YEAR END TECHNICAL REPORT
September 29, 2023 to September 28, 2024

Chemical Process Alternatives for Radioactive Waste

Date submitted:

June 13, 2025

Principal Investigator:

Leonel E. Lagos, Ph.D., PMP®

Florida International University Collaborators:

Dwayne McDaniel, Ph.D., P.E. (Project Manager)
Anthony Abrahao, M.S.
Aparna Aravelli, Ph.D.
Amer Awwad, M.S., P.E.
Mayren Echeverria Boan, Ph.D.
Mackenson Telusma, M.S.
DOE Fellows

Submitted to:

U.S. Department of Energy
Office of Environmental Management
Under Cooperative Agreement DE-EM0005213

FIU Applied Research Center
FLORIDA INTERNATIONAL UNIVERSITY

Addendum:

This document represents one (1) of five (5) reports that comprise the Year End Reports for the period of September 29, 2023 to September 28, 2024 prepared by the Applied Research Center at Florida International University for the U.S. Department of Energy Office of Environmental Management (DOE-EM) under Cooperative Agreement No. DE-EM0005213.

The complete set of FIU's Year End Reports for this reporting period includes the following documents:

Project 1: Chemical Process Alternatives for Radioactive Waste
Document number: FIU-ARC-2023-800012997-04b-009

Project 2: Environmental Remediation Science and Technology
Document number: FIU-ARC-2023-800013918-04b-006

Project 3: Waste and D&D Engineering and Technology Development
Document number: FIU-ARC-2023-800013919-04b-006

Project 4: DOE-FIU Science & Technology Workforce Development Initiative
Document number: FIU-ARC-2023-800013920-04b-015

Project 5: Long-Term Stewardship of Environmental Remedies: Contaminated Soils and Water and STEM Workforce Development
Document number: FIU-ARC-2023-800013922-04b-005

Each document will be submitted to OSTI separately under the respective project title and document number as shown above. In addition, the documents are available at the DOE Research website for the Cooperative Agreement between the U.S. Department of Energy Office of Environmental Management and the Applied Research Center at Florida International University: https://doeresearch.fiu.edu

DISCLAIMER

This report was prepared as an account of work sponsored by an agency of the United States government. Neither the United States government nor any agency thereof, nor any of their employees, nor any of its contractors, subcontractors, nor their employees makes any warranty, express or implied, or assumes any legal liability or responsibility for the accuracy, completeness, or usefulness of any information, apparatus, product, or process disclosed, or represents that its use would not infringe upon privately owned rights. Reference herein to any specific commercial product, process, or service by trade name, trademark, manufacturer, or otherwise does not necessarily constitute or imply its endorsement, recommendation, or favoring by the United States government or any other agency thereof. The views and opinions of authors expressed herein do not necessarily state or reflect those of the United States government or any agency thereof.

TABLE OF CONTENTS

LIST OF FIGURES

LIST OF TABLES

PROJECT 1 EXECUTIVE SUMMARY

The Department of Energy's (DOE's) Office of Environmental Management (EM) has a mission to clean up the contaminated soil, groundwater, buildings, and waste generated over the past 60 years by the R&D and production of nuclear weapons. The nation's nuclear weapons complex generated complex radioactive and chemical wastes. This project is focused on tasks to support the safe and effective storage, retrieval, and treatment of high-level waste (HLW) from tanks at Hanford and Savannah River sites. The objective of this project is to provide the sites with modeling, pilot-scale studies on simulated wastes, technology assessment and testing, and technology development to support critical issues related to HLW retrieval and processing. Florida International University (FIU) engineers work directly with site engineers to plan, execute, and analyze results of applied research and development. In addition, efforts focus on addressing waste disposal challenges at the sites and issues related to preserving the structural integrity of the H-Canyon Exhaust Tunnel at Savannah River.

DOE Fellows supporting this project include Brendon Cintas (Graduate, Ph.D., Mechanical Engineering), Bryant Pineda (graduate, M.S., Mechanical Engineering), David Rojas (undergraduate, Mechanical Engineering), Pedro Chaviano (Graduate, M.S., Electrical Engineering), Douglas Baptiste (Undergraduate, Civil Engineering), Gabriel Cerioni (Graduate, M.S., Mechanical Engineering), Joel Adams (Graduate, Ph.D., Mechanical Engineering), Nicholas Espinal (Undergraduate, Mechanical Engineering), Kevin Yulkowski (Undergraduate, Mechanical Engineering), Philip Moore (Graduate, M.S., Mechanical Engineering), Rafael Velasquez (Graduate, M.S., Electrical Engineering), Bryan Torres (Graduate, Mechanical Engineering) and Theophile Pierre (Undergraduate, Mechanical Engineering).

The following ARC researchers are supporting this project and mentoring the DOE-EM Fellows: Dwayne McDaniel (Ph.D., Engineering Mechanics, Project Manager), Anthony Abrahao (M.S., Mechanical Engineering, Task 18.4, 18.5, 18.7,Task Manager), Amer Awwad (M.S., Mechanical Engineering, Task 18.6, Task Manager), Aparna Aravelli (Ph.D., Mechanical Engineering, Task 17.2, 19.1, Task Manager), Jose Rivera (B.S., Civil Engineering, Task 18.6, Research Analyst), Mackenson Telusma (M.S., Mechanical Engineering, Task 18.3, Task Manager), Mayren Echeverria (Ph.D., Chemical Engineering, Task 20, Task Manager), Leonel Lagos (Ph.D., PMP®, Mechanical Eng./Civil/Env. Engineering, PI).

Although several tasks have been initiated and completed over the course of the cooperative agreement, at the end of this past year, there were 4 active tasks. These tasks are listed below, and this report contains a detailed summary of the work accomplished for FIU's Performance Year 4.

Task 17: Advanced Topics for HLW Mixing and Processes

In the U.S. Department of Energy's (US DOE) Savannah River Site (SRS) and Hanford site, systems of pipelines transport high-level radioactive liquid waste for waste processing and storage. After transporting the waste, the lines are flushed with water to ensure that no sludge or sludge solid sediments remain in the transfer line. Current guidelines that establish a minimum flush volume and flush water velocity required for post-transfer flushing operations to achieve a satisfactory cleanliness exist; however, the Defense Nuclear Facilities Safety Board (DNFSB) indicated a need for further investigation on the technical basis for the prescribed guidelines. Consequently, further studies that will assist SRS and Hanford in waste remediation are being done to optimize the operational conditions. This optimization would minimize the flush volume and consequent downstream waste, which ultimately would assist in preserving tank storage, preventing secondary waste processing, and minimizing changes to the waste's chemistry and rheology.

To perform these investigations, an expandable, 3-inch carbon steel experimental pipe loop was designed and constructed at Florida International University (FIU) to simulate flushing operations of non-Radioactive slurries. The test loop was designed to simulate sediment beds of solid materials and bed heights to investigate what parameters affect the efficiency of flushing operations at various concentrations. Testing was then conducted using non-Radioactive kaolin-water slurry simulants at various concentrations with various flush volume and flush modes to determine the effect of flush volumes for each configuration. These concentrations offer repeatability within the sediment beds inside the pipeline for fully flooded and gravity-drained conditions with one day, one week, and two-week sedimentation. By parametrizing the sediment height and conditions, the flush volume and flush velocity values could be optimized, which leads to satisfactory cleaning of transport lines of varying length with a minimal use of flush water.

This report presents the latest efforts in flush analyses to determine the efficiency of flushing operations. In this year of testing, efforts were redirected to assist in understanding the performance of flushing with a slurry as opposed to water which was used in previous studies. Recently the loop was modified to conduct the flushing tests with a slurry and a test plan was developed to evaluate how settling time effects the flush-to-line volume (FTLV) ratio. Multiple trials were conducted, and the data has led to suggestions for further investigation. The trials with 1 week and 16 week show similar data from the testing, but challenges still remain in estimating the exact time the line has been flush. We will continue to work with Savannah River engineers to update the test plan based on the results obtained.

Task 18: Technology Development and Instrumentation Evaluation

Scientists and engineers from the Hanford and Savannah River sites are constantly evaluating innovative technologies to alleviate the operational issues related to inspecting, sampling, and repairing aging nuclear infrastructure and tanks containing highly radioactive nuclear waste. In close collaboration with WRPS and SRNL, the Applied Robotics Laboratory at FIU has developed and deployed several specialized robotics tools tailored to the needs of the Hanford and Savannah River sites.

In collaboration with SRNL, FIU has developed a wall-crawler system (Subtask 18.3) to evaluate the H-Canyon exhaust tunnel for degradation and potentially apply a protective coating. The H-Canyon is America's only remaining chemical processing facility capable of reprocessing plutonium, highly enriched uranium, and other radioactive materials. Robotic inspections of the facility's exhaust tunnel revealed significant degradation of the reinforced concrete structure, primarily associated with acid attack compromising the tunnel's structural stability. Applying a protective coating on the degraded tunnel walls could mitigate and prevent further deterioration. During this performance period, energy consumption during vertical climbing was improved, transitions between orthogonal surfaces were made more efficient, additional sensors—including load sensors, depth cameras, and ultrasonic sensors—were added to the dual-fan system for enhanced performance and teleportational use, the complexity of the five-fan drive module was reduced to improve structural stability and decrease mechanical failure points during operation, the initial design of a high-fidelity large-scale mockup of a section of the H-canyon was completed, and work continued on transferring vector thrust technology from the dual-fan system to the five-fan unit.

FIU continues to collaborate with WRPS to investigate mobile robotic platforms (Subtask 18.4) and state-of-the-art field-deployable sensory suitable for improving worker health and safety across the site. Routine inspections at the Hanford site typically require personnel to enter hazardous facilities, where they carry sensors to collect environmental data. This data is analyzed after the inspection is complete. This procedure poses two significant challenges: first, the risk of personnel exposure to hazardous conditions increases the potential for accidents; second, there is often a significant delay between data collection and analysis, which can hinder timely decision-making. Remote mobile robotic platforms can serve as a substitute for personnel by performing inspections remotely. These robotic platforms, known for their versatility, can be outfitted with sensor payloads that capture environmental data like human inspectors. Furthermore, the data collected by these robots can be transmitted in real-time to a base station. At the base station, operators can immediately assess and analyze the data from the inspected area. By employing mobile robotic platforms for surveys, the need for personnel to physically enter hazardous facilities is eliminated, significantly reducing the risk of exposure to dangerous conditions. Additionally, the remote data capture capability ensures that the information becomes available for analysis much more quickly, thus improving the efficiency and effectiveness of the inspection process. The expected outcome of this study is to validate the effectiveness of mobile robotic platforms in conducting safe and efficient inspections at the Hanford tank farms. During this performance period, the team further continued development of the navigation capabilities of the robotic tools to implement frontier-based, fully autonomous movement for mapping and surveilling the environment. In addition to digital twin capture, environmental sensors were equipped to the robotic platform to perform radiation mapping and ammonia gas monitoring. This tool was deployed during the summer at WRPS' Cold Test Facility, with a focus on the needs of stakeholders from the WRPS Industrial Hygiene (IH) and Radiation Control (RadCon) organizations in accordance with the Technology Element Description Summary (TEDS) MTW-79 (see Appendix), which focuses on reducing the entries into the tank farms while collecting "vapor-related data in the worker breathing zone". During this field work, the focus was to implement, test, and deploy sensors that would assist workers in conducting routine surveillance operations to emergency response.

In another collaboration with WRPS, FIU has developed several specialized inspection tools (Subtask 18.5) tailored to single-shell and double-shell tanks. The effort is part of the WRPS's Engineering and the Chief Technology Officer (CTO) partnership with FIU to develop technologies to alleviate operation burdens at Hanford's tank farms. During this performance period, sampling capability was successfully incorporated into the miniature rover (Subtask 18.5.1). The system improvements will continue with the objective of demonstrating and testing at Hanford to retrieve sample material under the DSTs in 2026. The lateral gamma scanner (Subtask 18.5.2) was successfully demonstrated and tested for the second time at Hanford's Cold Test Facility. The system support will continue. The discussions regarding a possible 2025 demonstration of the LGS at Hanford's tank farm will continue with WRPS. An off-riser sampler system (Subtask 18.5.3) prototype was finalized and demonstrated at Hanford's Cold Test Facility during the summer of 2025. The team will continue streamlining the pneumatic arm's components and joint controls, resume designing a deployment cable hoist system, and start implementing a stabilization mechanism.

Finally, in collaboration with WRPS, FIU has developed a Robotic Vacuum System (Subtask 18.6) and the In-Tank Sonar System for DST Applications (Subtask 18.7). The systems were successfully demonstrated at Hanford Cold Test Facility and Atkins Technology Center. These demonstrations represent significant progress toward addressing the operational challenges in tank waste management at Hanford site. The successful demonstrations and positive stakeholder feedback indicate that these technologies are advancing toward operational readiness, with clear pathways for future improvements and deployments in 2025.

Task 19: Pipeline Integrity and Analysis

The Hanford Site Tank Farm has implemented a Fitness-for-Service (FFS) program for the Waste Transfer System. The FFS program, based on API-579-1/ASME FFS-1, examines structural parameters of the waste transfer systems in order to develop erosion/corrosion rates for relevant system components. The FFS information is acquired from opportunistic evaluations of pipelines that have been removed from service.

One of the objectives of this research is to test and demonstrate that the SRNL erosion and mass loss coupons can provide an in-situ method for collecting erosion and mass loss rates from a pipeline using the stainless steel and carbon steel coupons during operation.The real-time particle erosion effect on the SRNL coupons was verified and validated on an engineering scale test bed using a combination of sand and glass replicating SRNL's DWPF glass frit. Experimental results showed much less change in erosion in stainless steel when compared to the carbon steel coupons.

Another objective is to test and demonstrate that the SRNL coupons could provide static and dynamic methods for collecting corrosion rates from pipelines using stainless steel and carbon steel coupons. For this, a bench scale loop was custom designed and installed for testing replicate caustic simulants with various concentrations. Findings of the research summarize that carbon steel underwent high levels of caustic corrosion with 6M salt simulants over a period of 3 years. Results of static testing will be shared with SRNL for future material and design considerations.

A final objective involves CFD simulations for erosion corrosion detection and model development in data analytics. Fluid flow simulations using COMSOL software have been conducted by developing corrosion models for particle flow in U-bends of the pipe sections. The research provides a basis to combine the CFD simulations with experimental results that can potentially be used to develop comprehensive realistic multi-physics-based models for flow in the HLW transfer process. The machine learning models developed using the particle erosion data can be used to predict erosion in pipes based on statistical methods. In the future, a comparative study of all simulant mixtures and their simultaneous effect can be investigated.

Task 20: Corrosion Protection and Characterization of EM Infrastructure

FIU has been working with the Savannah River site engineers in the search and evaluation of potential coatings for the mitigation and protection of the degraded concrete walls of the H-Canyon infrastructure (subtask 20.1). Remote inspection of the H-Canyon Exhaust tunnel has shown degradation of the reinforced concrete walls, with the loss of more than 2 inches of material, protruded coarse aggregates and in some areas, exposure of the steel rebar (initially embedded), all this due to the aggressive environment inside the tunnel. Hence, the search for solutions to mitigate and prevent further degradation is necessary. The identification, evaluation and selection of the best coating candidate that can be applied to the tunnel's degraded concrete walls constitute the main goal of this investigation. The investigation has been divided into different phases: 1) development and evaluation of aged concrete surfaces under accelerated aging conditions, 2) identification and evaluation of potential coatings applied on aged and non-aged concrete under accelerated aging conditions (preliminary results presented in this report) and 3) selection of best coating candidates from research findings.

Previous efforts were focused on 1) the development and evaluation of aged and non-aged concrete surfaces to evaluate potential coatings and 2) the identification and preliminary evaluation of potential coating candidates for the protection of the degraded concrete walls of the HCAEX tunnel. A comprehensive test plan for the evaluation of the coated surfaces was developed and executed including key variables such as 1) surface preparation, 2) aging conditions of the substrate and 3) presence of rebar. Previous results included the completion of the aging and evaluation of three (Carboline, Sherwin-Williams and Belzona) of the four potential coatings selected for the study. The accelerated aging of the samples consisted of exposing the top surface to a 0.5M nitric acid solution and erosion.

In this year, the Framatome polyurea coating system, completed the accelerated aging and evaluation through visual inspection, failure analysis, thickness and impedance measurements. Visual inspection results showed no major failures, except some erosion with loss of coating material and color change suggesting some chemical degradation of the coating. The coating system showed high impedance values indicative of good protective properties. The reduction of thickness over time indicated degradation and loss of protective properties, motivated by the erosion of the surface. In addition, a ranking of the potential coating candidates was established. The ranking was based on the coating's performance to the accelerated aging conditions, 0.5M nitric acid solution and erosion. Parameters considered for the ranking included the results on 1) visual inspection, 2) coating failures, 3) thickness loss and 4) impedance.

FIU is also working on a new task (20.2) with the Hanford Site. A current challenge for DOE and relevant DOE sites is to understand the durability of the steel containers that will contain low-activity waste (LAW) and secondary waste forms, encapsulated in glass and grout respectively, and that will be placed within the Integrated Disposal Facility (IDF) at Hanford. Currently, corrosion data of the steel and weld regions of the containers at Hanford that is exposed to groundwater is limited. In addition, there is limited information on the corrosion behavior of container materials in groundwater that has also contacted grout waste forms following the initial container breach. It is of interest to study the corrosion of container materials when exposed to grout-contacted solutions to get information of the container-waste form (grout-waste form) interface. The objective of this subtask is to evaluate material behavior of the containers in environments similar to IDF conditions and obtain site-specific corrosion data through electrochemical measurements. Previous efforts were concentrated on completing the evaluation of potential container materials such as 304 and 316 stainless steels in contact with a Hanford simulated groundwater solution through electrochemical measurements. For comparative purposes, another solution containing only the chloride ions of the previous recipe was also used.

In this year, 304SS and 316SS potential container materials exposed to grout-pore water solutions from Hanford's Cast Stone samples completed the evaluation. Also, carbon steel samples initiated the corrosion testing. Polarization graphs of 304SS and 316SS, in the three solutions, showed that the anodic branches were controlled by passive film formation followed by rupture of the film due to pitting formation or some current instability. The corrosion rates of 304SS and 316SS in the three solutions are very low, between 0.006-0.008 mm/y, indicating that the material is very stable. The highest impedance modulus is for the materials immersed in the most concentrated grout-pore water solution (GPW1) on day 1, ~ 1E9 Ω, compared to the two diluted solutions, GPW2 and GPW3, with values ~ 1E7 Ω.

MAJOR TECHNICAL ACCOMPLISHMENTS

Task 17: Advanced Topics for HLW Mixing and Processes

- The flushing loop was modified and a test matrix was generated to allow for the flushing and resuspension of sediment using a slurry.
- Initial testing was conducted that the modifications to the loop and the additional instrumentation added were functioning appropriately.
- Two trials were conducted – a 1-week and 16-week settling time for a 10% kaolin water slurry mix.
- Operational information was obtained that suggests additional efforts need to be addressed regarding steady state values of the density and determining at what point in time and what line volume is needed to completely flush the line.

Task 18: Technology Development and Instrumentation Evaluation

- The second DOE, FIU, and WRPS Technology Development Collaboration Meeting was hosted at FIU on February 14 and 15, 2024. Officials from the DOE-EM TD Office, WRPS, and Savannah River National Laboratory attended the meeting.
- Professional track posters and oral presentations based on Project 1 research results were presented at the WM2024 Symposia in Phoenix, AZ in March 2024.
- DOE Fellows continued researching their FIU robotic projects at SRNL and WRPS during their summer internships.

Wall-Climbing Platform (Subtask 18.3)

- Successfully redesigned the large EDF drive module, transitioning from 2-DOF to 1-DOF, improving overall performance and reliability
- Integrated load cell sensors into the platform chassis for real-time monitoring of thrust forces
- Enhanced surface transition capabilities through extensive testing of ground-to-wall and wall-to-ceiling movements
- Successfully developed and tested a spray mechanism for coating application on vertical surfaces
- Initiated construction of a comprehensive H-Canyon tunnel mockup incorporating critical environmental factors

Long-Term Surveillance Systems (Subtask 18.4)

- Enhanced autonomous navigation capabilities for outdoor and unstructured environments
- Implemented frontier-based navigation techniques with 3D LiDAR sensor integration
- Developed custom GUI for robot operation and telemetry visualization

- Successfully integrated and tested radiation mapping capabilities using Bayesian Optimization
- Demonstrated technology at Hanford's Cold Test Facility with positive stakeholder feedback

Robotic Systems for DOE Sites (Subtask 18.5)

Miniature Inspection Rover

- Transitioned from single-PCB to dual-PCB design for enhanced functionality
- Developed new tether quick-connect system using pogo-pins
- Successfully manufactured critical components in-house using AL 6061-T6 materials

Off-Riser Sampler System

- Developed and tested novel multi-joint pneumatic manipulator
- Successfully integrated diverse end-effector tooling (augers, drills, air hammers, scoops)
- Achieved payload capacity exceeding 10 lbs
- Successfully demonstrated at WRPS's Cold Test Facility
- Effectively sampled various materials including concrete, loose sand, and KMAG simulant

Vacuum Crawler System (Subtask 18.6)

- Successfully developed and tested dual EXAIR Line Vac pneumatic vacuum modules
- Achieved up to 95% debris removal efficiency in testing
- Demonstrated successful navigation over ½-inch obstacles
- Implemented precise control system with joystick interface
- Successfully tested at Cold Test Facility with positive stakeholder feedback

In-Tank Sonar System (Subtask 18.7)

- Successfully designed and fabricated corrosion-resistant deployment system
- Developed effective gimbal control system with mechanical stop solution
- Conducted successful imaging tests in various tank sizes
- Demonstrated system capabilities at Atkins Technology Center
- Achieved 98.7% accuracy in tank dimension measurements
- Successfully mapped submerged features and simulant materials in 30-foot diameter test pool

Task 19: Pipeline Integrity and Analysis

- The real-time particle erosion effect on the SRNL coupons has been verified and validated on an engineering scale test bed using a combination of sand and glass replicating SRNL’s DWPF glass frit. Experimental results showed much less change in erosion in stainless steel when compared to the carbon steel coupons.

- The effect of simulated caustic solutions replicating the chemical composition of HLW at Hanford and Savannah River sites is studied on waste transfer pipes. Two materials have been considered for corrosion due to the varying molar concentrations of the chemical simulants. Immersion experiments were conducted using SRNL's patented coupons. Visual inspection, weight change and thickness changes are quantified. Findings of the research summarize that carbon steel underwent high levels of caustic corrosion with 6M salt simulants over a period of 3 years.

- Computational Fluid Dynamics (CFD) analysis was conducted to investigate the flow velocities and pressure changes in the pipe sections to identify hot spots (regions prone to high velocities/pressures). The research provides a basis to combine the CFD simulations with experimental results that can potentially be used to develop comprehensive realistic multi-physics-based models for flow in the HLW transfer process. The machine learning models developed using the particle erosion data can be used to predict erosion in pipes based on statistical methods.

Task 20: Corrosion Protection and Characterization of EM Infrastructure

- FIU presented a poster with some research results of the 20.1 tasks at the WM2024 Symposia in Phoenix, Arizona. The poster was <u>selected as Best Poster of Track 6</u> of Deactivation and Decommissioning, and the manuscript achieved the rating of a <u>"Superior"</u> paper at the Conference.
- The Framatome polyurea coating system completed the aging and evaluation.
- Laboratory research findings of the four potential coatings supported the establishment of a ranking.
- Impedance measurements supported the evaluation of the coating's protective properties.
- Completed the evaluation of 304 and 316 stainless steels exposed to grout-pore water solutions from Hanford's Cast Stone samples.
- Corrosion parameters such as corrosion potential, corrosion current, corrosion rate and corrosion current density were obtained from Tafel slopes and calculations.
- Evaluated the effect of grout-pore water solution concentration on the corrosion behavior of 304 stainless steel and 316 stainless steel containers materials.

TASK 17: ADVANCED TOPICS FOR HLW MIXING AND PROCESSES

Subtask 17.2: Evaluation of Pipeline Flushing Requirements for HLW at Hanford and Savannah River Site

Subtask 17.2: Introduction

Transfer of high-level nuclear waste through pipelines at Hanford, Savannah River and other sites require operations above critical velocities for transporting slurry mixtures to prevent formation of stationary or moving beds of solid sediments. The formation of sediment beds within the pipeline can result in partial line plugging (which may lead to an excessive pumping load and erosion) or full line plugging (which may lead to a pump burst or pipeline failure). The design strategy of the high-level waste pretreatment facility requires that the process lines be flushed with water after each slurry transfer to minimize the likelihood of pipeline plugging. The Defense Nuclear Facilities Safety Board (DNFSB/TECH-40, 2016) has indicated the need for an investigation into the technical basis for prescribing flush velocities in pipelines. Also, the results of previous flushing and critical velocity tests using several simulants were reviewed. Poloski et al. (2009) and Yokuda et al. (2009) reported the following results: (1) the minimum number of flush volumes were higher than the values in the design guidelines (Hall 2006), (2) the flush velocities in the pipeline were higher than the maximum velocity stated in the flushing guidelines, and (3) no assessments of the post-flush pipeline cleanness have been reported. Hence, it is essential to minimize the volume of water needed to achieve effective flushing operations as well as to develop additional guidelines in support of literature developed flushing standards (Nguyen et al. 2016).

Research has been conducted by FIU recently to investigate and estimate the flush to line volume required for a clean flush in the pipelines. [Cintas et al. 2023]. Varying concentrations of slurry mixtures with water and kaolin have been used to investigate the particle resuspension and settling characteristics with varying settling time of the slurry in the loop. These studies were conducted under both gravity-drained and fully flooded conditions.

The objective of this effort is to build upon the findings of previous testing to determine the capability of using slurry to flush the pipelines and to make sure there is minimum to no deposition at the bottom of the lines. If successful, it will aid in minimizing the additional clean water currently being used for flushing the lines and thus minimizing additional waste creation on site. Successful execution of this effort will require the creation and characterization of sediment beds, a variety of flushing modes for comparison, and an evaluation of the operational effectiveness through measurement of post-flush pipeline residues. To extend the previous flushing studies, a set of case studies will be created, each targeting flushing with slurry of kaolin water simulant mixtures in a closed pipe loop. For each phase of testing, a specific simulant and a fixed pipe length will be used while varying the influential parameters, including the flush volume/time and the initial conditions (gravity drained, and fully flooded systems). To achieve the objectives of this task, a 165-ft test loop made of 3-inch schedule 40 carbon steel pipes and fittings will be utilized. The closed test loop has been previously constructed and tested at FIU. This test loop will also include cameras and ultra sonic sensors for sediment bed characterization and a Coriolis meter to determine flow rate and solid concentrations. A description of the loop and its operation is provided in later sections.

Subtask 17.2: Objectives

The objective of this effort is to provide a technical basis for flush volume used in the waste transfer process when a slurry is used to flush a transfer line. This includes:

- Developing a testing procedure to determine at what time/volume, a line is flushed with a slurry.
- Understanding how length of sitting time for the settled solids effects the performance of the flush.

Subtask 17.2: Methodology

An experimental test loop with the ability of operating in different operational modes was designed (Figure 1). The operational modes include slurry circulation (to load the system), draining, flushing (for gravity-drained and fully flooded initial conditions), post-flush circulation, pump cleaning and water/solids recycling.

A slurry pump capable of delivering 230 gpm of water at 93 feet of head will be used for slurry circulation, flushing, and post-flush evaluations. This pump can also be controlled manually by a variable frequency drive to achieve target flow rates. A Coriolis meter will measure density and mass flow rate of the flow during the slurry circulation mode (to adjust concentrations inside the mixer tank), during flushing mode (to indicate the time for switching between high and low velocity values) and during post-flush evaluations (to assess the presence of post-flush solid residues). High resolution cameras, potential borescopes and ultrasonic transducers will be used to characterize sediment bed height inside the pipeline before, during, and after flushing operations. The test loop will be equipped with safety elements such as relief valves and a burst disk (to avoid over pressurization of the lines and to provide quick venting) to protect the system elements, particularly the slurry pump. Pressure transducers and gauges will be used to monitor the system pressure at different locations and detect/locate possible plug formations. This monitoring will help characterize the system in terms of pressure losses, protect the slurry pump, and indicate the need for quick unplugging using a drain snake as well as cleaning/replacing the filters used for capturing post-flush solid residual and cleaning the recycling water. An ultrasonic tank level gauge will trigger an alarm for termination of the flushing operation when water in the flushing tank drops to the target levels.

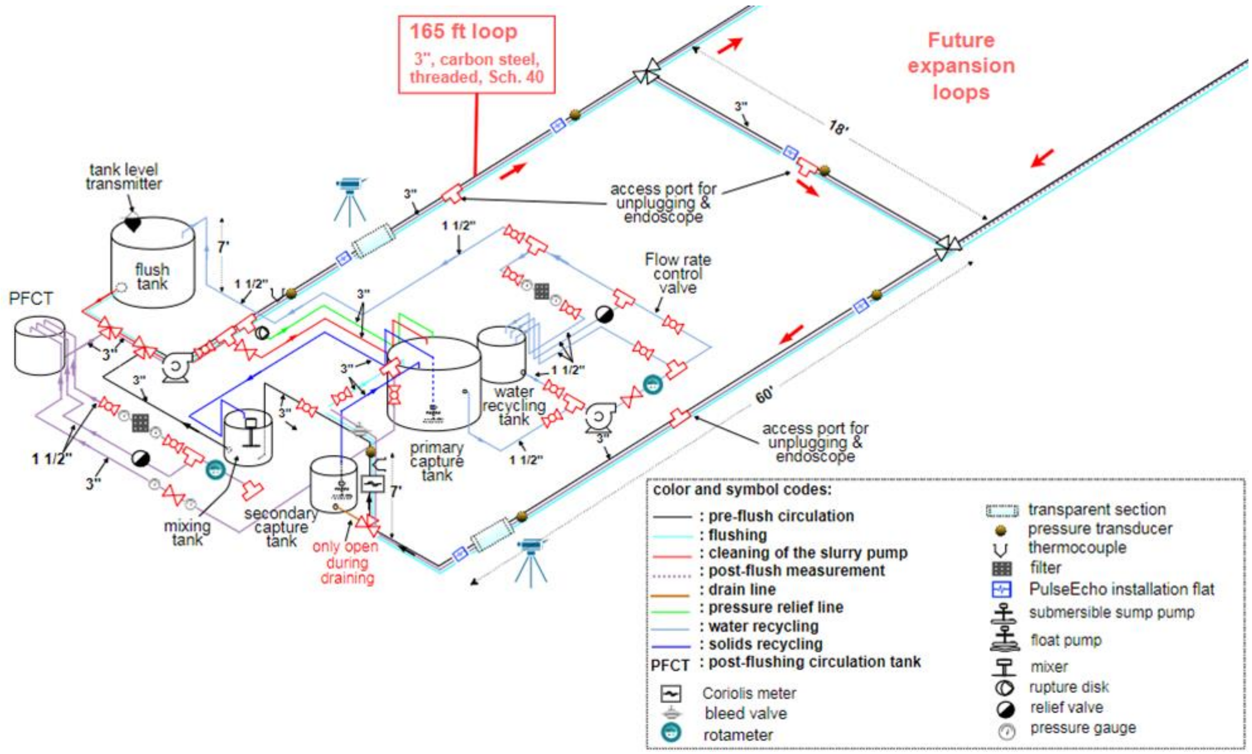

Figure 1. Layout of the flushing test loop.

Two initial condition modes, gravity-drained and fully flooded, can be utilized depending on the conditions required (Figure 2). For the transfer applications at Savannah River, gravity drained will be the focus for these testing trials.

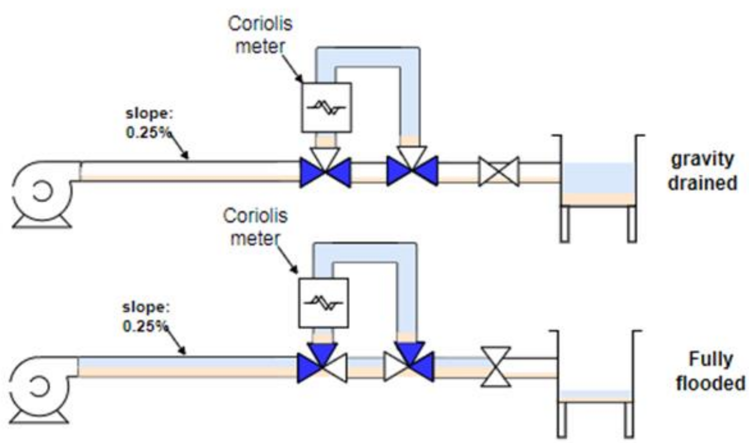

Figure 2. Two initial condition modes for the flushing studies.

The loop was built according to the schematics using 3-inch carbon steel pipe components (straight sections and elbows). Flow control valves were installed at various sections to maintain and regulate the flow of water and slurry mixtures. Three clear sections were installed for visual inspection before, during and after the experimental tests. The major equipment and instrumentation for the test loop are the slurry pump, variable frequency drive, Coriolis meter, submersible pumps for the primary capture and secondary capture tanks, centrifugal pump for the water retrieval system, filters/housing, mixer, tanks, ultra sonic transducers, cameras, and tank level sensors. Figure 3 shows the currently installed and tested loop at FIU with a length of 165 ft which will be used for these trials.

Figure 3. Experimental flushing pipe loop with storage and flushing tanks.

Subtask 17.2: Initial Testing

Initial testing of the system was conducted to: (1) ensure smooth operation and accurate functionality of all system elements, including the pump, valves, pressure transducers, mixer, and Coriolis meter, as well as the absence of any air pockets or leaks; (2) ensure consistency of the initial conditions created for each flushing experiment; (3) test the ability of the ultrasonic sensors to determine the sediment bed thickness inside the pipeline in both static and dynamic conditions;

Efforts during the initial testing will focus on creating repeatable sediment beds inside the pipeline for gravity-drained systems. The material composition used to create sediment beds (mixing tank contents) as well as the loop length will be fixed (a 165 ft loop will be used). Bed parameters such as height, solids concentration, and rheology will be measured to ensure consistency of the initial conditions between tests. FIU will control parameters such as the rate of the slurry pump shut-down and delay time, which affect sediment build-up, to attain consistent initial conditions.

Selection of a simulant for the flushing tests has been discussed between FIU and engineers from SRNL. A mixture of 10 wt% kaolin in water is expected to result in the appropriate ranges of interest for density, viscosity and yield stress. In previous studies [Cintas 2023], FIU has investigated and verified the EPK kaolin for initial characterization (density, rheology, settlement rate, and particle size analysis) and performance testing as the simulant material. Hence, it will be used for the current testing. Pipelines in the flushing tests are primarily made of carbon steel threaded pipes with PVC in some sections of the pipe loop including the post-flush water/slurry circulation and water filtration loops. Slurry will be used as the flushing medium for these trials.

Subtask 17.2: Experimental Approach

Fulfillment of the flushing criteria will be investigated using ultrasonic, visual, and solids entrapment methods. A post-flush circulation loop will be used to gradually filter out the solids. Determination of post-flush residuals will be conducted through measurement of the accumulated mass of solids inside the filter as well as the density of the post-flush-circulation tank contents. Variation of the density will be monitored via a Coriolis meter as part of this circulation loop.

Approaches/parameters/controls are as follows:

- Use of a modular pipe loop with a length of 165 feet,
- Use of a single slurry pump controlled by a variable frequency driver (VFD) for system loading, flushing, and post flush evaluations,
- Preparation of a simulant with properties within the recommended ranges (10% weight percent) in a circulation loop,
- Creation and characterization of initial conditions (sediment bed) in both drained and fully flooded modes by stopping the flow in the circulation loop and using visual/camera and PulseEcho methods,
- Monitoring of the sediment bed erosion during flushing using video recordings of the flow,
- Timely control of flushing operations by precise monitoring of density and flow rate (using a Coriolis meter) and water usage (using an ultrasonic tank level transmitter),
- Post-flush evaluations and inspections using (1) visual (camera and endoscope) and PulseEcho methods for residual detection, and (2) density monitoring by a Coriolis meter as well as solids filtration during continuous recirculation,
- Solids and water retrieval for subsequent flushing studies,
- Removal of potential granular plugs as detected by pressure transducers via pressure pulsation by slurry pump, compressed air introduced in via three-way connectors, and drain snakes.

The following approach will be utilized for each trial:

- Ensure appropriate slurry concentration in the slurry tank and the fresh water in the supply tank.
- Fully flood the system (loop) with slurry.
- Use the gravity drained mode for testing and vary the wait time after draining for each trial.
- Collect data in each mode.
- Conduct data analysis to test the resuspension and flushing ability of slurry during the waste transfer process.

Details of the experimental procedure with step-by-step instructions for instrument operations are provided below:

- Fill the system by adding water to the mixing tank while the loop outlet is routed to the mixing tank. Start the slurry pump at low speed using a VFD to circulate the water in the loop and continue adding water to the mixing tank. Stop adding water to the mixing tank when all the air is removed, which can be accomplished with a bleed valve mounted at the highest point of the system. The absence of air in the system can also be verified by considering the stability of the density signal at the Coriolis meter.
- Start the mixer inside the mixing tank and slowly add kaolin. Observe the density variations in the Coriolis meter until the desired concentration is achieved. The concentration of 10% will be used. With a submersible pump and a hose, transfer the contents from the mixing tank to one of the reservoir tanks that only function as an inlet to the loop.

- Repeat step 2 until the desired volume is achieved in the reservoir tank, the pipeline is fully flooded, and the water-kaolin mixture in the tanks and the pipeline is at the targeted ratio.
- *Pump Calibration*: Increase pump speed to achieve a flow velocity of 10 ft/s. Record the associated frequency indicated by the VFD for both water and slurry modes. Slowly reduce the pump speed until the pump is fully stopped.
- Set the frequency of the VFD to the recorded value (10 ft/s). Start the slurry pump and simultaneously open the flush valve. Stop the slurry pump after a minimum of 3 lines of slurry is transferred through the loop to ensure fully flooded condition.
- Let the slurry in the pipeline settle for the appropriate test duration. Attempt to monitor sediment bed height with visual inspection in the clear sections, ultrasonic sensors, and possible borescopes. Periodically mix the contents of the water reservoir tank with a submersible pump to prevent it from settling.
- After the specified settling time, open the drain value to remove the liquid from the pipe, leaving the solids at the bottom. Observe the height of the sediment through the clear sections and measure the height at various locations through the access ports.
- Repeat step 5 to flush the loop with the kaolin-water mixture from the reservoir tank to the capture tank.
- Transfer the remaining material from the primary capture tank to the mixing tank using a submersible slurry pump with an agitator.
- Clean the loop by flushing with water and observe the residual sediment levels remaining in the loop via the density measurements.

Subtask 17.2: Results and Discussion

For this performance period, efforts focused on creating a procedure to test flushing requirements when a slurry is used to flush a transfer line. After modifications were made to the test loop and the initial commission tests were completed, two trials were conducted with different settling/wait times. The times used were 1 and 16 weeks. Results from the 1-week trial are shown in the figure below.

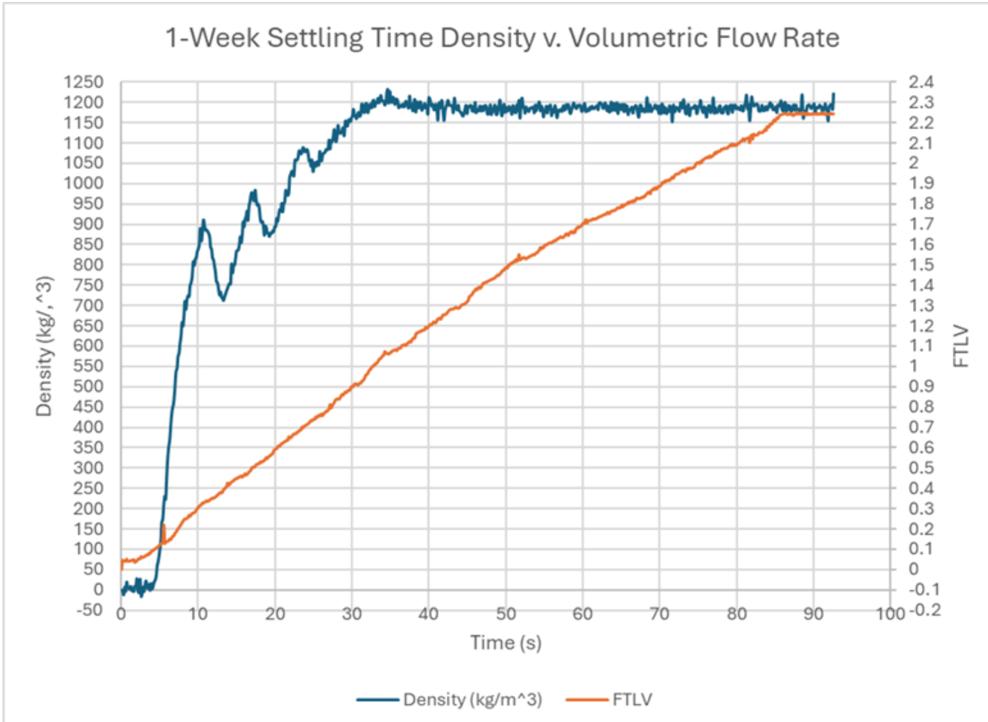

Figure 4. Density and FTLV ratio for 1-week settling trial.

Figure 4 shows the change in density along with the FTLV as a function of time. There are initial variations in density as the air gaps are pushed through the system but the density appears to settle between 1150 and 1200 kg/m^3. This is expected as the density of the 10% kaolin/water slurry is approximately 1165 kg/m^3. As expected, results show the density increase to a maximum value as the solids in the pipe are resuspended and then returns to a steady state value. The FTLV is also plotted as a function of time, but the challenge is to determine at what exact time the system is completely flushed. We will need to investigate the raw data more closely to see if the variation in the steady state density is the expected density of the slurry. It appears that the data reaches a steady value at approximately 1.2-1.3 lines of volume. Additional methods will also be needed to verify all the material has been resuspended.

Results from the 16-week settling trial are shown in the figure below.

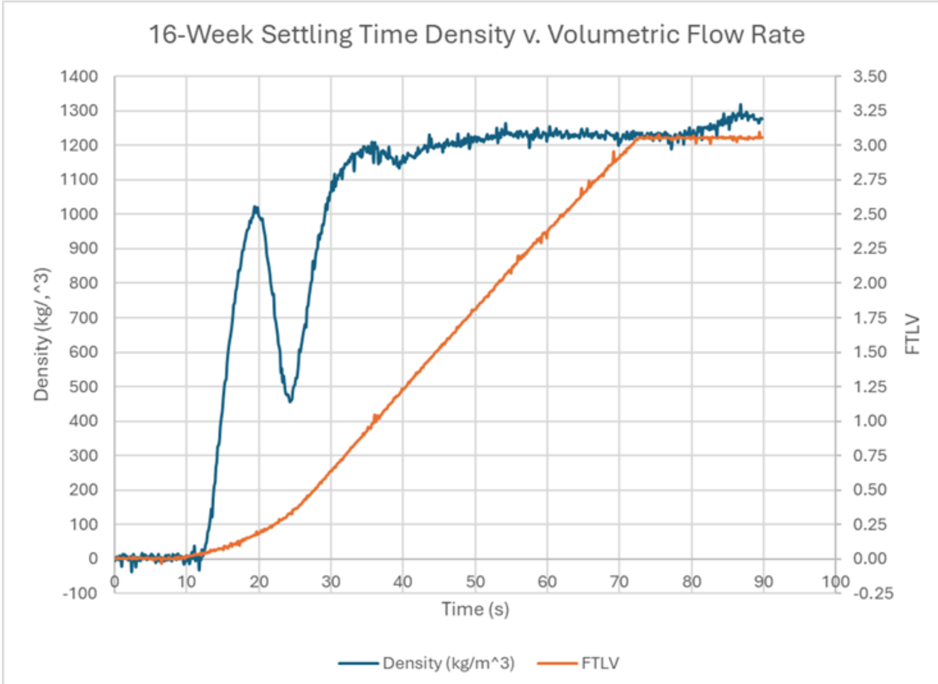

Figure 5. Density and FTLV ratio for 16-week settling trial.

The 16-week settling time trial appears to show similar trends but there are slight differences with the 1-week settling time trial. The density appears to settle at a higher value and has a slight increase toward the end of the run. It should be noted that there were a few unintended operational differences between the two trials that provide significant lessons learned. In this trial, 3 lines of volume were used so the tank configuration was different requiring addition transport from a mixing tank to the tank used in the flush. In the first trial, 2 lines of volume were used so that the flushing slurry was mixed within the tank used to flush the lines. In addition, in the first trial, the pump frequency was set to a value that provided a flow velocity of approximately 5 ft/s and in the second trial the flow velocity was found to be just over 9 ft/s. There doesn't appear to be a significant difference with the two trials, but further analysis is needed.

Subtask 17.2: Conclusions

An approach has been created to assess flushing performance using a slurry to resuspend sediment in a pipe. A test plan was generated that utilized a 165 ft 3-inch diameter pipe to evaluate the flushing performance. Different settling times can be used for the resuspension of a slurry with 10% kaolin and water. The results show promise that the approach can be used for this application but there are additional challenges that still need to be addressed. Lessons learned from the testing include the following:

- Consider adding flow velocity as a potential variable to the test matrix.
- Prior to the flush, evaluate the density of the slurry while cycling it through the loop. This will provide a basis for the required steady state value.
- Remove the clear sections after flushing to validate the line is completely flushed.
- Utilize one mixing tank which limits testing to only 2 lines of volume.

- Rerun all trials for consistency of data.
- Analyze the density data to get a better understanding of the exact time and volume used when the pipe is completely flushed. One approach to address this is to use a specified volume (1, 1.5 and 2 line volumes) and remove the clear sections to determine if the line has material remaining.

Subtask 17.2: References

1. Kazban, A., “Plugging and Wear of Process Piping at The Waste Treatment and Immobilization Plant”, DNFSB/TECH-40 (2016)
2. A. Poloski, M. L. Bonebrake, A. M. Casella, M. D. Johnson, P. J. MacFarlan, J. J. Toth, H. E. Adkins, J. Chun, K. M. Denslow, M. L. Luna, J. M. Tingey, “Deposition Velocities of Newtonian and Non-Newtonian Slurries in Pipelines”, PNNL-17639, WTP-RPT-175 Rev. 0, (2009)
3. S. T. Yokuda, A. P. Poloski, H. E. Adkins, A. M. Casella, R. E. Hohimer, N. K. Karri, M. Luna, M. J. Minette, J. M. Tingey, “A Qualitative Investigation of Deposition Velocities of a Non-Newtonian Slurry in Complex Pipeline Geometries”, PNNL-17973, WTP-RPT-178 Rev. 0, (2009)
4. N. Hall, “Minimum Flow Velocity for Slurry Lines”, 24590-WTP-GPG-M-0058, Rev 0 (2006)
5. Nguyen V.C., Fountain M.S., Enderlin C.W., Fuher A.J.L., Pease L.F., 2016, One System River Protection Project Integrated Flowsheet-Slurry Waste Transfer Line Flushing Study, RPP-RPT-59600, Rev. 0
6. Cintas, B., McDaniel, D., Aravelli, A., Sinnott, D., Poirier, M., “Engineering-Scale Evaluation of Flushing Requirements for High-Level Liquid Waste at Savannah River and Hanford Sites”, Proceedings of the Waste Management Symposia 2023, Phoenix, AZ, February 26 - March 2, 2023.

TASK 18: TECHNOLOGY DEVELOPMENT AND INSTRUMENTATION EVALUATION

As a major highlight of 2024, FIU's applied robotics and AI teams hosted the second DOE, FIU, and WRPS Technology Development Collaboration Meeting at FIU on February 14 and 15, 2024. Figure 6 shows pictures of the two-day collaboration meeting. Officials from the DOE-EM TD Office, WRPS, and Savannah River National Laboratory were in attendance.

Figure 6. DOE, FIU, and WRPS Technology Development Collaboration Meeting.

The meeting covered a comprehensive range of technical discussions and demonstrations focused on robotics, AI, and technology development for tank inspection and maintenance. Key topics included solid-liquid interface monitoring, tool development including the minirover and vacuum cleaner systems, leak detection technologies, tank farm surveillance, and remote repair capabilities.

The agenda included facility tours of the Applied Robotics and AI laboratories, High Bay area featuring a double shell tank mockup, and an outdoor testing facility.

The meeting also included a special demonstration of a robotic remote system project involving FIU, ANL, SRNL, and WRPS, and concluded with discussions about summer intern activities and potential projects for 2025.

Subtask 18.3: Development of a Coating Deployment Platform for the H-Canyon Exhaust Tunnel

Subtask 18.3: Introduction

The H-Canyon is the only remaining chemical processing facility in America capable of reprocessing plutonium, highly enriched uranium, and other radioactive materials [1]. The exhaust air flow from the H-canyon chemical processing areas and HB-line is transported through the H-Canyon Exhaust (HCAEX) tunnel, where radioactive contamination is removed. Robotic inspections of the tunnel have revealed significant ongoing degradation of the reinforced concrete structure that was associated with acid attack. The degradation observed could compromise the mechanical strength of the structure. Hence, the search for solutions to mitigate and prevent further degradation is necessary [2-3]. The application of a protective coating on the degraded tunnel walls could mitigate and prevent further degradation, which constitutes the main goal of this investigation. This research effort has been divided into two phases: 1) Development and evaluation of aged concrete under accelerated aging conditions and 2) Evaluation of potential coatings applied on aged and non-aged concrete under simulated aggressive conditions.

In the preliminary stage of the investigation, a comprehensive literature review was performed and major findings included: 1) the characterization of the tunnel degradation conditions, 2) the identification of the chemical attack and erosion as the primary degradation mechanisms affecting the tunnel concrete walls, 3) the identification of the acid-type immersion tests as a well-known method for evaluating the materials' resistance to acid attack and, 4) the preliminary selection of potential coatings for aggressive environments similar to the tunnel [3].

Lessons learned and research findings of the initial testing of concrete in acid solutions supported the development and ongoing execution of a comprehensive test plan that will be presented in this report. The test plan execution is an ongoing task allowing the development and evaluation of aged concrete surfaces, with 1) protruded aggregates, 2) exposed steel rebar, and 3) chemically damaged, similar to the tunnel walls after more than 60 years of operation. The degraded (aged) concrete surfaces were developed through various accelerated aging conditions including the effect of some variables such as acid concentration, erosion, mode of action of the aggressive agent, and the presence of steel rebar [3]. Finally, the developed aged concrete surfaces will be used as the substrate for the evaluation of potential coatings in a further stage of the investigation. Because this is an ongoing investigation, preliminary results of the accelerated aging of concrete specimens will be presented in this report.

Due to the hostile environment of the HCAEX tunnel, the ability to enter the tunnel and perform any type of investigative, or in this case damage mitigation to the concrete walls, have been restricted to the use of robotic platforms equipped with the tools necessary to accomplish said goals. The robotic platform would need to work in tandem with another larger ground platform capable of traversing the difficult terrain of the tunnel. The ground platform would need to deploy the secondary platform onto the concrete walls to apply a down selected coating.

The secondary robotic platform will need to be capable of traversing the HCAEX tunnel concrete walls in a manner that does not further damage the surface of the walls and allows accurate positioning of the platform to apply the coating. A literature review regarding the different methods available that would allow a mobile platform to maintain contact with the walls, regardless of the platform's orientation, will be highlighted in this report.

After developing and testing a single fan-based platform, which creates the appropriate adhesion mechanism, the results obtained from constructing a multi-fan omnidirectional platform will be detailed in this report. The goal of the report will also be to show the viability of the platform as an option to a unit capable of traversing a concrete surface without introducing further damage to the wall's surface and at the same time, maneuvering across the surface to reach a desired location when tele-operated.

Subtask 18.3: Objectives

The primary objective is to develop a robotic mobile platform capable of traversing vertical walls with varying surface conditions and applying a coating to the walls with the aim of preventing further surface degradation inside the HCAEX tunnel. The aim is to develop a robotic mobile platform capable of traversing vertical walls with varying surface conditions using a thrust based adhesion mechanism [4,5].

A scaled mockup concrete wall will be constructed using the information from Savannah River Site engineers, and the platform will be evaluated for its ability to maneuver along walls with varying surface conditions. The performance of the platform will also be quantified and used as a baseline to compare to future iterations of the platform as improvements are made during the project cycle.

The platform will be equipped with a coating application system which will be developed for the purpose of applying a selected coating to the concrete walls of the HCAEX tunnel. The application system will be designed to be modular in nature so that it can be incorporated into mobile platforms of varying sizes and configurations.

Subtask 18.3.1: Improvement of Mobile Platform Efficiency

Subtask 18.3.1: Methodology

The implementation of the current wall-climbing platform in the H-Canyon tunnel will enable the deployment of a protective coating that extends the facility's working life, particularly in the daily operation of reprocessing nuclear materials for continued scientific applications. Applying this coating will help mitigate the degradation of the tunnel walls, enhancing both safety and efficiency within the facility. The addition of sensors—such as load cells—the improved robustness of the large EDF drive module, and extensive lab testing regarding the performance of the mobile platform will play crucial roles in the wall crawler's success during deployment tasks. These advancements not only ensure precise application of the coating but also provide valuable data for monitoring the platform's operation and the structural integrity of the tunnel.

Furthermore, the development of a wall-climbing platform capable of operating on non-magnetic surfaces and equipped with a coating deployment mechanism has numerous applications beyond the H-Canyon tunnel. Such technology can be utilized in various industries for maintenance, inspection, and repair of large structures like bridges, dams, and high-rise buildings, where manual access is challenging or hazardous. The versatility and adaptability of this platform make it a valuable tool for extending the lifespan and safety of critical infrastructures, thereby contributing significantly to engineering and maintenance practices across multiple sectors.

Large EDF Drive Module Design Update

The initial design of the drive module for the large, 5-fan, wall crawling platform operated with 2-DOF allowing for more complex platform maneuvering along a surface. Initially, this proved to very helpful in positioning the platform chassis in an orientation that required less drive time and steps if done using a standard drive system. However, during operation on a vertical surface the servo motors were not able to minimize the associated angle deflection of the lower half of the module when countering the weight of the platform. The drive unit, pictured in Figure 7 below, consisted of a high torque servo for actuation of the second half of the drive unit at different angles. The lower half consisted of a DC motor which provided the means of moving the platform along a surface. The electronics required to operate the original drive module consisted of a motor controller, voltage regulators, a microcontroller and associated wiring for power delivery and communication.

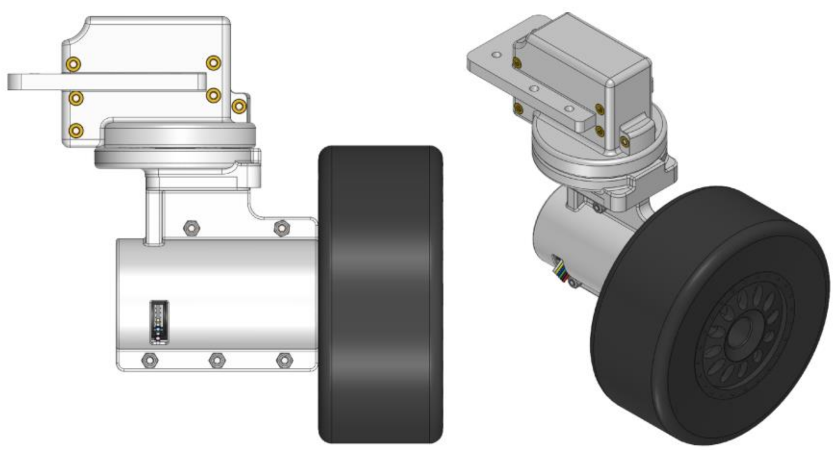

Figure 7. Original 2-DOF drive module for the large EDF platform.

In order to improve the overall performance of the drive module, the servo motor was removed, and the upper half of the drive module was made static. The new design, pictured in Figure 8 below, was achieved utilizing topological optimizing techniques along with completing an FEA study to minimize the deflection of the module while subjected the forces associated to the weight of the large wall crawling platform, thrust adhesion forces generated by the EDF units and traction forces while driving along a vertical surface. The redesigned drive module operates in 1-DOF and makes use a single high torque DC motor selected for this particular application. The associated electronic package has also been simplified as only a single voltage regulator and motor driver is required for operation.

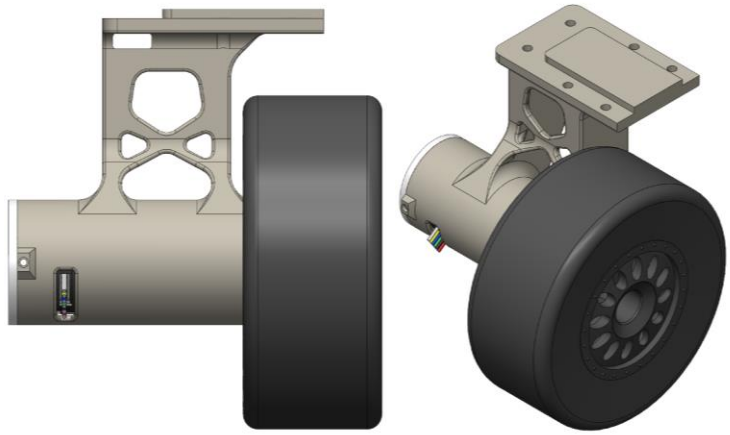

Figure 8. Redesigned drive module for the large EDF platform.

Load Cell Sensor Application

The semiautonomous capability of the dual-EDF wall crawling platform, where based on the orientation of the platform, the microcontroller on the platform will determine the required thrust that needs to be generated to create the adhesion forces necessary for climbing a vertical surface. Many successful tests have been completed using this model however, it is limited to the specific testbed that the data was collected from along with a regression function that was used to relate the pitch angle to accepted thrust value. In order to expand the operational use of this technology, a load cell, Figure 9, was integrated into the chassis of the dual-EDF platform, which would allow for real-time monitoring of the thrust force from the EDF units and also allow for the integration of a feedback control model improve the robustness of the semiautonomous capability of the platform when operating under varying environmental conditions.

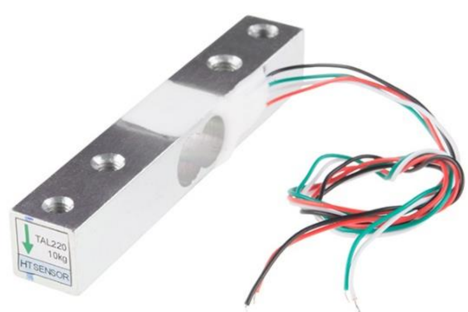

Figure 9. Load cell candidate integrated onto the chassis of the dual-EDF platform.

Each drive module, Figure 10, which will be directly attached to the chassis of the dual-EDF platform will make use of two load cells which will provide data reading for normal force experienced by each wheel during the operational testing of the platform. Special design considerations were implemented onto the drive module in order to minimize deflection along the center brace as to not skew the load readings when subjected to a force as well.

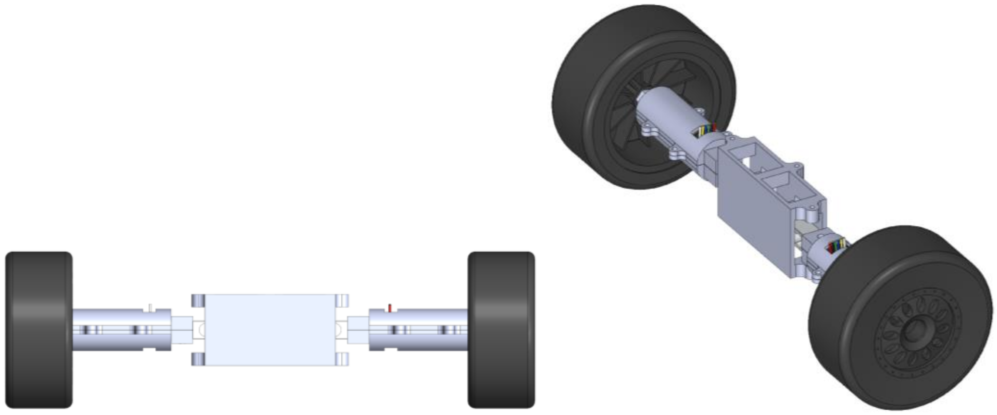

Figure 10. New load cell drive unit for dual-EDF platform.

Surface Transition Testing

Testing the transition capabilities of wall-crawling platforms from the ground to the wall and from the wall to the ceiling in a tunnel structure is crucial when deploying a wall coating mechanism. These transitions are complex maneuvers that challenge the platform's stability, adhesion, and control systems. By thoroughly testing these capabilities, we ensure that the platform can navigate seamlessly across different surfaces and orientations, which is essential for the uniform application of the protective coating. Successful transitions enable the platform to reach all areas of the tunnel, including hard-to-access spots, thereby enhancing the overall effectiveness of the coating process. Additionally, testing helps identify and mitigate potential issues related to mechanical stress and control algorithms during orientation changes, ultimately improving the platform's reliability and the safety of the deployment operation.

Subtask 18.3.1: Results and Discussion

Building upon these advancements, this results section presents the work completed on updating the design of the large-EDF platform to enhance its performance and reliability. We also detail the development and testing of a load cell drive module for the dual-EDF unit, which provides valuable data for monitoring the platform's operation and ensures precise application of the coating. Additionally, we analyze test data from the large-EDF unit during transition maneuvers from ground to vertical and vertical to upside-down orientations. These findings contribute to a comprehensive understanding of the platform's capabilities and the tunnel's structural integrity under various operational conditions.

Drive Module Testing and Evaluation

The base design of the original 2-DOF drive module was used as the foundation of new unit to propagate the existing design parameters for the chassis fitting. An extensive FEA study was completed on the base design to locate areas of concern which were then modified to minimize the associated deflection along the different axes. The completion of this FEA study was then followed with a topological optimizing procedure to remove material that did not directly contribute to the overall rigidity of the design while trying to maximize the strength characteristic of the design. The results of an FEA study and mass removal via topological optimization are depicted in Figure 11 below. The result was a drive module that weighed less than the original design with no motors installed, and a more user-friendly design for troubleshooting and installation.

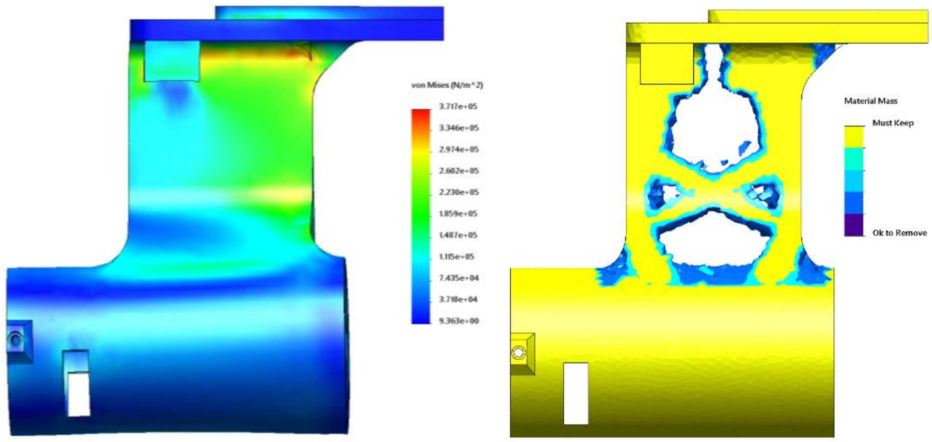

Figure 11. FEA study (left) and topological study (right) on the redesigned drive module.

The integration of the redesigned drive module onto the large wall crawling platform, Figure 12, was also made more straightforward with the redesign where the only connections needed for operation are the wires that are utilized for power and encoder readings.

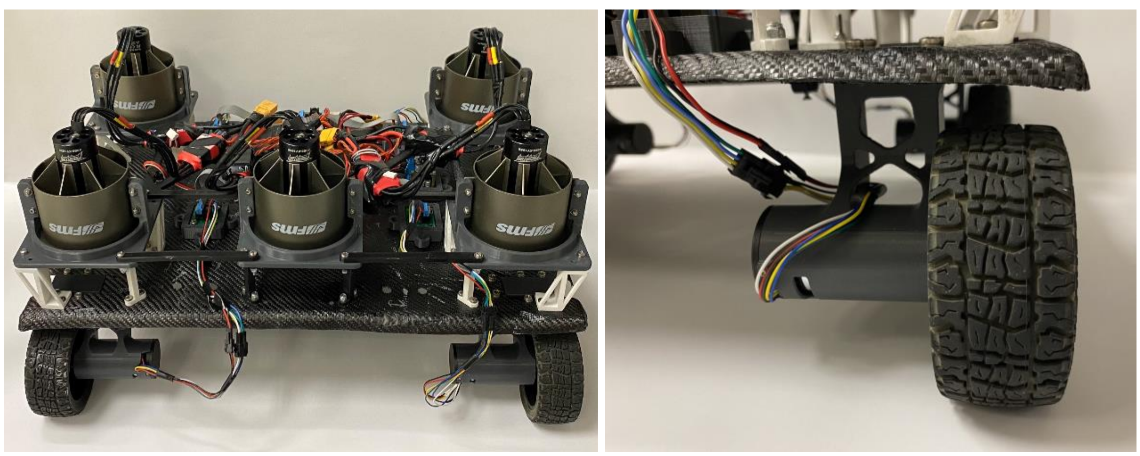

Figure 12. Integration and testing of redesigned drive module on large EDF platform.

Load Cell Integration and Testing

In this results section, we present the findings from our experiments aimed at evaluating the performance of the wall-crawling platform during critical transitions from the ground to the wall and from the wall to the ceiling within a tunnel structure. These tests were essential to assess the platform's stability, adhesion, and control systems when deploying a wall coating mechanism in complex environments. Additionally, we examined the effectiveness of the newly integrated load cell design in measuring the forces experienced by the platform's wheel at various pitch angles. The data collected, including load versus time and pitch angle versus time graphs, provide valuable insights into the platform's operational capabilities and the utility of the load cell in enhancing control and stability during transition maneuvers.

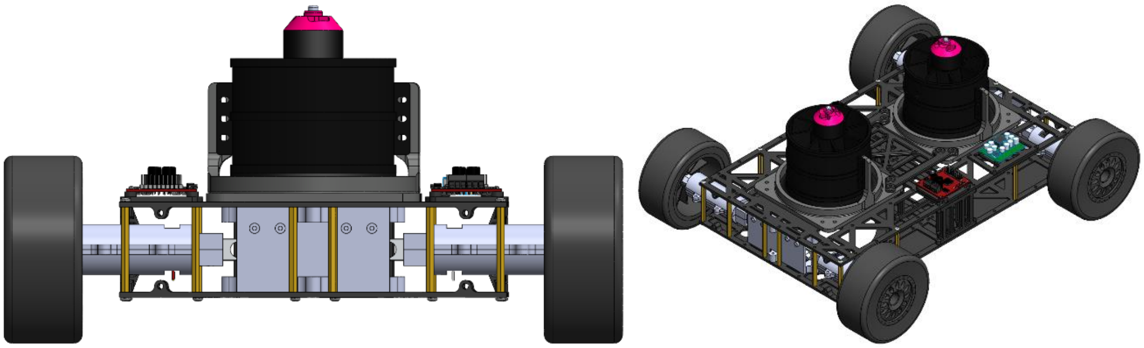

Figure 13. Integration of load cell sensor onto dual-EDF platform.

Testing the transition capabilities of wall-crawling platforms from the ground to the wall and from the wall to the ceiling in a tunnel structure is crucial when deploying a wall coating mechanism. These transitions are complex maneuvers that challenge the platform's stability, adhesion, and control systems. By thoroughly testing these capabilities, we ensure that the platform can navigate seamlessly across different surfaces and orientations, which is essential for the uniform application of the protective coating. Successful transitions enable the platform to reach all areas of the tunnel, including hard-to-access spots, thereby enhancing the overall effectiveness of the coating process. Additionally, testing helps identify and mitigate potential issues related to mechanical stress and control algorithms during orientation changes, ultimately improving the platform's reliability and the safety of the deployment operation.

Figure 14. Assembly of load cell drive unit (left) and testing on dual-EDF platform (right).

Graphs depicting load versus time and pitch angle versus time, Figure 15 below, from our experiments highlight the utility of the new load cell design on the wall-crawling platform. The load vs. time graph shows how the normal force on the wheel varies as the platform transitions through different pitch angles. As the pitch angle increases, the load cell data indicates a decrease in the normal force due to the changing gravitational components acting on the wheel. The pitch angle vs. time graph corresponds with these findings, illustrating the moments when the platform adjusts its orientation. These results demonstrate that the load cell effectively measures the forces experienced by the wheel in real-time, allowing for precise control adjustments. This capability is crucial for maintaining traction and stability during complex maneuvers, such as transitioning from the ground to the wall or from the wall to the ceiling. The data gathered validates the new design's effectiveness in enhancing the platform's performance during deployment tasks involving a wall coating mechanism.

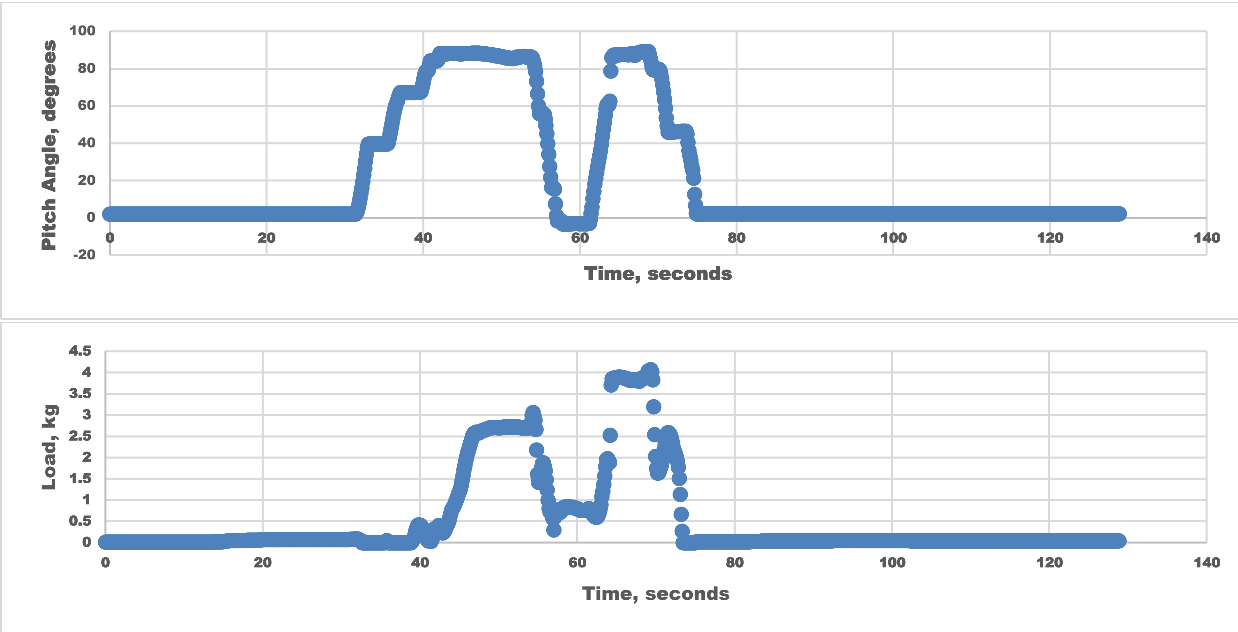

Figure 15. Graphs of pitch angle and associated adhesion thrust.

Surface Transition Improvement

Multiple transition tests were completed during this performance period in order to observe any areas of improvement during the transition process from either ground to vertical or vertical to upside-down. Initial tests began using the dual-EDF platform where the lessons learned from those experiments were translated to the large, 5-fan, wall crawling platform, Figure 16 below. During these tests, data related to the pitch, roll and yaw angles of the unit were collected along with the associated current draw from each of the EDF units on the large platform. Further analysis is needed to develop an accurate model representing the relationship between the mentioned parameters in order to improve the overall platform performance.

Figure 16. Transition testing of the large-EDF platform.

Subtask 18.3.1: Conclusions

In summary, the enhancements to the large-EDF platform—including the updated design and the integration of a redesigned load cell drive module—have significantly improved its performance and reliability. Finite Element Analysis (FEA) and topological optimization led to a lighter, more user-friendly drive module that is easier to integrate and operate. Experimental evaluations during critical transitions from ground to vertical and vertical to upside-down orientations demonstrated the platform's ability to maintain stability, adhesion, and control, which are essential for the uniform application of protective coatings in complex environments. The load cell data, depicting load versus time and pitch angle versus time, provided valuable insights into the forces experienced by the platform during transitions. These findings validate the effectiveness of the new design in enhancing control and stability. While further analysis is required to develop an accurate model of the relationships between the collected parameters, the results contribute to a comprehensive understanding of the platform's capabilities and lay the groundwork for future performance improvements.

Subtask 18.3.1: References

1. Gilliam, Bob J., Ray, J., and Giddings, B. "Inspection and assessment of the H-Canyon ventilation system at The Savannah River Site". Phoenix, Arizona, 2015. Waste Management Conference.
2. Staff Report, Defense nuclear facilities safety board. "H-Canyon exhaust tunnel fragility analysis input and assumptions". 2018.
3. Echeverria, M., Nunez Abreu, A., Lagos, L., McDaniel, D. "Aging of concrete for the evaluation of repair materials to protect the HCAEX tunnel at Savannah River". Waste Management 2020 Conference, Phoenix, AZ, March 2020. (Best Poster of Track). Paper # 20301
4. Telusma, M., Natividad, J., Lagos, L., McDaniel, D. “Development of an Omnidirectional Wall Crawling Mobile Platform, Designed to Aid in the Repair of H-Canyon’s Concrete Walls”. Waste Management 2021 Conference, Phoenix, AZ, March 2021.
5. Lattanzi, D., Miller, G. “Review of Robotic Infrastructure Inspection Systems”. Journal of Infrastructure Systems Vol. 23, Issue 3 (September 2017)

Subtask 18.3.2: Integration of the Coating Application System

Subtask 18.3.2: Methodology

An experimental study was conducted to assess the effectiveness of integrating a spray mechanism into the large five-fan Electric Ducted Fan (EDF) unit, enabling it to perform programmed routines for creating specific patterns. The wall-crawling platform was first tested on a horizontal surface to identify the optimal control parameters necessary for task execution. These parameters included the platform's speed, movement direction, coating material viscosity, and the setting time required for the coating before moving to the next section. After fine-tuning these controls, the platform was transitioned to a vertical surface. The chassis design incorporated a barrier section to prevent coating material from entering the EDF inlets located on top of the chassis, thereby safeguarding the internal components.

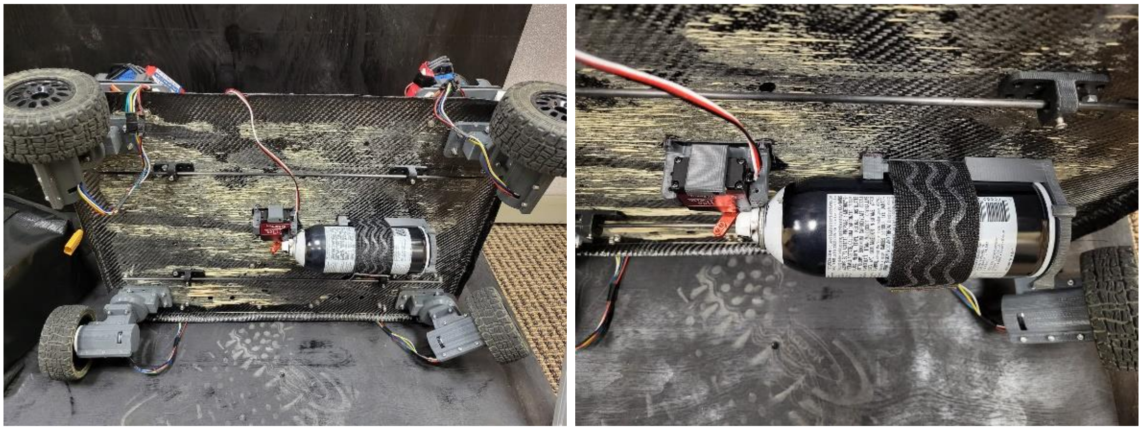

Figure 17. Spray mechanism for large wall crawler.

The platform was equipped with a redesigned spray mechanism, Figure 17 above, actuated by a servo motor with required actuation torque, aimed at generating patterns on a vertical surface. This redesign improved the actuation method to minimize misfiring of the spray can during testing procedures. The spray system was mounted on the underside of the large EDF platform, with the continued use of a four-inch clearance between the spray nozzle and the surface. Additionally, the redesigned mechanism has the capability to measure the reaction forces generated during spray tests, providing valuable data for optimizing the platform's stability and control.

Large-scale H-Canyon Mockup Model

A comprehensive CAD model of the large-scale SRNL H-Canyon tunnel mockup—which incorporates critical environmental factors such as temperature, humidity, wind speed, and concrete debris flow—the collection of experimental data regarding the effects of these conditions on tunnel performance will be the focus of this mockup build. The outside testing facility at ARC, Figure 18 below, will be used as the construction site for this mockup since it provides the team with stable foundation for construction and desired dimension layout for a section of the tunnel.

Figure 18. Outside testing facility and area of mockup construction.

Subtask 18.3.2: Results and Discussion

Multiple tests were conducted to enhance the spray capability of the large wall-crawling EDF platform while traversing vertical surfaces. The spray mechanism was redesigned to minimize misfiring of the spray can and to increase its robustness, leading to successful spray deployments during testing. The clear spray patterns observed indicate that the chassis barrier effectively allows the spray material to reach the surface with minimal interference from the EDF units. However, due to vibrations associated with thrust generation from the EDF units, excessive noise was introduced when gathering data on the reaction forces during spray tests. This noise hindered the accurate measurement of reaction forces. Despite this challenge, the results demonstrate that the redesigned spray mechanism significantly improves the platform's ability to apply coatings to vertical surfaces.

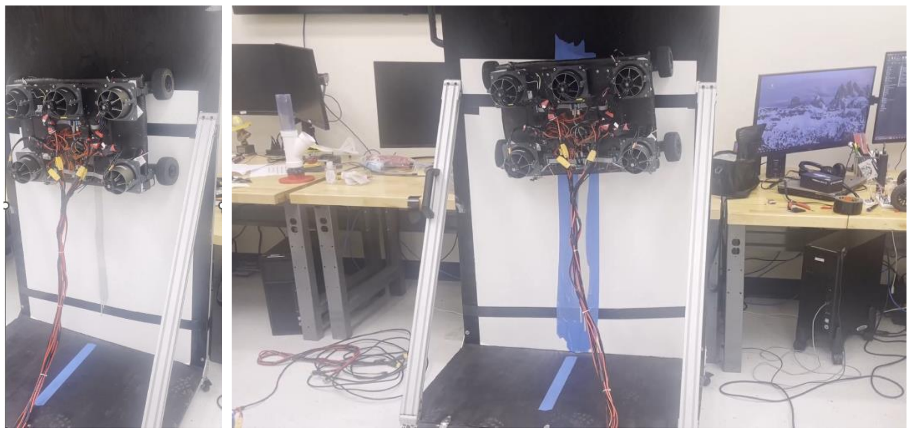

Figure 19. Successful spray deployment on vertical surface.

High-fidelity Mockup of H-Canyon Tunnel Section

The CAD model of the mockup for the SRNL H-Canyon tunnel has will provide accurate and full specifications for the construction of the mockup along with the installation of the required machinery, Figure 20 below. This model integrates crucial environmental factors such as temperature, humidity, wind speed, and concrete debris flow to simulate realistic conditions. To represent mechanical degradation observed inside the H-Cayon tunnel, the mockup includes concrete walls with exposed aggregate and rebar, closely mimicking the tunnel's aging state. Large fans are incorporated into the design to generate the necessary wind speeds for testing, enabling the study of debris flow and its impact on the structure. The mockup will include a concrete wall section with overhead section and insulation will be used to minimize temperature loss to external environment.

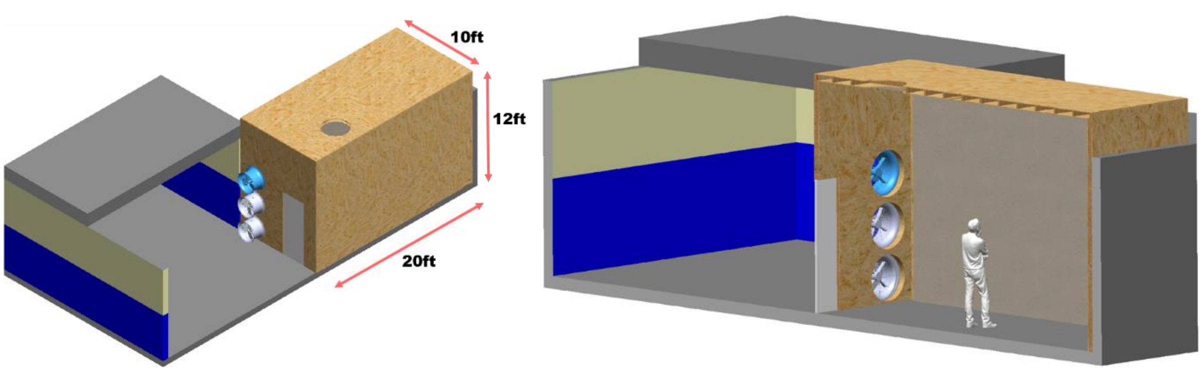

Figure 20. CAD layout for H-Canyon tunnel mockup.

Subtask 18.3.2: Conclusions

The large five-fan EDF platform, equipped with a redesigned spray mechanism, effectively deployed coatings onto vertical surfaces. The improved actuation minimized misfiring and measuring reaction forces enhanced platform stability and control. Mounted with a four-inch nozzle clearance, the spray system successfully created patterns. Using the comprehensive CAD model of the SRNL H-Canyon tunnel mockup—which incorporates environmental factors like temperature, humidity, wind speed, and concrete debris flow—we collected data on platform performance under various conditions. These results indicate that the enhanced spray mechanism and optimized controls improve coating effectiveness, advancing the platform's readiness for complex environments.

Subtask 18.3.2: References

- Telusma, M., Natividad, J., Lagos, L., McDaniel, D. *"Development of an Omnidirectional Wall Crawling Mobile Platform, Designed to Aid in the Repair of H-Canyon's Concrete Walls"*. Waste Management 2021 Conference, Phoenix, AZ, March 2021.

Subtask 18.4: Long-Term Surveillance of Nuclear Facilities and Repositories using Mobile Systems

Subtask 18.4: Introduction

Ongoing surveillance of nuclear facilities and repositories is essential for effectively managing and understanding radiological environmental impacts, guiding cleanup efforts, and meeting the quality assurance standards set by the U.S. Department of Energy. Advanced mobile surveillance systems offer a safe, efficient, and cost-effective solution for monitoring these sites. By employing state-of-the-art instrumentation, these systems reduce radiation exposure risks for workers while addressing the challenges posed by the large size of facilities, the high cost of radiation sensors, and the nature of radiological sources. Mobile systems also enable frequent periodic surveillance, delivering continuous radiation measurements while integrating data from multiple embedded sensors. This capability supports the long-term tracking of environmental changes, aiding in the assessment and documentation of facility conditions throughout operations, decommissioning, and final evaluation phases.

In continued collaboration with Washington River Protection Solutions site engineers, this subtask explored robotic platforms and advanced field-deployable sensory technologies for long-term monitoring of nuclear facilities to stakeholders that would benefit from the use of the proposed technologies.

Subtask 18.4: Objectives

This task's primary goal is to investigate assisted teleoperated, semi-autonomous, and fully autonomous off-the-shelf multi-use robotics technologies suitable for surveying nuclear facilities and repositories across the DOE complex. Our investigations focused on achieving the following objectives:

- Develop and deploy a platform agnostic sensor package coupled with a robust autonomous radiological and potentially emission gas survey framework to be deployed at Hanford's mobile platforms during the summer.

- Continue support in robotics of the research efforts in computer vision and machine learning applied to waste segregation on Project 3, Task 9, controlling a robotic manipulator.

Subtask 18.4: Methodology

Fully autonomous surveillance technologies are valuable tools for decision-making because they allow managers to consider numerous spatial data points and trends, leading to more optimal and safer decisions based on updated, abundant, and reliable information. Mobile platforms hold significant potential in automating data collection, offering the comprehensive quality data often required for Artificial Intelligence and Big Data systems. These statistical learning tools are sensitive to random errors, abnormal events, and inadequate or insufficient data, where potential human errors can compromise the accuracy and performance of trained systems. Automated data collection strategies thus play a crucial role in successfully deploying modern technologies driven by Machine Learning.

Conventional surveying methods of taking radiation measurements by hand within or around containment areas and analyzing the collected data to obtain results are ineffective and have exposed scientists to unnecessary radiation risks. The Chief Technology Office (CTO) supports Hanford's cleanup mission under the Department of Energy (DOE) Office of Environmental Management (EM) by advancing technologies that enhance worker health, safety, and engineering efficiency across the site. A key focus of the CTO's current work, as outlined in their Technology and Innovation Roadmap (TEDS MTW-79), is reducing the need for personnel to enter hazardous environments, particularly within the Hanford tank farms, where exposure to vapor-related data and radiation presents significant risks. To address these risks, the CTO is exploring and refining off-the-shelf robotic systems that can be deployed autonomously or semi-autonomously to collect data and monitor these environments. These platforms can perform routine inspections and rapid response operations, thereby improving worker safety and operational efficiency. The potential benefits include minimizing exposure to hazards in line with "As Low as Reasonably Achievable" (ALARA) principles, enhancing data reliability and consistency, and reducing costs for stakeholders by leveraging robotic solutions.

As shown in Figure 21, the retrieval operations at Hanford's Tank Farm have led to frequent changes that require site engineers to manually reconfigure the surveillance mobile platform's mission plan, adding to the challenges of analyzing the captured data over time.

Figure 21. Hanford's Tank Farm retrieval operations in September 2016 (left) and 2018 (right).

The methodology for this task expands on existing autonomous navigation frameworks by implementing a novel onboard information-driven planning and control system tailored to environmental and spatial surveillance of large-scale facilities. This expansion includes online adaptive planning algorithms [2] that consider not only navigation goals and battery constraints, but also sensing objectives such as increasing coverage to route the optimal path that would decrease the uncertainty in the overall radiation map and reduce geometric uncertainties in the mapped environment over time. Additionally, the framework will include basic terrain risk awareness and advanced perception capabilities, which are critical advancements for transitioning fully autonomous surveillance systems from controlled laboratory or mockup environments to real-world facilities and repositories.

The core areas of development of FIU's Mapping and Robust Localization Framework are:

1) Information-driven planning and control in radiological and hazardous environments,
2) Remote assisted teleoperation powered by terrain risk awareness in dynamic and unstructured environments, and
3) Advanced perception in complex environments.

Information-driven planning and control in radiological environments

The proposed framework leverages fully autonomous robots as intelligent agents to sense locations, dynamically determine the optimal sequence of measurements, and adjust radiation sensor acquisition parameters in real-time such as dwell time and surface proximity. This approach aims to enhance the accuracy of radiation mapping while addressing challenges associated with irregularly spaced data, noise, low count measurements, obstructions, and existing background radiation and other hazards.

Terrain risk awareness in dynamic and unstructured environments

The proposed framework incorporates a computer vision module supported by a semi-supervised machine learning system to classify terrain conditions. Surrounding video images captured by onboard cameras are processed to segment terrain features based on LiDAR data elevation. A convolutional neural network (CNN) is trained to identify surface types such as carpet, vinyl, water, and grass. For surfaces with low classification confidence, they are treated as obstacles to ensure safety. Unknown surface types can later be manually classified by an operator, integrating human oversight into the system.

This adaptive framework enhances terrain awareness over time, ensuring the safety of the platform in unexpected floor conditions. This capability is particularly crucial for unsupervised robots operating in outdoor repositories, especially after weather events, where terrain changes pose significant challenges.

Advanced perception in complex environments

The proposed framework uses several heterogeneous imaging sensors and gamma radiation detectors to construct an immersive environmental map, as illustrated by Figure 22. The framework stores high-resolution maps for digital twin reconstruction while maintaining reduced-order maps optimized for navigation and control. Additionally, it incorporates an innovative robust localization algorithm that fuses multiple odometry sources - specifically Iterative Closest Point (ICP), Inertial Measurement Units (IMUs), and visual odometry. This approach is particularly well-suited for monotonous environments like hallways and tunnels, where traditional localization methods may struggle to maintain accuracy.

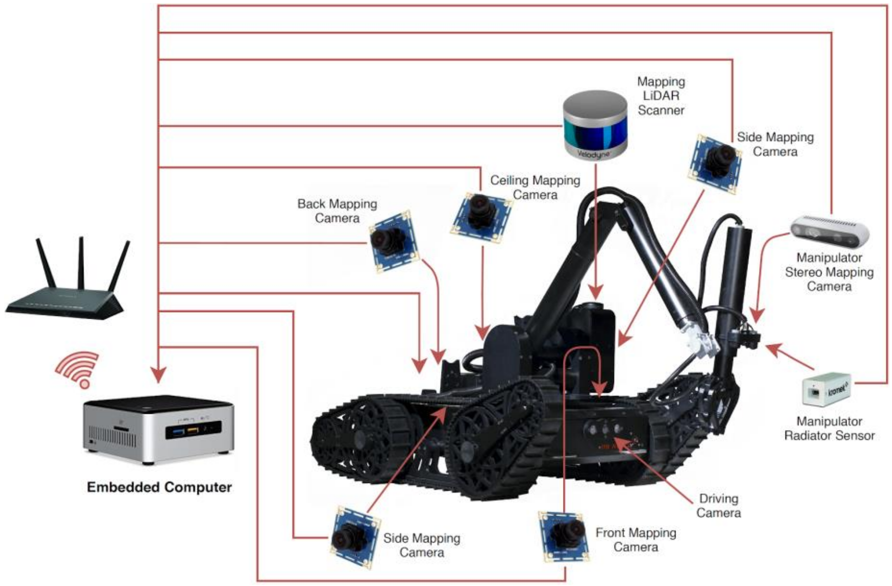

Figure 22. Mobile platform integration.

Figure 23 shows the ground mobile platforms that have been used in our in-house tests have been customized to include a variety of perception, gamma radiation, and ammonia sensors. These modifications enable the platforms to navigate nuclear facilities effectively and generate high-fidelity three-dimensional environmental maps.

Figure 23. FIU's mobile ground platforms.

Subtask 18.4: Results and Discussion

During this performance period, FIU enhanced its robotic capabilities by focusing on outdoor navigation in unstructured environments. This included implementing new behaviors and mapping strategies tailored for such complex scenarios. Formalized experiment trials were designed and conducted to validate results within the laboratory environment. These trials served to validate the improved navigation system's performance and adaptability to real-world challenges.

FIU also expanded its autonomous surveillance framework by integrating frontier-based navigation techniques to complement the existing system. The new approach utilized a 3D LiDAR sensor for high-fidelity spatial scanning and enhanced the robot's camera capabilities for real-time obstacle and landmark recognition. This included integrating visual data into the navigation framework, improving environmental understanding. A custom graphical user interface (GUI) was developed to facilitate robot operation and telemetry visualization. These advancements culminated in a second site deployment at Hanford's Cold Test Facility, where FIU showcased the technology's capabilities to site engineers and sought collaborative opportunities for continuous improvement.

Outdoor Navigation Testing

The autonomous navigation capabilities were improved via further tuning on the software side and testing in a real-world environment shown below in Figure 24.

Figure 24. Spot platform autonomously navigating an unstructured outdoor environment.

The changes involved included adding noise filters to try to address tall blades of grass being perceived as solid obstacles, adjustments to how the robot creates trajectories on a large and small scale and experimenting with different tolerances for buffer zones around objects. The testing enabled the robot to better utilize its flexible four-legged form factor and traverse uneven and highly unpredictable terrain.

Experimentation with Vision Output

To aid the robot in performing actions such as deploying its arm to take measurements, various strategies were implemented and tested such as using the robot's vision systems to derive possible sampling locations by filtering out excess and noisy information. An example is shown below in Figure 25 where the Spot robot is perceiving its surroundings, cropping a section in front of it, and breaking it down into manageable points to serve as measurement candidates.

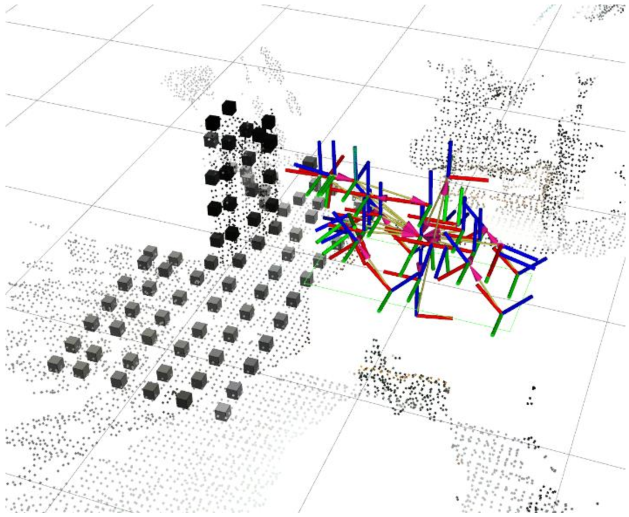

Figure 25. Visualization of Spot robot's joint locations and the perceived environment via its depth camera as well as filtered vision information.

These kinds of programs that clean up, combine, or transform information for the robot adds to its arsenal of tools to leverage for creating a robust mapping system.

Point Measuring using Bayesian Optimization

A form of optimization was integrated called Bayesian Optimization that creates a guess of the radiation map based on limited information and intelligently determines which points to measure next to gain the most amount of information about the map. Shown below in Figure 26, the robot can take measurements of an artificial radiation map generated by a mathematical function. The robot is operating in the real world and its location determines where on the map it will take a sample.

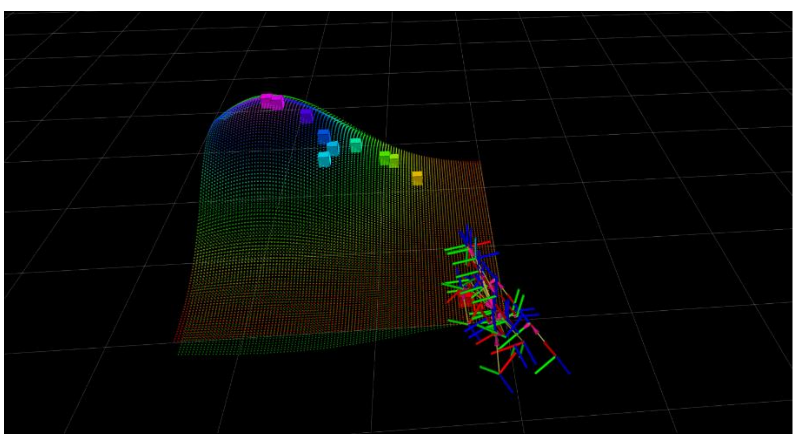

Figure 26. Visualization of an artificial radiation map and selected measurement points where the robot pseudo-sampled in the real-world.

New behaviors were modeled for the robot to achieve further robust mapping behavior with a combination of the platform's arm and body. The arm retracts when detecting too much sustained force from the environment, overcoming a challenge regarding the arm's inability to avoid obstacles during operation. It additionally reconfigures optimization parameters based on its history of arm retractions during its runs. The arm also returns to a safety position before moving on to measure a new point. Various behavior changes such as these were tested in the lab environment shown below in Figure 27**.**

Figure 27. Mapping environment with Cesium source in the ground and various obstacles crowding the region.

These tests with environments of various configurations having different degrees of difficulty for the robot has demonstrated an enhanced capacity for real-world operation in unstructured surroundings. Diverse types of obstacles were tested such as tubes that are free to roll on the ground when stepped on, traffic cones, and box shaped items of different heights. Further behavioral modifications were made based on these results to maximize the safety of the robot and reduce the chance of tripping.

Experiments

Finally, experiment trials were formalized and tested with a Cesium source after the integration of a radiation sensor, the Kromek GR1. Multiple radiation sensors were tested such as Kromek's Sigma50, and a USB-RAD121 Geiger Counter by Magnii Technologies. The use of the USB-RAD121 was deemed inadequate for our purposes and the Kromek sensors both are viable options. The trials controlled for the obstacle-rich and obstacle-free settings, as well as dynamic and static options for optimization parameters. Shown in Figure 28 below is one such radiation map generated via Bayesian Optimization where a peak is visible where a small Cesium source was placed under an orange cap on the ground visible in the right-side photo.

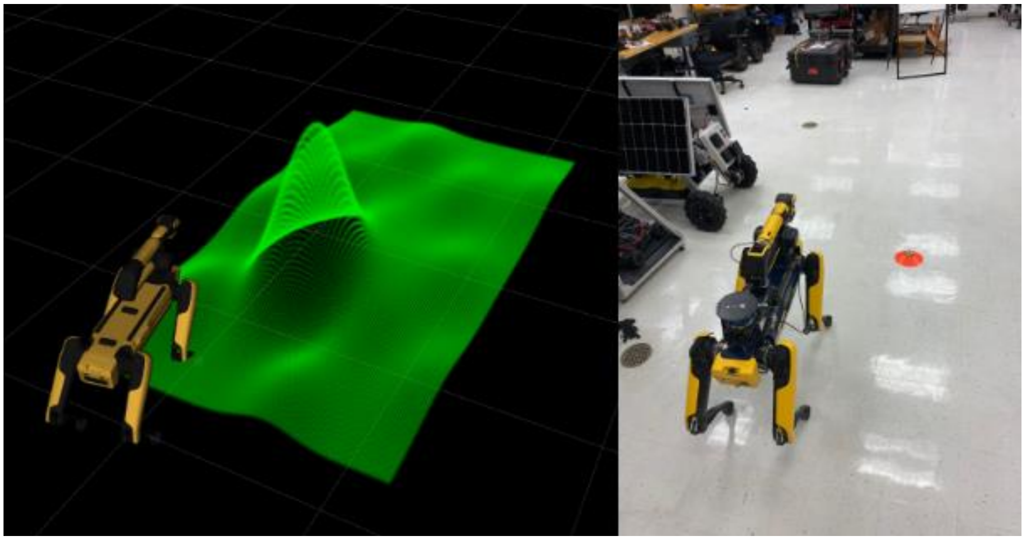

Figure 28. Visualization of robot and estimated radiation map (left) and real-world view of mapped environment including Cesium source location (right).

The experiment validates the custom behaviors that were modeled and the software pipeline that was developed for making the radiation mapping operation possible. This sets the foundation for the team to deploy the robot into larger environments and test with other Spot robots to work collaboratively.

Frontier Exploration and Improved LiDAR Captures

The existing navigation framework was improved by implementing an algorithm that utilizes data from generated from the navigation stack developed in the previous year. The robot utilizes the ROS2 Navigation2 stack, which integrates costmaps and odometry data to enable semi-autonomous and fully autonomous exploration. Costmaps are generated from voxelized point clouds, where the environment is divided into three-dimensional grids (voxels) to represent obstacles and free space, which is shown in Figure 29, which is a spatial representation of a portion of the office building at CTF. In Figure 29, the dark blue spaces represent *free space* – any space in which the robot can move without obstruction, such as corridors and vacant rooms; the magenta space represents *occupied space* – areas in which the robot is unable to traverse, such as walls and large objects; lastly, the teal spaces represent *buffer space,* which is an indicator to the robot that it is approaching an *occupied space*, so that the robot can correct itself. This voxelization process allowed the robot to assess its surroundings and create detailed maps for safe navigation. In frontier-based navigation, the robot autonomously planned its trajectory based on these costmaps, simultaneously creating real-time 2D maps of its environment. In this performance period, the efforts in automation expanded on the previous work by testing both forms of navigation on real hardware rather than in simulation, with odometry powered through a fusion of an inertial measurement unit (IMU), the improved camera system, and a 3D LiDAR.

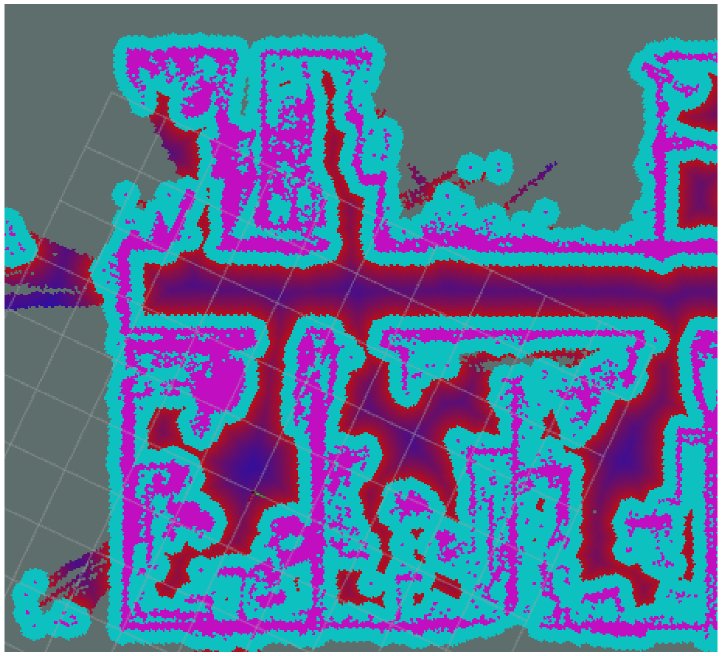

Figure 29. Partial costmap generated at a demonstration at Hanford CTF.

The costmaps generated in the previous figure are generated from a broader dataset from the 3D LiDAR, which was another point of improvement in this performance year. The LiDAR data is additionally stored in databases on the robot as it executes the frontier-based operations, and could be off-loaded for analysis, visualization, and post-processing. This iterative process, when repeated across multiple instances, contributes to the compilation of an evolving historical record of the facility that the robot has monitored. Figure 30 shows one of these databases during a series of frontier-based trials, in which several features, such as office cubicles and personnel working within the facility, can be noticed.

Figure 30. 3D LiDAR scan of the ARC Office Cubicle Space, at FIU Engineering Center (EC).

Custom Designed Graphical User Interface (GUI)

To address the challenges of initializing, driving, and monitoring the robot and its environment, one of the key efforts was to develop a custom graphical user interface (GUI). The user interface is a sophisticated real-time monitoring and control application designed for a robotics platform. The GUI, shown across Figure 31, Figure 32, and Figure 33, provides a graphical representation of data received from the robot via ROS2 topics, allowing operators to monitor and control the robot's operations efficiently. The main window of the interface is divided into several key sections, each serving a distinct purpose in providing real-time feedback and control over the robot's functions.

Menu Bar and Visualizers

At the top of the main window is the **Menu Bar (a)**, which includes essential functions like saving the current data state and exiting the program safely. Below the menu, the **Map Visualizer (b)** section displays the robot's perception of its environment. This feature updates dynamically with data from the `/map` ROS topic, reflecting changes as the robot navigates and explores its surroundings. The visualization is crucial for understanding the robot's location and the layout of the environment it is mapping. Additionally, a **Camera Visualizer (c)** allows the operator to see from the front-facing camera installed.

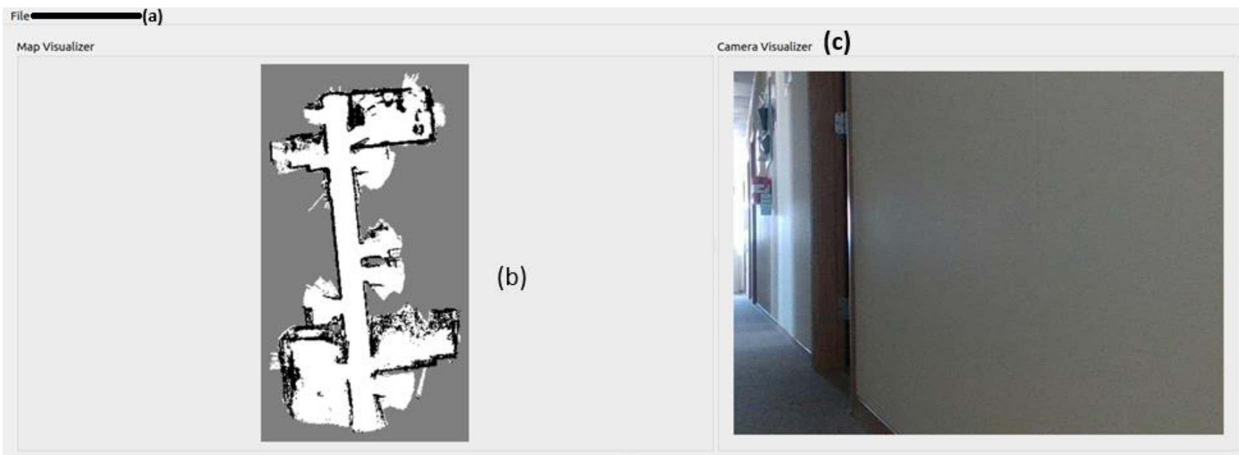

Figure 31. Menu bar (a), map (b), and camera visualizer (c) within the GUI.

Environmental Monitors

Adjacent to the Map Visualizer are the **Radiation Monitor (d)** and **Ammonia Monitor (e)** sections, placed side by side for a comprehensive view of environmental hazards. The Radiation Monitor displays a graph of radiation levels over time, showing counts per minute (CPM) and millirem per hour (mR/hr) data. This section updates in real-time based on the `/rad` ROS topic, allowing operators to monitor radiation exposure and its variations. Similarly, the Ammonia Monitor visualizes ammonia concentration levels detected by the robot, focusing on the primary value extracted from the `/ammonia_ocr` topic. A shared time slider is available for both monitors, enabling synchronized adjustments to view historical data trends over different time intervals, which helps in analyzing patterns and changes.

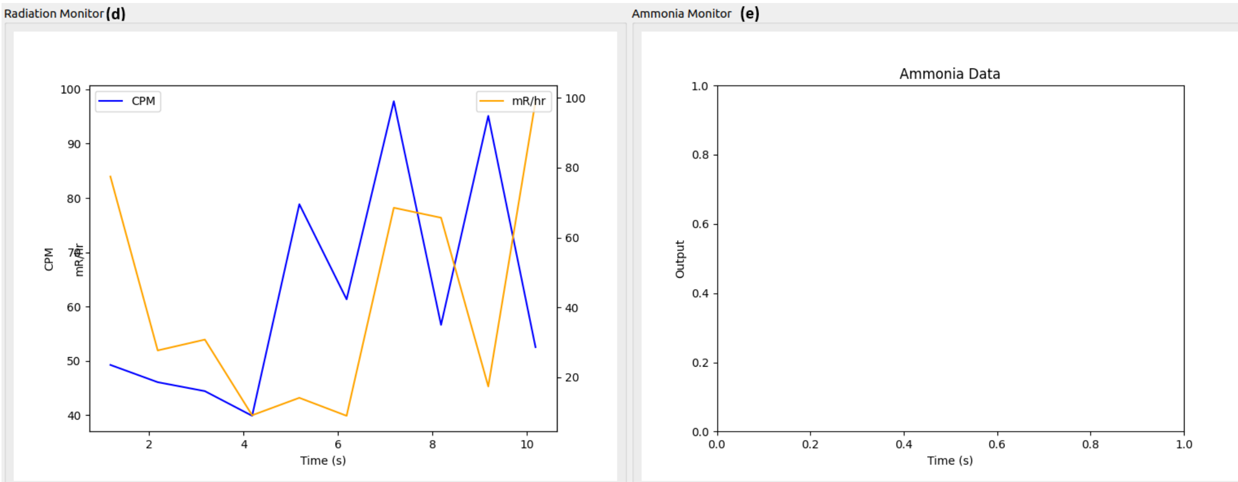

Figure 32. Environmental monitors for radiation (d) and ammonia (e) within the GUI.

Telemetry and Robot Controls

On the right side of the interface, the **Telemetry Display (f)** provides real-time feedback on the robot's movement and orientation. It includes information about linear and angular velocities along the X, Y, and Z axes, as well as translation and rotation data. This display also features an operation mode indicator that shows the current operational state of the robot, such as Teleop for manual control or Frontier for autonomous exploration. Accompanying the telemetry data are several control buttons: **Stop (g)**, **Teleop (h)**, and **Frontier (i)**. The Stop button immediately halts all robot operations in emergencies, while the Teleop button toggles manual control. The Frontier button is used to start or stop autonomous exploration, which is designed for mapping unknown areas.

Additionally, the user interface included a **3D Model Placeholder (j)**, intended for future integration with a 3D model visualization of the robot. Currently, it displays static text indicating its purpose, but is designed to eventually provide an interactive 3D representation based on the robot telemetry in **(e)**. Below the visual displays is a shared **time slider** for the Radiation and Ammonia Monitors, allowing users to adjust the time scale and explore data over different periods. This feature aids in comprehensively analyzing environmental conditions and how they evolve.

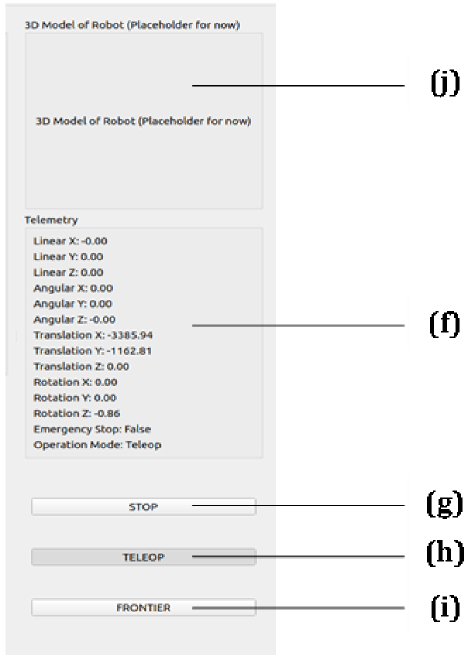

Figure 33. Teleoperation and telemetry features within the GUI.

Summer Deployment at Hanford

Finally, a portion of this task involved a deployment of the surveillance platform to the Hanford site to demonstrate the technology to relevant stakeholders. Although a large-scale demonstration was not conducted, consistent communication with stakeholders was maintained through regular presentations during staff meetings organized by the respective engineering groups. These presentations included both slideshows and live demonstrations of the current efforts. Following the demonstrations, discussions were held between the engineers developing the robotic platforms and the stakeholders. The goal of these discussions was to assess the robot's current state from the end-user’s perspective, gather feedback on the development, and identify potential improvements that would benefit the stakeholders.

One key point of discussion within IH was the challenges associated with fugitive emissions at the Hanford Site. Fugitive emissions refer to the unintended or irregular release of gases or vapors from pressurized equipment due to leaks and other unintended breaches. Currently, WRPS conducts fugitive emissions rounds as part of their ongoing efforts to monitor and manage these emissions. These rounds involve IH technicians performing daily checks on potential emission sources such as capped-off risers, passive breathers, and other penetrations that may leak gases.

Looking ahead, one of the potential applications of the LTS-UGV would address the challenges posed by the height difference between the robotic platforms used for monitoring and the actual emission points. Since the rounds often involve "sniffing" around a flange or similar structure, it's crucial that the robots are equipped or designed to reach the height of these emission points effectively. This may involve adapting the robot's design or developing attachments that can extend the sensor array to the necessary height. One such candidate for adapting the robot’s design is the Curtis-Wright "PackBot", shown in Figure 34 has been identified as a potential platform that could better accommodate the deployment of sensors like the Ventis Pro.

Figure 34. Curtis-Wright PackBot candidate robot for fugitive emissions detection.

Waste Segregation Task Support

The team also supported Project 3, Task 9, controlling a waste segregation robotic manipulator. The efforts mainly included the construction of a computer vision application and furthering our research in reinforcement and learning training methods for robot manipulators.

This performance period focused on training new DOE Fellows joining the project. The training program covered essential components of our in-house robotic framework, including manipulator fundamentals, machine learning principles, and computer vision techniques. Fellows also gained hands-on experience with the Robot Operating System (ROS2), which serves as the core software platform for our robotic implementation. The training combined theoretical concepts with practical implementation, ensuring Fellows could effectively contribute to the project's ongoing development while maintaining technical rigor.

Figure 35 illustrates detection efficacy test of the proposed computer vision framework in waste segregation applications. The system demonstrates robust capability in performing polygonal segmentation, effectively delineating object boundaries with high spatial precision. This boundary extraction methodology proves instrumental in generating the requisite spatial coordinates and geometric parameters that govern the manipulator's pick-and-place trajectories.

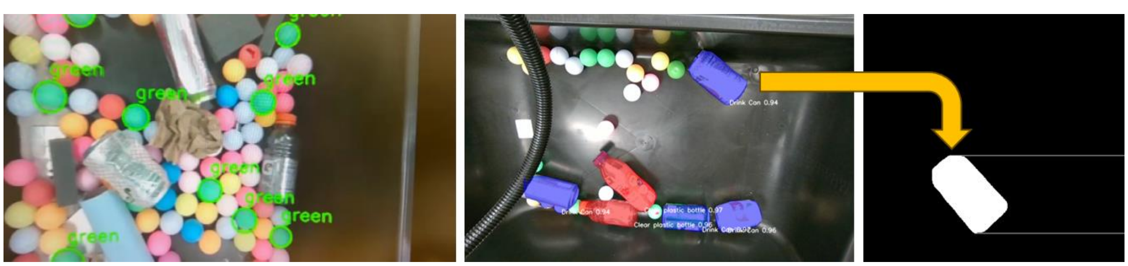

Figure 35. FIU's computer vision and object selection.

The implemented vision algorithm utilizes instance segmentation techniques to generate high-fidelity object masks, facilitating precise geometric interpretation of waste items within the manipulator's workspace. These masks, represented as polygonal approximations of object contours, provide critical topological information that enables the robotic system to execute manipulation strategies. The integration of this vision-based geometric reasoning enhances the system's capacity to perform autonomous waste segregation tasks with improved accuracy and reliability.

The preliminary validation of autonomous manipulation capabilities is illustrated in Figure 36, which demonstrates the system's pick-and-place operational sequences. The robotic end-effector is equipped with a pneumatic tool-changing device, enabling dynamic gripper selection based on waste material characteristics. This modular end-effector configuration facilitates adaptive grasping strategies through automated tool interchange, allowing the system to optimize its manipulation approach according to the physical properties and morphological features of the identified waste objects.

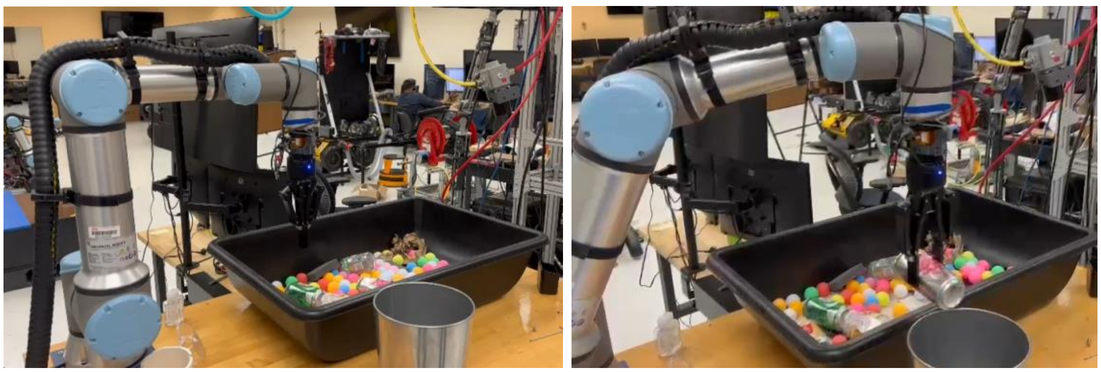

Figure 36. Waste sorting tests.

Figure 37 illustrates the implementation of this reconfigurable grasping system enhances the versatility of the waste sorting operation, enabling efficient handling of diverse material categories through appropriate end-of-arm tooling selection.

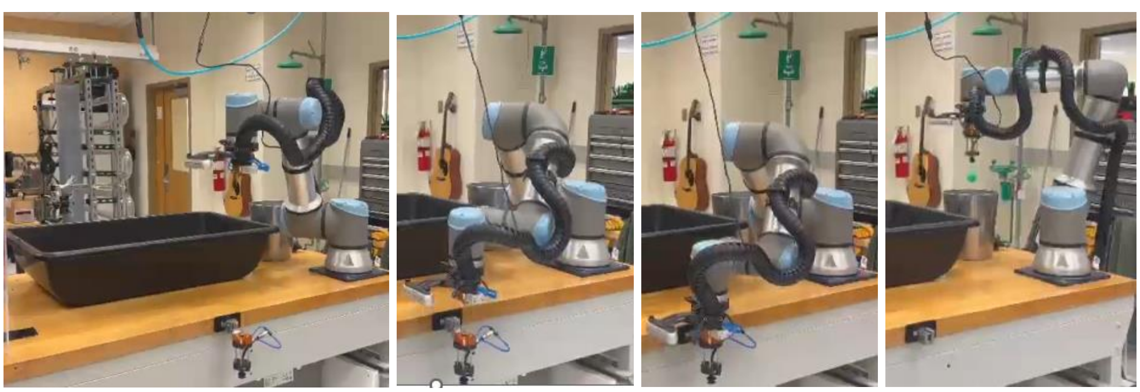

Figure 37. Manipulator gripper change.

The pneumatic tool changer provides rapid actuator interchange capabilities, minimizing operational downtime during gripper transitions while maintaining system reliability and manipulation precision

Testbed

Research efforts were invested in the development of a sorting mockup that more accurately simulates the conditions encountered in nuclear waste repacking operations, particularly focusing on drum-stored waste scenarios. The refined manipulator workspace, detailed in Figure 38, incorporates key environmental and spatial constraints representative of actual nuclear waste handling facilities. The upgraded testbed was specifically designed to replicate the geometric constraints, material arrangements, and operational challenges inherent in drum-stored waste manipulation tasks.

Figure 38. Nuclear waste repacking mockup.

The revised mockup configuration enables the validation of robotic manipulation strategies under conditions that closely approximate real-world nuclear waste handling scenarios, including representative drum geometries, waste object distributions, and spatial accessibility constraints. This enhanced experimental setup facilitates more rigorous testing of the system's capabilities while maintaining compliance with relevant safety and operational protocols typical of nuclear waste handling environments.

Subtask 18.4: Conclusions

This performance period, the team achieved significant progress in both autonomous surveillance and waste segregation capabilities. The surveillance platform showed enhanced performance in outdoor navigation through improved filtering algorithms and behavioral adaptations, successfully managing unstructured environments and varying terrain conditions. The integration of Bayesian Optimization for radiation mapping proved effective, as validated through formal laboratory trials using various radiation sensors, notably the Kromek GR1.

Key achievements include:

- Development of robust outdoor navigation capabilities with noise filtering and trajectory optimization.
- Implementation of frontier-based exploration with improved LiDAR integration.
- Creation of a comprehensive GUI for real-time monitoring and control.
- Successful deployment and demonstration at Hanford's Cold Test Facility.
- Advancement in waste segregation technologies through computer vision and adaptive gripping systems.

The waste segregation system demonstrated effective object detection and manipulation capabilities through polygonal segmentation and a reconfigurable pneumatic tool-changing system. The development of an enhanced mockup facility provides a more realistic testing environment for nuclear waste handling operations, enabling more rigorous validation of the robotic systems under representative conditions.

These developments lay a strong foundation for future work in autonomous radiation surveillance and waste handling operations, with potential applications in fugitive emissions detection and other nuclear facility maintenance tasks. The successful integration of new DOE Fellows and the continued collaboration with site stakeholders ensure sustained progress in these critical areas.

In Summer 2025, the long-term surveillance platforms will be sent for a third redeployment at Hanford with a specific focus on two tasks:

1) using the surveillance platform for assessing environmental conditions at "cold-and-dark" facilities deemed hazardous for entry and for generating a digital twin of the facility, and
2) potentially investigate automation for rapid/emergency response and routine monitoring of the Tank Farms.

Subtask 18.4: References

1. S. Ferrari and T. A. Wettergren. (2021). Information-Driven Planning and Control. The MIT Press.
2. C. Miskinis (2018, January). Combining digital twin simulations with virtual reality – what can we expect?. https://www.challenge.org/insights/virtual-reality-and-digital-twin
3. M. Berger, A. Tagliasacchi, L. Seversky, P. Alliez, G. Guennebaud, J. Levine, A. Sharf, C. Silva (2016). A Survey of Surface Reconstruction from Point Clouds. Computer Graphics Forum.

Subtask 18.5: Development of Robotic Systems for DOE Sites

Subtask 18.5: Introduction

Hanford's site scientists and engineers are constantly evaluating innovative technologies to alleviate the operational issues related to inspecting and sampling aging single-shell and double-shell tanks containing highly radioactive nuclear waste. In close collaboration with WRPS, the Applied Robotics Laboratory at FIU has developed and deployed specialized inspection tools tailored to Hanford's needs.

FIU's magnetic rover was successfully deployed at the Hanford tank farm, inspecting the AP-105 double-shell tank. WRPS's site personnel successfully operated the miniature inspection tool, navigating along the tank's inner liner walls from above ground to the tank's bottom floor, reaching the central plenum, and providing video feedback along the way. The miniature inspection tool's design incorporates several innovative features that are patent pending, from a flexible body tailored to overcoming oblique weld seams to magnetics wheel scups removing accumulated rust deposits. Figure 39 shows images of the tank farm deployment. WRPS technicians operated the rover through the riser located at grade and lowered it down via the deployment tray. Upon being lowered to the appropriate length, the rover traversed down the tank wall in the annulus and entered the refractory air slot. Upon the successful inspection of the refractory slot, the rover returned to the deployment tray and was retrieved successfully.

Figure 39. FIU's miniature inspection rover deployment at AP-105 DST.

FIU has also developed a lateral gamma scanner to autonomously monitor leaks underneath Hanford's single-shell tanks. The tool is designed to scan existing lateral pipelines underneath the tanks running across the diameter, measuring changes in the gamma radiation baseline. The device uses a pneumatic peristaltic crawler synchronized with an automated cable reel, providing a viable option for leak detection, does not require operator supervision, and reduces operational burdens on site personnel. The tool was successfully demonstrated at WRPS's cold test facility last summer. In the summer of 2023, the LGS was redeployed at Hanford's Cold Test Facility. The effort was part of the WRPS's Engineering and the Chief Technology Officer partnership with FIU to develop a technology that can detect possible leaks under single-shell tanks. The deployment received positive feedback from site engineers for a potential 2024 deployment at Hanford's SST tank farm. **Error! Reference source not found.** illustrates details of FIU's deployment efforts featured on WRPS social media.

WRPS collaborates with FIU to design tool for detecting single-shell tank leaks

Engineering and the Chief Technology Office (CTO) are continuing their partnership with Florida International University (FIU) to develop technology that can detect possible leaks under single-shell tanks (SSTs).

The "Lateral Gamma Scanner" project is one of three summer internships currently being sponsored by WRPS. The crawler moves through existing horizontal pipes by using mechanical grabbers that push and pull it along the inside of the pipe, while sensors detect possible leaks by measuring gamma radiation from cesium-137.

Josue Estrada, a WRPS intern and Department of Energy (DOE) Fellow, is part of the team continuing work from last year. He was present to help lead a recent demonstration at the Cold Test Facility (CTF).

"This year, we've furthered development of the system in its reliability, operability, and maintenance," he explained.

The crawler's gripper module has undergone significant design improvements, enhancing the previous gripping force from approximately 20 pounds to 45 pounds per module. The upgrade will allow the tool to crawl through more debris with relative ease. The improvements also include strengthened wheel guides. The guides center the crawler module to minimize friction and potential debris accumulation during inspections.

"We also enhanced operability by adding a more user-friendly interface that shows a video feed of the crawler moving forward and allows the operator to pause and resume the operation with a touchscreen button on a display monitor," said Estrada.

The design team integrated a quick-disconnect attachment into the inspection tools and redesigned the crawler's modules, which previously had wires soldered in place around the crawler's central piston. The new modules have hollow centers that allow cables to be inserted or removed as needed without soldering.

The recent demonstration tested the improved device in front of several WRPS engineers.

"I am impressed by the exceptional talent and unwavering dedication displayed by the students of the DOE Fellowship program at FIU," said Doug Reid, a WRPS mechanical engineer who is Estrada's mentor in CTO. "As a proud corporate sponsor, I have witnessed the remarkable partnership between academia and industry. The students' intelligence, creativity, and technical prowess have benefitted WRPS. Their passion for learning and innovation is a true testament to their potential as future leaders in technology."

"We are honored to have collaborated with these talented individuals and remain committed to supporting their continued success," he added.

In the upcoming fall semester, the robotics team at FIU's Applied Research Center will begin the integration and testing of a preliminary gamma sensor into the crawler system. This development aims to deliver a prototype ready for tank deployment in 2024.

The "Lateral Gamma Scanner" crawler bot is lowered down the pipe and retracted using a reel and cable system.

DOE Fellow and WRPS intern Josue Estrada explains how the design team has improved the crawler bot's ability to navigate debris in pipes during a demonstration at CTF.

The new interface allows an operator to interact with the crawler's automation system more easily.

The crawler bot uses small, mechanical grippers to push and pull itself along the inside of a pipe.

Page 5

Figure 40. LGS deployment featured on Hanford social media.

FIU has also developed an off-riser sampler manipulator to support Hanford's tank retrieval operations. The system uses existing small diameter tank risers to cable deploy a dexterous teleoperated robotic manipulator coupled with multiple end-effector tooling to sample ample residual waste material in single-shell tanks. The idealized concept was successfully demonstrated at WRPS's Cold Test Facility last summer using an industrial robotic manipulator scooping simulant sand.

In collaboration with WRPS, the following subtasks will be continued in Year 4 to support FIU's current efforts in developing and deploying novel tools at Hanford tank farms to alleviate operational burdens on tank integrity assessments and residual waste removal. The developed devices can also be outfitted with additional sensors providing environmental information within SSTs and DSTs and essential details on tank floor health.

Subtask 18.5.1 – Incorporation of Sampling Capability to Miniature Rover

FIU will continue enhancing the miniature inspection tool's capabilities. The sampling system's hardware and software will be streamlined and exhaustively tested at FIU's full-scale sectional mockup, targeting a potential deployment at Hanford's Double-Shell Tanks during summer 2025.

Subtask 18.5.2 – Lateral Gamma Scanner Development and Support

FIU will continue supporting the lateral gamma scanner task, integrating radiation sensors into the existing crawler's mock payload modules, and aiming for deployment at Hanford's Single Shell Tank Farm. FIU will work with WRPS to identify a hot deployment of this technology during FIU Year 4.

Subtask 18.5.3 – Off-riser Sampler Development

FIU will continue to develop a compact mechanical manipulator equipped with appropriate end-effector tooling to sample 4-inch risers at Hanford's single-shell tanks. Commercially available industrial manipulators typically are too wide to fit through these small risers. The considered operational scenarios include scooping mud or chipping off hard specimens.

Subtask 18.5.4 – In-Situ 3D Printing Concrete Structures for Waste Containment

Note: The research conducted under this subtask is now being reported under Project 4 as a separate student research project under Task 2: DOE-EM Research Identification and Assignments.

Subtask 18.5: Objectives

This task aims to develop and deploy novel inspection and sampling tools for tank integrity assessments, removal, and storage of residual waste. FIU engineers and DOE Fellows will continue to work directly with site engineers to build, and test systems that can improve site personnel's operational efficiency and safety by:

- Streamlining, adding functionalities, and strengthening the multiple tools previously developed at FIU.
- Leveraging lessons learned from site personnel interactions and deployments.
- Deploying and demonstrating technologies at the Hanford and SRNL sites during the summer.

Subtask 18.5: Methodology

The approach taken to develop inspection tools for use at the Hanford Site has been to start with concepts that address the necessary issues and work with Hanford engineers to down-select from the ideas and focus on the concepts. Once a concept has been vetted, FIU engineers design and develop an initial prototype. Bench scale tests are then conducted to demonstrate the validity of the concepts and develop an understanding of where improvements are needed. After a prototype has been developed and determined to be functional, the system is tested in a mockup built at FIU. Typically, after testing in our mockups, improvements are made to address issues noted during the trials. Issues such as improved functionality and durability are discussed then. Once engineers at Hanford or SNRL are satisfied that the system meets the requirements, the units are taken to the DOE site to test in their Cold Test Facility or for deployment.

Subtask 18.5: Results and Discussion

The lessons learned from summer internship at Hanford, coupled with coordinated site demonstrations and deployments and WRPS engineers' feedback has been crucial in guiding the design improvement presented in FIU's developed technologies.

Subtask 18.5.1 – Incorporation of Sampling Capability to Miniature Rover

FIU continued enhancing the miniature inspection tool's capabilities. WRPS site engineers requested that FIU incorporate a sampling mechanism at the front of the rover to retrieve samples of deposit material along the bottom during routine inspections in Hanford's double-shell tanks.

Design Improvement

Figure 41 shows the miniature inspection rover deployed at Hanford to inspect the bottom of the AP-105 DST in 2022.

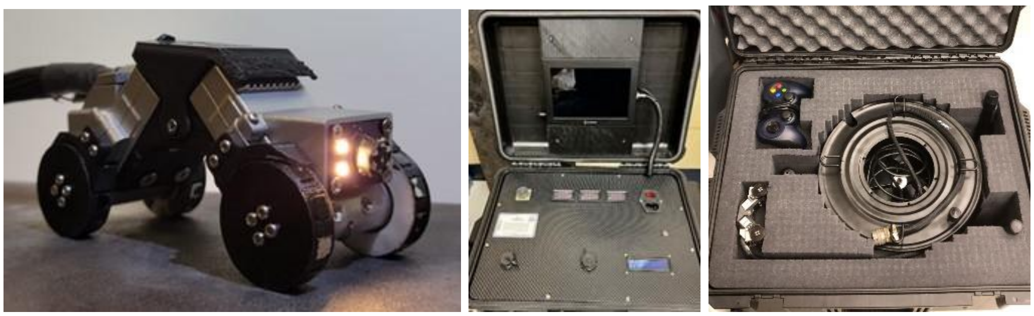

Figure 41. Deployed miniature inspection rover at AP-105 tank.

The miniature rover's embedded electronics were redesigned to accommodate the newly allotted space within the rover's chassis. With the newly allotted space came a redesign of the microcontroller layout to split functionality of the rover between a front and rear. The overall changes in the rover can be seen in Figure 42.

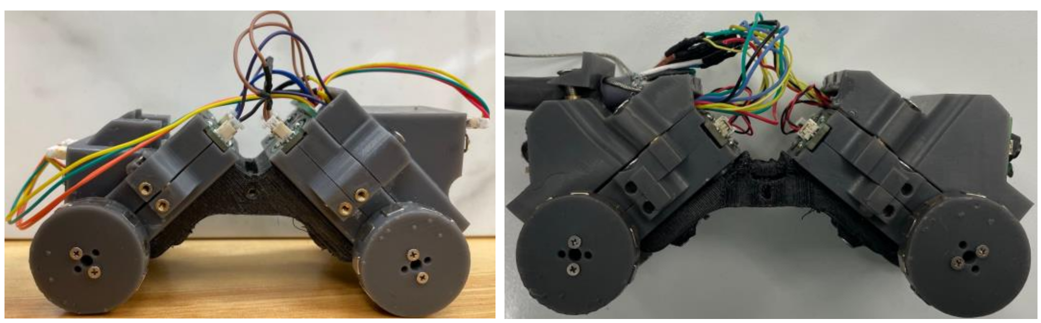

Figure 42 Previous single-PCB Miniature Rover (left) and new dual-PCB Miniature Rover (right).

The new board designed for the rover aimed to remove the clutter previously housed within the previous single-side design. This was especially sought after to better control the wires that had to crossover the flexible center of the rover. Now only a single set of wires crosses over. The current distribution of the rover is based on the prior systems that occupied the prior single board. This current iteration with the electronics exposed can be seen in Figure 43.

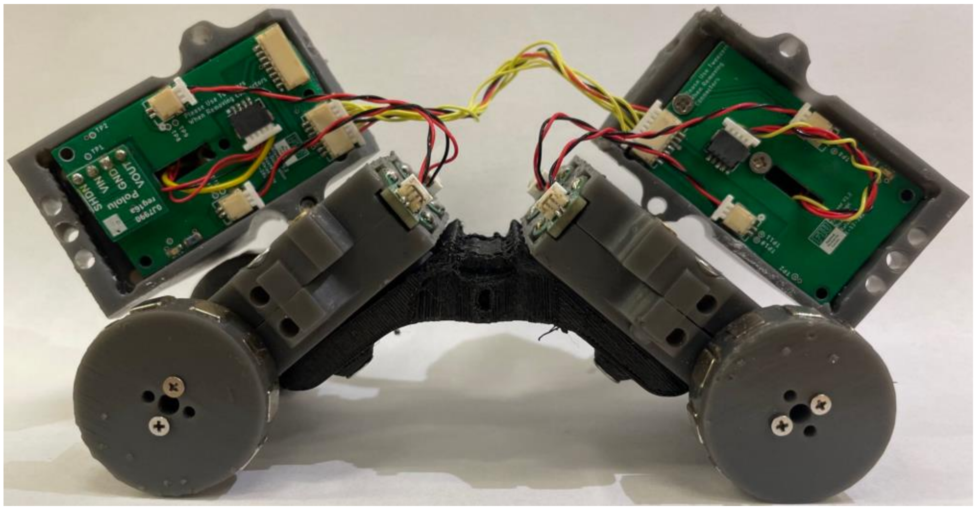

Figure 43. Dual-PCB rover internals.

Future systems for the miniature rover will take the space freed up for boards and incorporate an onboard logic processing microcontroller to more efficiently utilize the limited wires coming through the tether.

Except for the primary carrier boards board, the camera, motor, and control box boards remain functionally unchanged from the prior year. Minor revisions done to the camera and motor boards were the changing of the JST connectors from upright to right-angle configurations. This was done to repair an ongoing issue where connectors kept snapping off the boards. The right-angle configuration gave two additional anchor points. The camera boards had a minor change where the JST connections of the camera and distribution board are now placed on the back. This was done to better protect the camera cables from elements outside the rover.

A new board was designed to allow the quick connection of the tether from the miniature rover. The new board called the tether quick-connect board can be seen in Figure 44 and consists of a JST connector and exposed pads. The design behind this board is to facilitate connecting and disconnecting the tether from the rover. The prior system required the use of pliers to disconnect the tether. This system had the downside of placing tremendous strain on the brittle tether wires. This led to constant snapping on the tether connectors. Instead, the tether now has a header that contains a series of pogo-pin connectors. Upon connection, the pogo-pins are pressed against the exposed pads to send power and data. The redesigned tether connector can be seen in Figure 45.

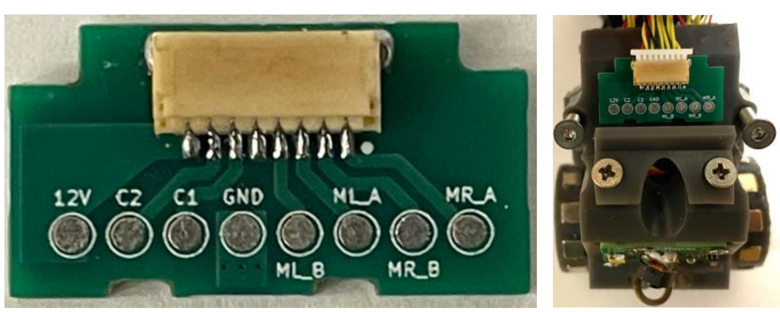

Figure 44. (Left) Tether quick-connect board and (Right) tether quick-connect attached to Miniature Rover.

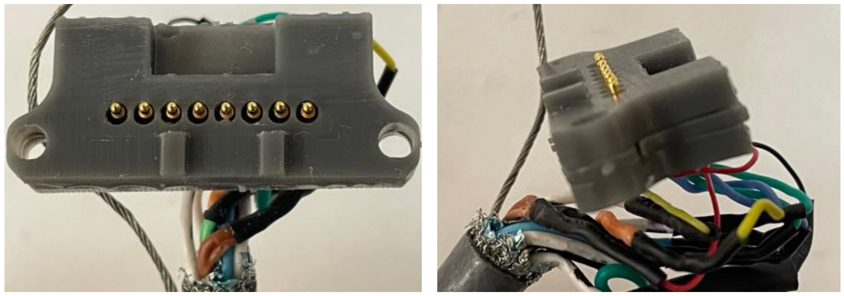

Figure 45. Redesigned tether end with Pogo-pins.

The current rover is still under redevelopment to better integrate the new tether connection. The current adapter as seen in Figure 46 was a proof of concept to test the viability of a connector and sought to be a fit-in replacement that required no modifications to the preexisting chassis.

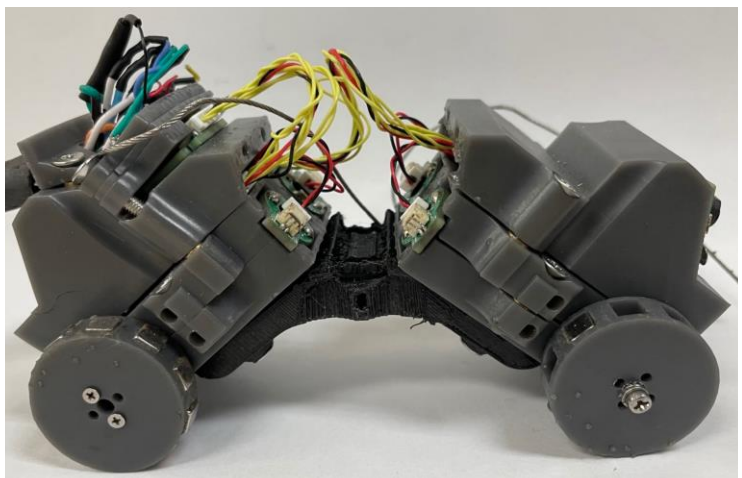

Figure 46. Assembled miniature rover with tether quick-connect.

The new rover incorporating the dual-PCB assembly and the quick connect tether were tested in November. These tests demonstrated that the current fit-in approach to the connector did not yield sustainable results under tension. The current design was found to place significant strain on the ethernet wires connected to the pogo pins. This led to constant wire snapping.

Work has commenced on designing a new microcontroller driver board to support the miniature rover's next-generation chassis. The microcontroller-driven rover aims to address limitations posed by the existing tether wire, which restricts the integration of a sampling mechanism. By replacing dedicated motor signal wires with onboard microcontroller commands, the new design simplifies signal transmission and enhances functionality.

The proposed microcontroller board will occupy the space currently used by the tether distribution board. In preparation for the dual-PCB rover chassis, an earlier version of this board was developed for the single-PCB rover, as shown in Figure 47. Although this initial design did not progress to manufacturing, its schematics will serve as a foundation for the dual-PCB microcontroller development.

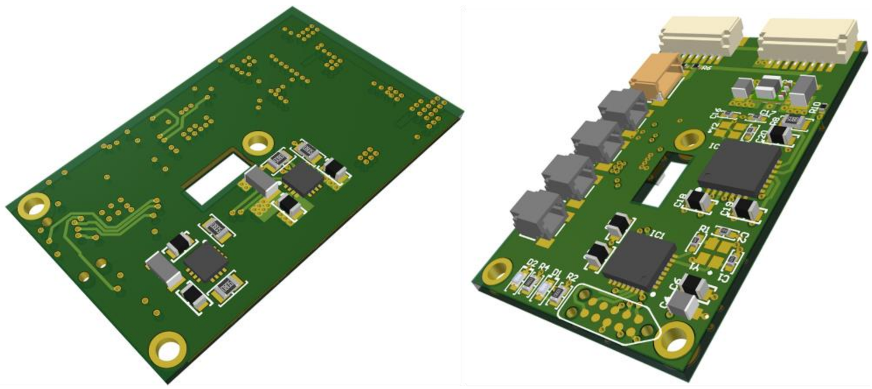

Figure 47. Single-PCB rover microcontroller board.

A significant change in transitioning from the single-board to the dual-board microcontroller variant is the individualization of each side of the rover. In this design, each side of the rover is equipped with its own microcontroller, connected via a shared CAN bus over the tether. This approach enhances error resilience and simplifies feature development. The block diagram in Figure 48 illustrates the planned layout for the interconnection of the boards in relation to the tether.

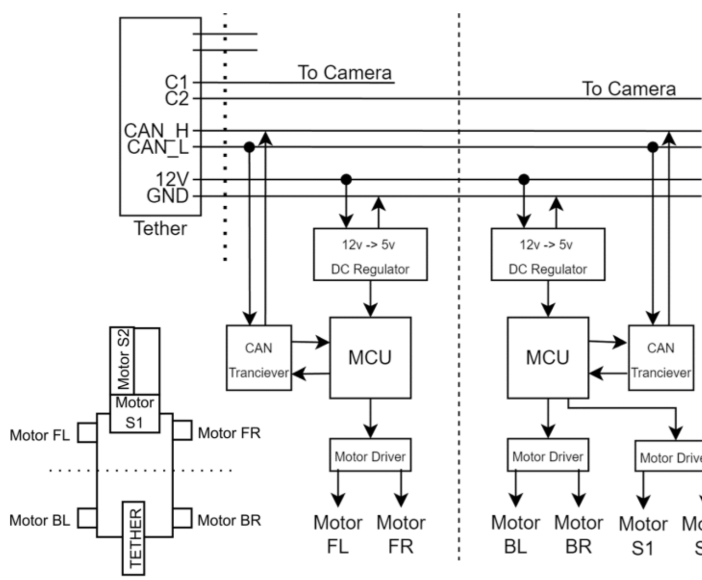

Figure 48. Dual-PCB rover control plan.

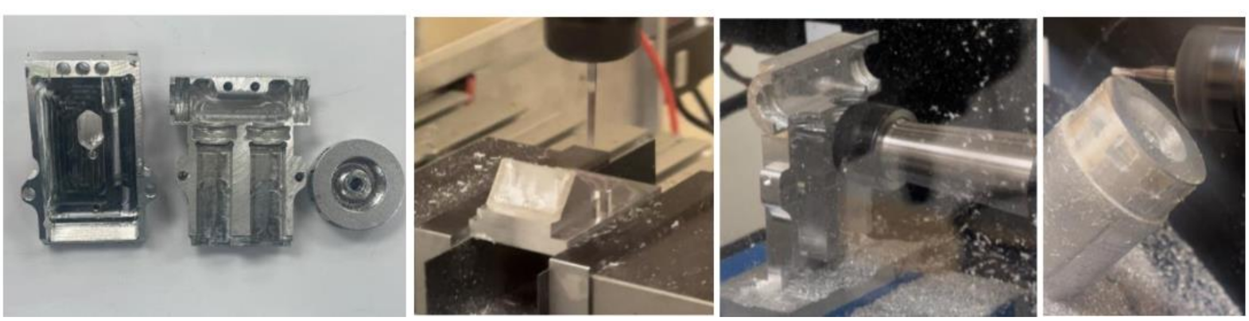

Figure 49. FIU in-house manufacturing of rover in AL 6061-T6.

With efforts to maximize the manufacturing capabilities of the robotics lab, various components were manufactured including: PCD housing, gearbox housing, and wheel. Shown in the Figure above, housing components being made on the CNC mill and 5-axis CNC.

Subtask 18.5.2 – Lateral Gamma Scanner Development and Support

FIU maintained the lateral gamma scanner system development, which has now achieved sufficient technological readiness for potential deployment at Hanford's SST farms. While the core technology is mature, the team made minor refinements to optimize the coordination between the crawler mechanism and the mechanized cable reel system during this reporting period.

Subtask 18.5.3 – Off-riser Sampler Development

The Off-Riser Sampler System (ORSS) underwent significant design upgrades in 2024, addressing limitations in existing waste sampling technologies. The ORSS integrates enhanced structural designs, transitioning to non-ferrous, corrosion-resistant materials such as AL6061-T6 aluminum and 304 stainless steels for robustness and durability. A novel multi-joint pneumatic manipulator was introduced, allowing wider operational ranges and increased mobility through pneumatic actuators that provide precise rotational motion and custom chain mechanisms for improved torque distribution. Modular end effectors, including augers, drills, air hammers, and scoops, were developed to facilitate diverse sampling operations. Additionally, a new control box was created with features like LCD displays for monitoring, emergency stop functions for safety, and modular electronics to ensure scalability.

During the fourth quarter of 2023, significant progress was made in refining the ORSS design. Testing of the motion carriage revealed design flaws when the joint failed at an 11-pound load. This identified weaknesses that informed subsequent improvements. In December, a major milestone was reached with the development of the rotational joint, a critical component of the pneumatic arm. This joint enables a fluid, multi-directional range of motion and was designed using advanced computer-aided design (CAD) software. Rigorous testing ensured the joint could withstand various stresses while maintaining smooth operation. Material selection focused on balancing strength, weight, and cost efficiency, resulting in a prototype that set the stage for full integration into the system. Additionally, a unique chain tensioner was developed during this period, featuring a dual-threaded rod mechanism for precise adjustments to chain tension. This innovation effectively prevents slack and slippage under variable loads, ensuring reliable operation.

During the first quarter of the year, the primary research and development efforts were dedicated to addressing the tension of the chain as shown in Figure 50. This new system uses threaded standoffs with jam nuts to secure them in place. After these modifications, the joint was able to successfully lift 45 pounds at a distance of 15.6” on the test mount. The chain tensioner was complemented by the design of an innovative sprocket chain clamp, which converts the linear motion of the pneumatic cylinder into rotational movement, simulating an elbow joint. This mechanism enhances the overall functionality of the pneumatic arm by ensuring smooth and consistent motion transfer. Alongside these mechanical innovations, the team devoted efforts to addressing stability challenges posed by the shifting center of gravity (COG) during arm movement. Two stabilization systems were explored: a tetrapod base for tank stabilization and a gyroscopic system similar to those used in maritime applications. While the tetrapod system provided initial insights, the gyroscopic approach showed greater promise in mitigating periodic motion caused by COG shifts.

From January to March 2024, efforts concentrated on refining the tetrapod stabilization system. A preliminary design was created to gauge its scale and functionality, followed by a scaled version incorporating carbon fiber rods for their lightness and rigidity. However, the design faced challenges, such as ensuring the system's compact profile to fit through a 4-inch riser and maintaining stability despite uneven tank terrain. Additionally, the legs needed to avoid interfering with the robot's workspace. While these issues posed significant hurdles, the insights gained gave the team confidence to manufacture parts for joints 2 and 3, culminating in a 3 Degree of Freedom (DoF) prototype.

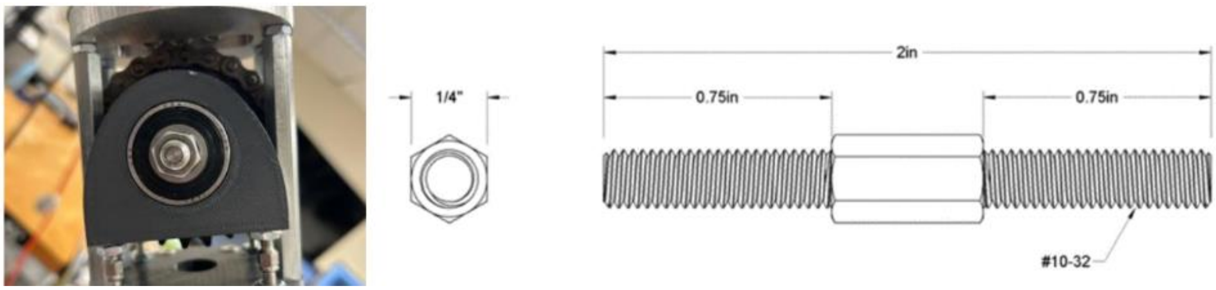

Figure 50. Standoff based tensioning system.

During the month of April, the focus was placed on meeting or exceeding the desired payload of 10 lbs. The prototype tests increase the pressure to the maximum for which the pneumatic solenoid valves are rated, illustrated in Figure 51

Figure 51. Payload testing

Simultaneously, illustrated by Figure 54, a new, machinable version of the arm was designed, shown in Figure 52, to be produced in aluminum using CNC and manual milling machine. This increased strength and reduced weight compared to the original prototype, which was constructed of 3D-printed plastic and stainless-steel hardware.

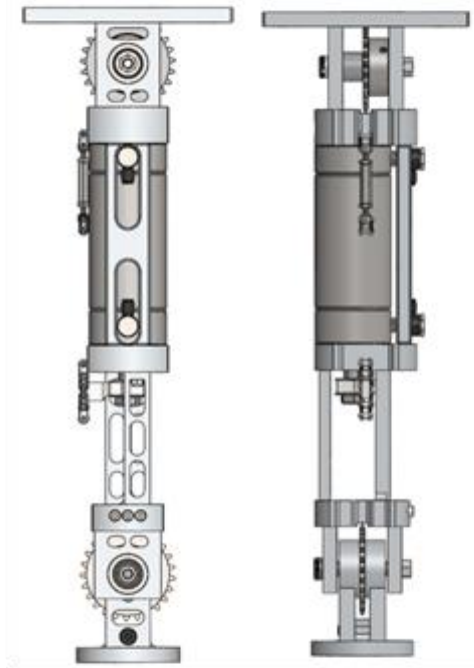

Figure 52. Front and side view joint of the Off-Riser Sampler System (ORSS).

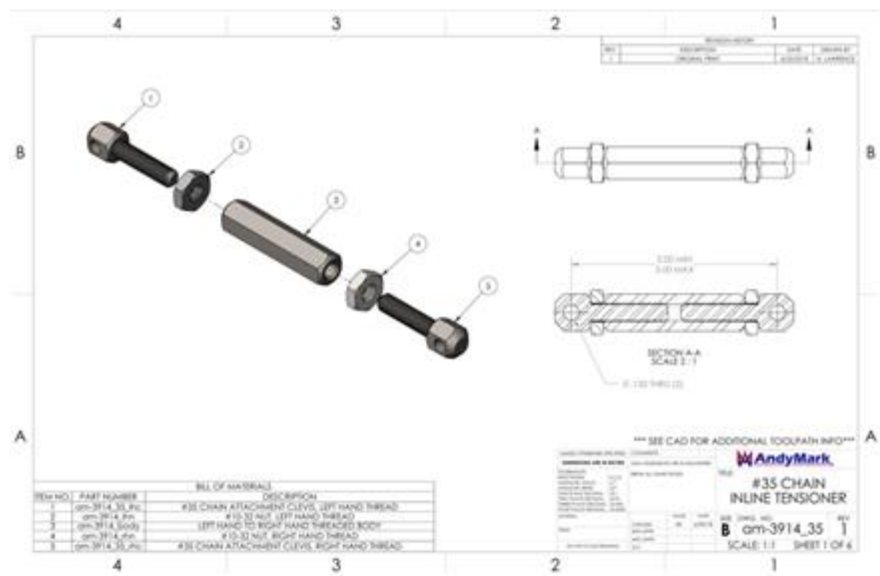

Figure 53. New #35 Chain inline tensioner.

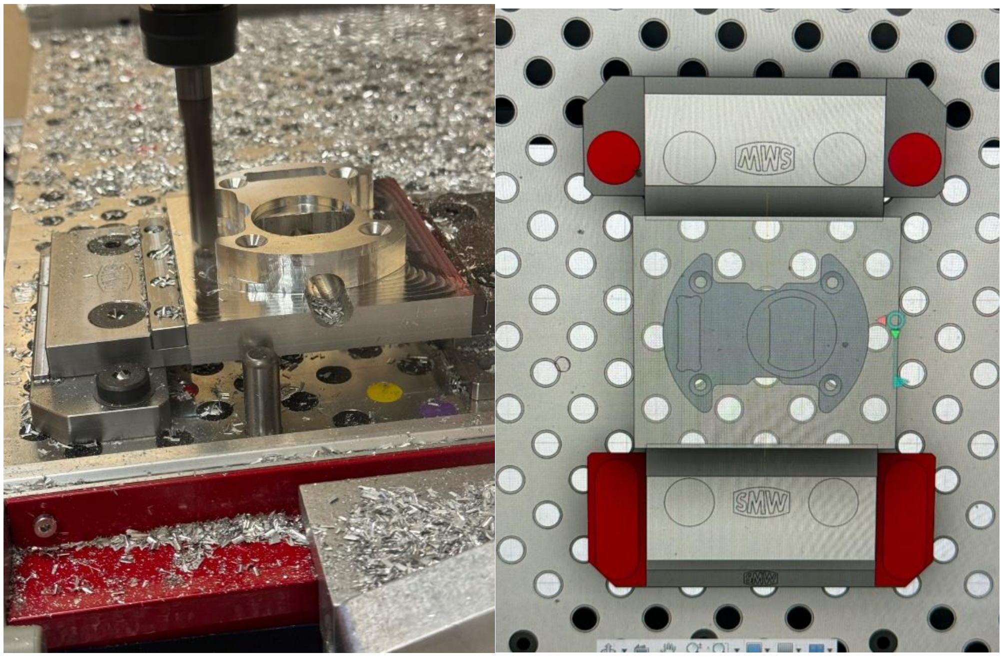

Figure 54. Machining components for off riser sampler at FIU.

This new design was machined and assembled in May, coinciding with DOE Fellow Theophile Pierre's internship at WRPS in Richland, Washington. Coordination with WRPS engineers led to plans for a technology demonstration at WRPS's Cold Test Facility (CTF). The robot and test stand were disassembled and prepared for shipping, along with necessary tools for reassembly. Upon arriving in Richland in late May, Fellow Pierre completed onboarding training and badging.

Figure 55. Shipment preparation for Hanford

Summer Development at Hanford

In June, work in Washington focused on streamlining the manipulator design and controls. A new end-of-arm tooling was developed to sample various waste consistencies in tank environments. The off-riser tank prototype was fully assembled at WRPS with a final demonstration date scheduled for July. These efforts refined the system's performance and positioned the ORSS for its next phase of evaluation and development.

Figure 56. New controls box developed at Hanford.

A major milestone was achieved during the July 16th demonstration at the Hanford Cold Test Facility. This event showcased the ORSS's capabilities to stakeholders, highlighting its performance and versatility. DOE Fellow Theophile Pierre played a key role during this period as part of his 10-week internship with WRPS in Richland, Washington. He focused on streamlining the manipulator design and controls and collaborated with WRPS stakeholders to create a list of requested tooling and end effectors, including drills, augers, and scoops. New tooling and a control box were developed to enhance safety and operational smoothness. Additionally, Pierre coordinated activities and prepared the robotic system for FIU's technology demonstration at WRPS's Cold Test Facility, completed successfully in July. The auger efficiently sampled loose sand without compaction, while the air hammer successfully fragmented dense concrete blocks, demonstrating its effectiveness on tough materials. The Venturi-based vacuum system maintained a clean operational environment by efficiently managing debris. Stakeholders expressed satisfaction with the system's proof-of-concept and showed interest in further development and deployment in future phases.

Figure 57. July 16th demonstration of pneumatic hammer on concrete block.

Figure 58. ORSS end effectors developed at Hanford.

Error! Reference source not found. illustrates details of FIU's deployment efforts featured on WRPS social media.

From coast to coast

WRPS & FIU partnership bolsters DOE workforce, advances Hanford cleanup

The summer arrival of four students from Miami-based Florida International University (FIU) highlights the continuing collaboration between WRPS, the university, and DOE's Office of Environmental Management. The partnership, formed through the DOE Fellows Program, seeks to grow and diversify the DOE workforce while furthering cleanup efforts at DOE sites across the country.

At Hanford, WRPS' Chief Technology Office (CTO) leads a collaborative effort to identify cleanup needs and opportunities for innovation at the Tank Farms. As needs are identified, FIU interns engage with stakeholders alongside their CTO mentors and manage their respective projects with the goal of providing innovative solutions in hazardous waste management and nuclear facility maintenance.

WRPS is sponsoring four FIU projects in 2024.

Theo Pierre is a graduate student pursing a master's in mechanical engineering. His project is the development of a pneumatic manipulator for off-riser tank waste sampling.

Current waste sampling operations rely primarily on collecting waste from the areas where waste sampling devices are deployed directly beneath risers. This project aims to improve the efficiency and effectiveness of sampling operations by advancing sampling manipulator technology to reach beyond those areas.

Pierre's off-riser sampler concept does that in perhaps the most literal kind of way — with a robotic "arm" that, once deployed through a riser, can be remotely controlled to reach up to five feet away. To accommodate different tank waste sampling conditions, the robotic arm is being developed to accept various attachments including a scooper, chisel, rake, and auger. Its enhanced design, precision control, and overall development were demonstrated at the Cold Test Facility (CTF) in July.

Pierre will continue developing various improvements based on the feedback he received during the demo. Additionally, he plans to finalize the control box and develop a solution for stabilizing the arm up to 50 feet deep.

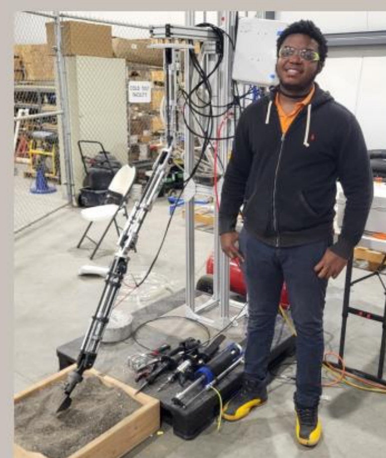

Figure 59. Off-riser sampler featured on Hanford social media.

In August, the Off-Riser Sampler was shipped back to FIU-ARC and unpackaged. Unfortunately, various components were damaged during transit and will need to be replaced prior to further development. This setback highlights the importance of robust packaging and careful handling during transportation to ensure the integrity of the system.

In September, the Off-Riser Sampler began undergoing repairs to address damage sustained during transit. Simultaneously, areas for potential improvement were identified and are being investigated. Research into control systems for pneumatics was also initiated, focusing on integration opportunities within the Off-Riser Sampler to enhance its performance and reliability.

In October, the Off-Riser Sampler was successfully reassembled and made operational again. Research on pneumatic control systems and potential integration opportunities continued, further advancing the system's capabilities and addressing areas for improvement identified in the previous months.

In November, research began on creating a control algorithm for the ORSS. A mathematical model of the pneumatic actuator was developed during this time, though further validation is required to ensure accuracy. These advancements mark a critical step toward achieving more precise and efficient system control.

Figure 60. KMag simulant.

In addition to the demonstration, extensive testing was conducted to evaluate the ORSS's performance under simulated tank conditions. These tests included handling materials such as concrete, loose sand, and potassium magnesium sulfate (KMAG). The auger and vacuum system excelled in handling sand and KMAG, demonstrating the system’s adaptability and efficiency. The air hammer proved its utility in tackling dense and resistant materials, showcasing the system's robustness. Iterative modifications improved the manipulator’s stability, with enhancements addressing joint flexibility and vibration dampening, ensuring optimal performance under varying loads.

Looking ahead, the development goals focus on several critical advancements. Stabilization enhancements, such as incorporating gyroscope and gimbal technology or applying crane theory, will improve the operational stability of the manipulator. Expanding the range of tools is another priority, with plans to develop an Automatic Tool Changer (ATC) for seamless switching and an increased library of end effectors to meet diverse operational needs. Further refinements to the Off-Riser Pneumatic Control System (ORPCS) will ensure precision and automation, streamlining the system's operation and enhancing its reliability.

The ORSS has demonstrated promising advancements in design and functionality, successfully addressing the challenges of hazardous waste sampling. The integration of innovative mechanical components, rigorous testing under realistic conditions, and stakeholder feedback have paved the way for further refinement. With continued development, collaboration, and validation, the ORSS is poised for deployment in operational environments, contributing to the mission of safe and efficient waste management. This year’s achievements mark a significant step forward, underscoring the potential of the ORSS as a cutting-edge solution for complex environmental challenges.

Subtask 18.5: Conclusions

The development and deployment of robotic systems for DOE sites demonstrated significant progress across multiple initiatives, with each system showing promise for addressing specific operational challenges at the Hanford Site.

The miniature inspection rover undergone substantial improvements in its electronic architecture, transitioning from a single-PCB to a dual-PCB design that offers better space utilization and enhanced functionality. Key developments include:

- Implementation of a new tether quick-connect system using pogo-pins, though further refinement is needed to address wire tension issues.
- Development of a microcontroller-driven design to overcome tether limitations and support sampling mechanism integration.
- Successful in-house manufacturing of critical components using AL 6061-T6 materials
- Planned redeployment at Hanford in 2025 with enhanced sampling capabilities

The Lateral Gamma Scanner reached a mature technological readiness level, positioning it for potential deployment in Hanford's SST farms. Recent achievements include:

- Successful second demonstration at Hanford's Cold Test Facility
- Refinement of coordination between the crawler mechanism and cable reel system
- Preparation for potential 2025 deployment at Hanford's tank farm
- Ongoing development of additional sensor integration capabilities as requested by WRPS

The Off-Riser Sampler System demonstrated significant advancement in its design and operational capabilities through:

- Successful development and testing of a novel multi-joint pneumatic manipulator
- Integration of diverse end-effector tooling including augers, drills, air hammers, and scoops
- Successful demonstration at WRPS's Cold Test Facility with positive stakeholder feedback
- Achievement of payload capacity exceeding 10 lbs
- Effective sampling of various materials including concrete, loose sand, and KMAG simulant

These developments represent significant progress toward addressing the operational challenges in nuclear waste management at Hanford site. The successful demonstrations and positive stakeholder feedback indicate that these technologies are advancing toward operational readiness, with clear pathways for future improvements and deployments.

Subtask 18.5: References

1. Randall, R. and Price, R. K., 2006, Gamma Surveys of the Single-Shell Tank Lateral for A and SX Tank Farms, CH2M Hill, RPP-RPT-27605, Rev. 0.
2. Engeman, J.K., Girardot, C.L., Harlow, D.G., Rosenkrance, C.L. , 2012, Tank 241-AY-102 Leak Assessment Report, Washington River Protection Solutions, RPP-ASMT-53793, Rev.
3. DOE (2018, November). Post-Retrieval Activities Changing Hanford Tank Farm Footprint. https://www.energy.gov/em/articles/post-retrieval-activities-changing-hanford-tank-farm-footprint

Subtask 18.6: Development of a Robotic Vacuum System

Subtask 18.6: Introduction

The Department of Energy’s Office of Environmental Management (EM) has a mission to clean up the contaminated soils, groundwater, buildings, and wastes generated over the past 60 years by the R&D and production of nuclear weapons. Hanford's site scientists and engineers are constantly evaluating innovative technologies to alleviate the operational issues related to inspecting and sampling aging single-shell and double-shell tanks containing highly radioactive nuclear waste. Since the primary linear failed in AY-102, there is significant concern regarding the health of other underground tanks at Hanford, prompting the need for developing specialized inspection tools that can assess the health of the primary liners in the Hanford Tanks. In close collaboration with Washington River Protection Solutions (WRPS), the Applied Robotics Laboratory at Florida International University (FIU) has developed and deployed specialized inspection tools tailored to Hanford's needs. FIU has been committed to conducting applied user-driven research and development to resolve technical problems associated with high-level radioactive waste (HLW) management: mobilization/retrieval, processing/immobilization, and final disposition.

Inspection of the double shell tanks (DST) (Figure 61) include ultrasonic testing of the primary tank walls as well as the secondary tank bottoms to test for wall thinning. The primary tank wall must be corrosion free before ultrasonic testing could be performed. The removal of this corrosion from the tank walls results in significant amounts of debris on the annulus floor. This debris interferes with efforts to perform ultrasonic testing on the secondary tank bottom. The annulus is an area surrounding the primary tank that is approximately 30” wide with four access points for tool deployment that range from 12” to 24” in diameter.

Subtask 18.6: Objectives

The objective of this research is to the development of a vacuum crawler system (VCS) that will be capable of cleaning the annulus floor and removing debris around the primary tanks. The VCS will meet the following major design requirements:

- All electrical components of the system will be NRTL (Nationally Recognized Testing Laboratory) certified.
- Will be capable of being deployed through a riser that is 24” in diameter or less.
- Will have forward and backward facing cameras.
- Capable of maneuvering around obstacles and operating within the width of the annulus.
- Will be remotely controlled with an umbilical cord that is capable of manually retrieving the robot in the event of a failure.

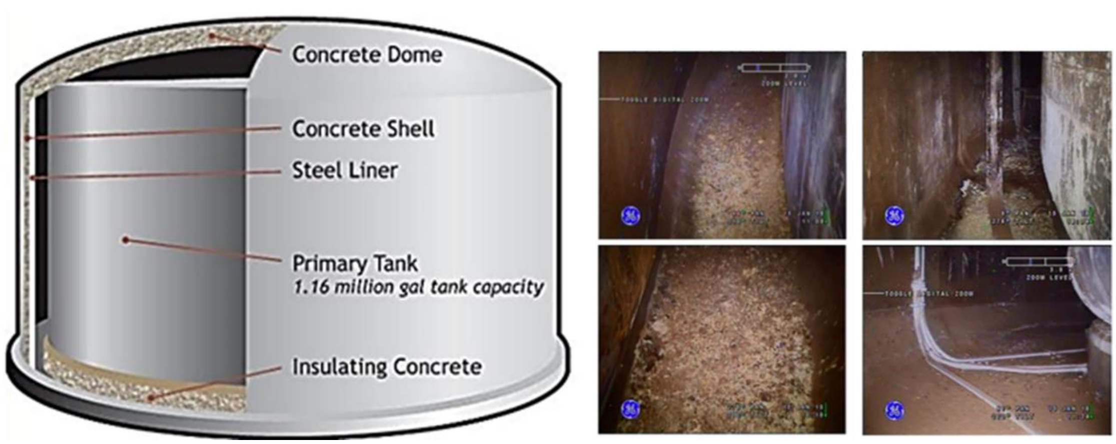

Figure 61. Double-shell tank.

This is just one of FIU ARC’s technology solutions to aid the engineering staff at the sites in autonomous inspection of their DSTs while mitigating risk and protecting worker health and safety. Successful completion of these activities will result in cost savings and risk minimization, which will lead to increased environmental safety in the management and disposal of the stored radioactive waste at the DOE sites.

Subtask 18.6: Methodology

Design of Robotic Platform

To accomplish this task, a robotic platform was designed that has the following features:

- 4-wheel drive with 4" diameter wheels to allow the robot to go over obstacles in the tank annulus such as electrical conduits.
- Pneumatically operated vacuum system with no moving parts to minimize points of failure.
- Forward and backward facing cameras.

After evaluating several vacuum motor designs, a pneumatic unit that has no moving parts was selected (Figure 62). Since this vacuum motor only needs a compressed air source to operate, it will make the robotic platform simple and reliable.

Figure 62. Pneumatic vacuum motor.

The ability to convey abrasive media was crucial to system success. The Line Vac's no-moving-parts design ensures reliability and maintenance-free operation, as demonstrated in Figure 20.

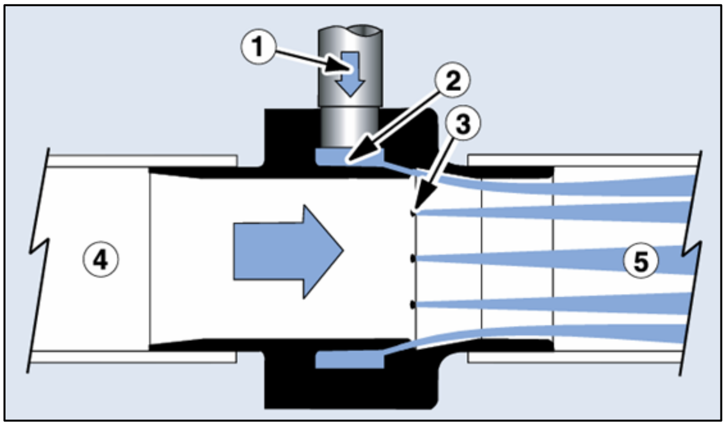

Figure 63. Pneumatic vacuum motor cross section.

(1) into an annular plenum chamber (2) It is then injected into the throat through directed nozzles (3), creating a vacuum at the intake (4), which draws in material and accelerates it through the unit (5) for conveyance over long vertical or horizontal distances.

A unit that uses ¾" hoses for vacuum as well as discharge was purchased and tested. Figure 64 shows the vacuum motor being used to vacuum damp dirt.

Figure 64. Vacuum motor test.

Even though the vacuum motor did successfully pick up the dirt, it was decided that a bigger motor would provide better vacuuming capability. A larger capacity motor was acquired and was tested. It was determined to have a better cleaning effect that the original one did on rock aggregate sizes recommended by WRPS personnel to simulate real-world conditions.

Once the preliminary design of the robotic platform (Figure 65) was finalized, the main platform components were ordering or fabricated. This included ordering the drive motors, motor controllers and wheels as well as 3D printing the frame of the robot.

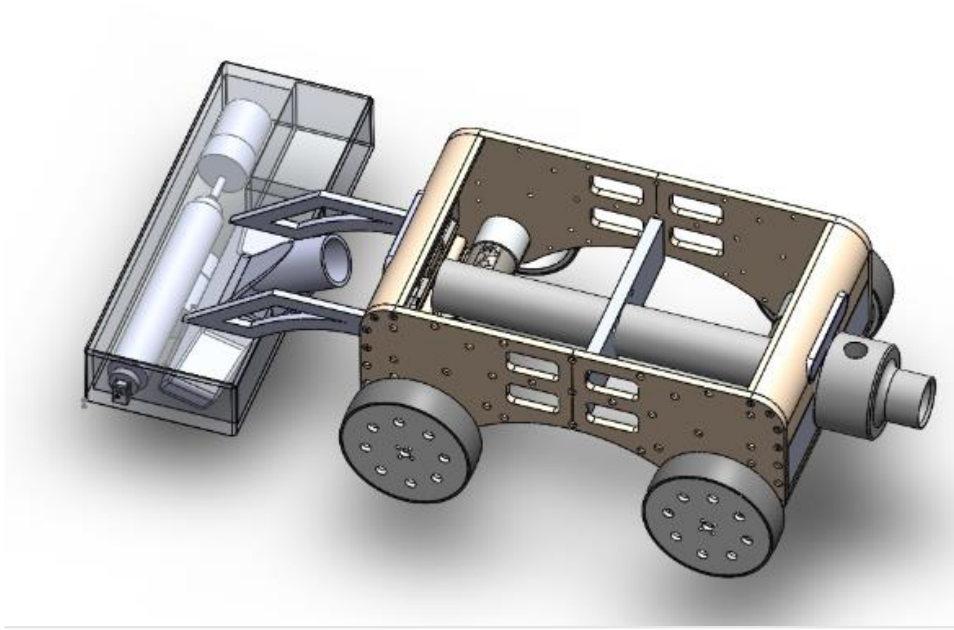

Figure 65. Preliminary VCS robotic platform design.

Options for the cleaning head design were researched, including turbo brush, DC powered brush, AC powered brush, and air nozzle. In addition, FIU evaluated different drive configurations such as direct drive, parallel drive, and right-angled drive (Figure 66). A basic vacuum nozzle was selected for the initial baseline testing.

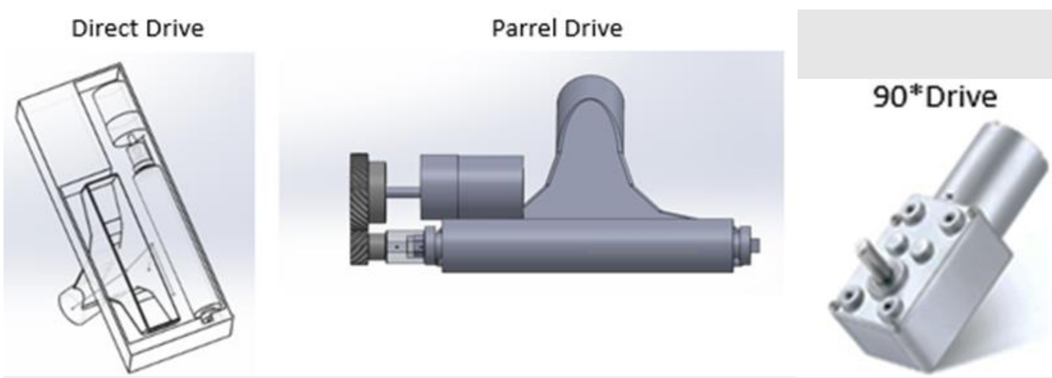

Figure 66. Different drive configurations evaluated.

System Fabrication

Once the designs of the major components were completed, fabrication of the robot commenced. The parts for the base robotic platform body were 3D printed and assembled. In addition, the motors and wheels were then installed on the platform body (Figure 67).

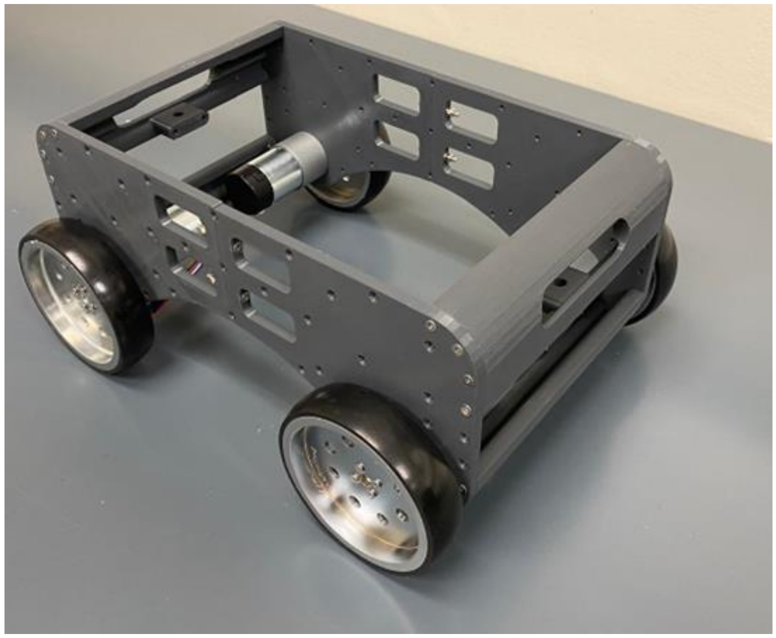

Figure 67. Base VCS robotic platform with motors and wheels.

Once the main components of the VCS were designed and fabricated, work began on the drive motor control circuit and fine-tuning of the encoders to regulate velocity control, and accuracy to ensuring precise motor movements (Figure 68). In addition, a joystick control of all four motors was integrated into the system to enhancing user interface and system operation.

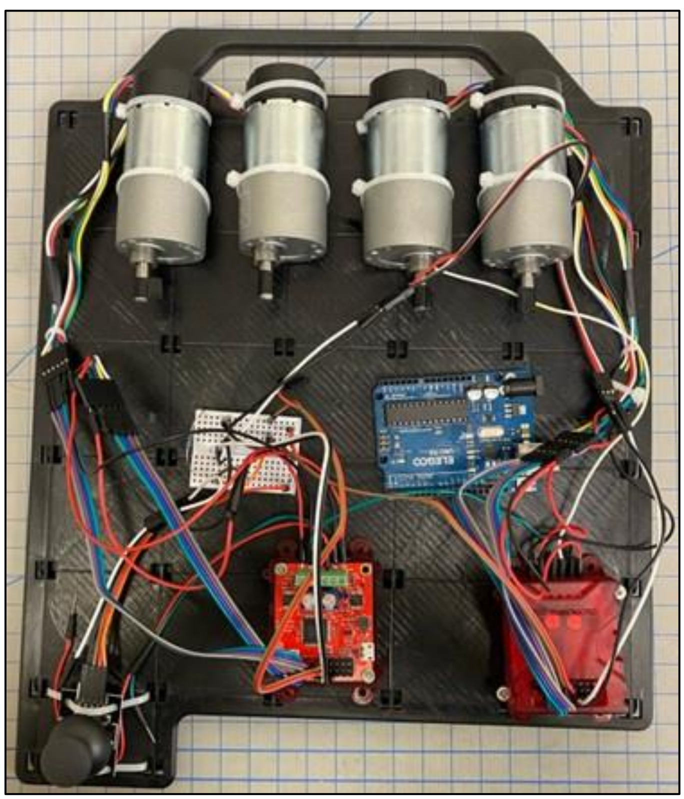

Figure 68. Drive motor control circuit being tested before installation.

System In-house Testing

After the VCS was assembled, it was run through various tests. These tests included its ability to vacuum gravel and dirt that is representative of what is in the tank anulus (Figure 69). In addition, FIU tested the robot's maneuverability on a curved steel surface that simulates the annulus of a waste storage tank. Fellow Pedro Chaviano continued testing the robot at WRPS's Cold Test Facility during his summer internship.

Figure 69. Testing the VCS's ability to vacuum similar gravel to that in the tank anulus.

System Testing at WRPS's Cold Test Facility

Pedro's internship focused on addressing critical engineering challenges such as suction power, maneuverability, and deployment strategies. Testing at the Cold Test Facility (CTF), as shown in (Figure 70), demonstrated the crawler's ability to navigate complex geometries and remove debris effectively.

Figure 70. Cold Test Facility.

The VCS underwent rigorous testing at CTF to evaluate its performance under conditions simulating the DST environment. Key testing procedures included:

- **Deployment Strategies**

  The initial stage of the testing focused on developing a deployment method for the crawler through the Mockup Riser at the Cold Test Facility (Figure 71). Key considerations included maintaining a controlled descent speed and ensuring the crawler remains parallel to the floor to prevent the front nozzle from crashing into the floor. This was achieved by integrating an additional suspension cable, secured within the umbilical cord sleeve, to prevent entanglement with the main safety suspension cable. This design ensures that the crawler can be manually retrieved in the event of a mechanical failure.

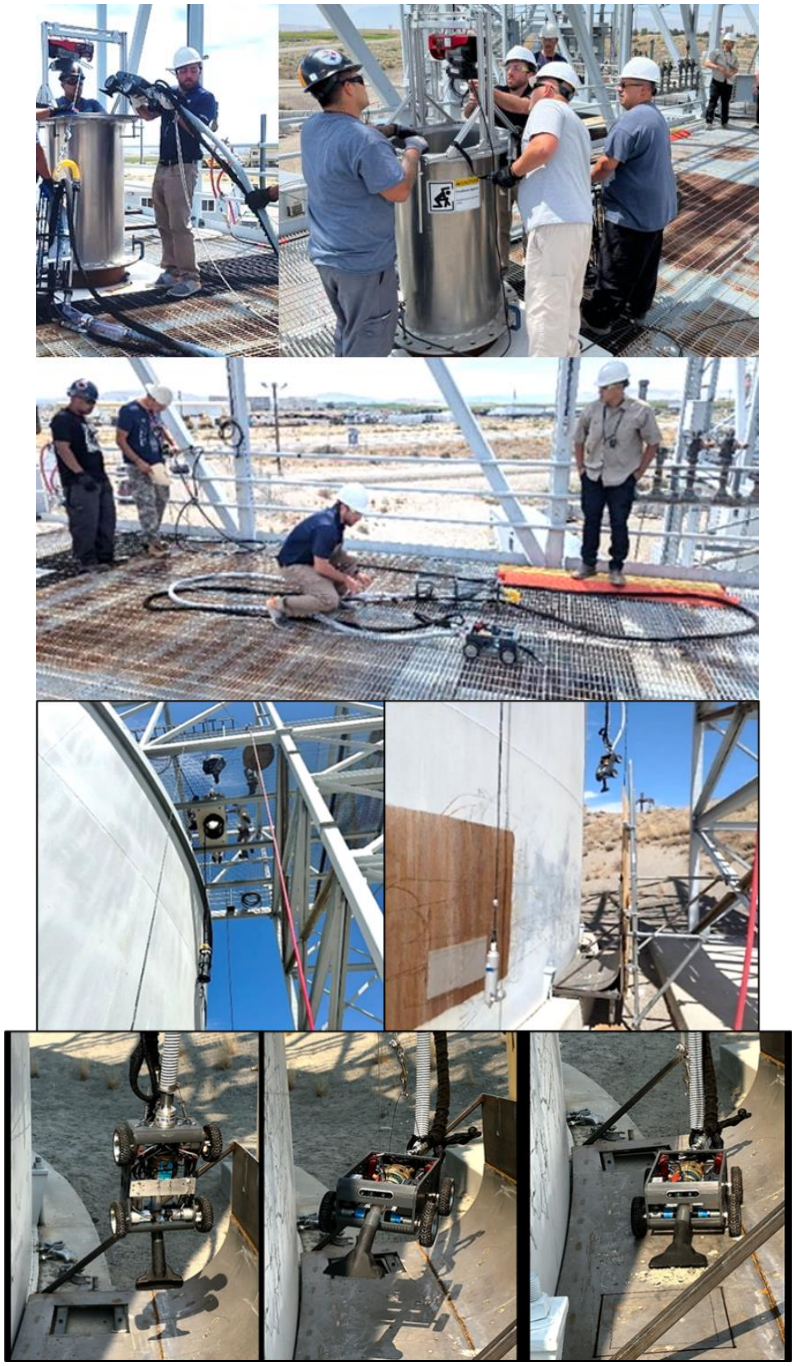

Figure 71. Deployment VCS through the mockup riser at the Hanford Cold Test Facility.

- **Vacuum Performance Testing:**

  The suction power and airflow of the Exair Line Vac modules were tested using various aggregates of debris and rocks. Tests were conducted on both 1” and 1-½” vacuum lines to validate the system's ability to handle different debris sizes and types. The system’s ability to maintain suction and prevent clogging was assessed by running the vacuum module continuously while navigating the mock annulus.

- **Maneuverability Testing:**

  The crawler's ability to traverse obstacles and navigate around welds up to ½ inch in height was tested. The system's design and ground clearance were evaluated to ensure reliable performance on warped liner bottoms and slopes within the annulus (Figure 72). Differential drive control systems were fine-tuned to optimize the crawler's responsiveness and stability during operation.

Figure 72. Control room camera feed.

- **Control System Validation:**

  The analog control circuits were tested and validated to ensure reliable operation without dependencies on software or firmware. The joystick interface was programmed to control all motors, and the system's response time to operator inputs was measured to be within 1 second, using a manual timer and adjustments to the joystick calibration.

Figure 73 illustrates details of FIU's deployment efforts featured on WRPS social media.

From coast to coast

WRPS & FIU partnership bolsters DOE workforce, advances Hanford cleanup

The summer arrival of four students from Miami-based Florida International University (FIU) highlights the continuing collaboration between WRPS, the university, and DOE's Office of Environmental Management. The partnership, formed through the DOE Fellows Program, seeks to grow and diversify the DOE workforce while furthering cleanup efforts at DOE sites across the country.

At Hanford, WRPS' Chief Technology Office (CTO) leads a collaborative effort to identify cleanup needs and opportunities for innovation at the Tank Farms. As needs are identified, FIU interns engage with stakeholders alongside their CTO mentors and manage their respective projects with the goal of providing innovative solutions in hazardous waste management and nuclear facility maintenance.

WRPS is sponsoring four FIU projects in 2024.

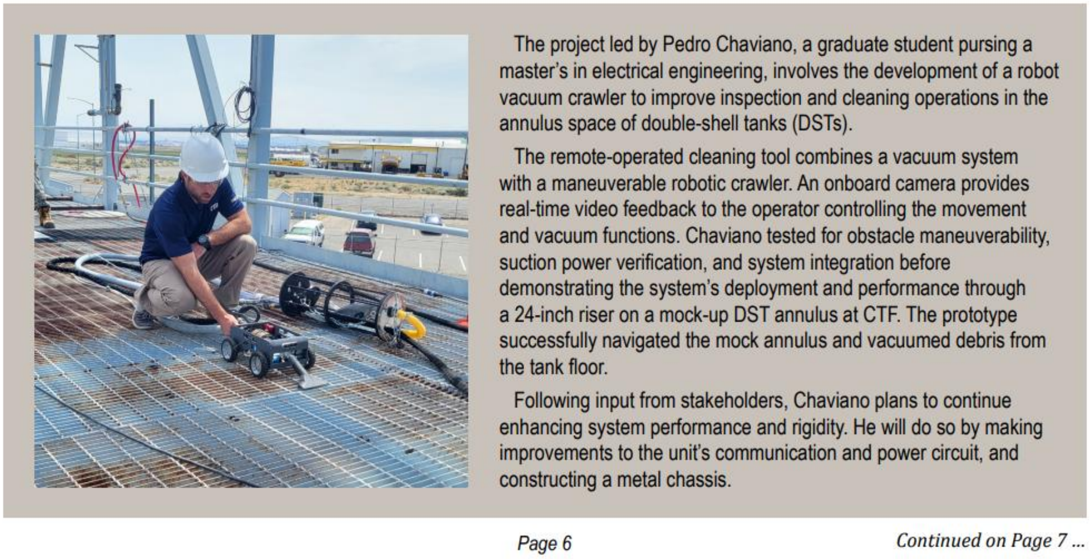
The project led by Pedro Chaviano, a graduate student pursing a master's in electrical engineering, involves the development of a robot vacuum crawler to improve inspection and cleaning operations in the annulus space of double-shell tanks (DSTs).

The remote-operated cleaning tool combines a vacuum system with a maneuverable robotic crawler. An onboard camera provides real-time video feedback to the operator controlling the movement and vacuum functions. Chaviano tested for obstacle maneuverability, suction power verification, and system integration before demonstrating the system's deployment and performance through a 24-inch riser on a mock-up DST annulus at CTF. The prototype successfully navigated the mock annulus and vacuumed debris from the tank floor.

Following input from stakeholders, Chaviano plans to continue enhancing system performance and rigidity. He will do so by making improvements to the unit's communication and power circuit, and constructing a metal chassis.

Page 6

Continued on Page 7 ...

Figure 73. Vacuum robot demonstration featured on Hanford social media.

Subtask 18.6: Results and Discussion

The VCS underwent a series of tests at CTF to evaluate its performance in simulating the conditions within the annulus space of DSTs. The key areas tested included suction power, maneuverability, debris removal efficiency, and control system responsiveness.

Vacuum Module Configuration:
The system used dual EXAIR Line Vac pneumatic vacuum modules arranged in series. These modules, connected to standard hoses or tubes, act as in-line conveyors, efficiently moving large volumes of material over long distances. Compressed air is injected through nozzles, creating a vacuum that generates high output flows. The design features a large, smooth bore to maximize material throughput, and its maintenance-free operation is ensured by the absence of moving parts. During the tests, the supply air flowrate entering the vacuum motors was measured using flowmeters (Figure 74) and compared the percentage of dirt that was removed. The system was tested using the 1” and 1 ½” diameter motors individually as well as both motors in series.

Figure 74. Collecting air flow data.

The conveying rate is influenced by various factors, including the size and mass of the material, as well as the length, lift, and bends in the hose or tube. Hands-on testing is crucial for optimizing configurations, such as selecting appropriate fittings, to ensure efficient flow rates. The data collected during these trials are shown in Table 1.

Table 1. Vacuum Performance and Debris Removal Efficiency

Media	Test	Line Vac Diameter	Vertical Rise (ft)	Rate (scfm)	Aggregate Debris (g)	Debris Removed (g)	Percentage Removed (%)
Aggregates of debris and rocks (Density: 68 lbs./ft^3)	1	6081 (1" Aluminum)	15	4	500	385	77.0%
	2	6083 (1 ½" Aluminum)	30	2	500	110	22.0%
	Vac lines in Series						
	3	1 + 1 ½"	15	7	500	475	95.0%
	4	1 + 1 ½"	30	6	500	425	85.0%

It was observed that optimal performance of the EXAIR Line Vac requires maintaining a steady supply of compressed air at the correct pressure. Factors such as compressor output pressure, airflow rate, piping diameter, and internal pipe smoothness can significantly affect performance. The air compressor must provide both sufficient pressure and flow; inadequate flow can impair performance even if the pressure is sufficient. A Sullair air compressor, capable of supplying up to 185 scfm at 120 psig, was used (Figure 75).

Figure 75. Sullair 185 air compressor.

During testing, it was observed that operating below 80 psig can reduce performance, while operating above this pressure may provide only marginal gains but at the cost of increased energy consumption. Proper selection of connectors and fittings is crucial to avoid restricting airflow, as restrictions can significantly impact tool performance. Quick connectors with smaller diameters can diminish airflow, so selecting the correct pipe size is essential to minimize pressure loss over distance.

Maneuverability:
The crawler successfully navigated the required obstacle height of 1/2 inch, validating the robustness of the differential drive system. Maintaining consistent speed while overcoming obstacles is crucial for reliable operation in the challenging annulus environment, as detailed in Table 2. Future tests will be necessary to account for the additional weight from the metal chassis redesign. Additionally, the crawler executed a full 360-degree turn within the 30-inch gap and incline of the shell.

Table 2. Maneuverability and Obstacle Traversed Ability

Test	Crawlers Weight (lbs.)	Obstacle Height (in)	Travel Time in 2ft (sec)	Obstacle Traversed (Y/N)
1	10	0	8	Y
2	10	⅜	12	Y
3	15	½	22	Y
4	15	¾	27	Y
5	10	1 ½	NA	N

Control System Performance:
The control system, featuring a joystick interface and analog circuits, delivered excellent precision. This precision is crucial for maintaining the stability of the crawler and ensuring smooth, reliable operation in the confined and complex environment of the annulus space. The system's responsiveness and accuracy instill confidence in the crawler's ability to navigate tight spaces and perform tasks with minimal operator intervention.

Subtask 18.6: Conclusion

The development and testing of the vacuum crawler system successfully demonstrated its capability to address the critical challenges associated with the inspection and cleaning of the annulus space in Double-Shell Tanks at the DOE's Hanford site. The crawler effectively utilized the dual Exair Line Vac pneumatic vacuum modules to achieve high debris removal efficiency, while the robust design ensured reliable maneuverability over obstacles up to ½ inch in height. The control system provided precise operation, with low-latency video feedback and accurate joystick control contributing to the overall effectiveness of the system. The crawler effectively performed its primary function of debris removal, achieving removal rates of up to 95% under various testing conditions, thus validating its design and operational capabilities.

The success of the initial testing trials indicated that the vacuum crawler system is well-positioned to advance into further stages of development, with the potential to significantly enhance the safety and efficiency of hazardous waste management in nuclear facilities. Insights gained from these trials will guide the next steps in refining the system's design. Planned upgrades include replacing the prototype chassis with a more robust design using stainless steel or anodized aluminum to withstand the harsh conditions within DSTs. Further development will improve vacuum efficiency, focusing on enhancing debris collection with upgrades to the vacuum module and brush assemblies. The multistage mechanical system will be refined to ensure reliable retrieval and containment of foreign objects, along with enhancements to the brush assembly and debris container. Additionally, the control system will be upgraded with added sensor data feedback, such as temperature, pressure, and flow, providing operators with more comprehensive monitoring capabilities. These planned enhancements aim to optimize the vacuum system and integrate additional mechanical assemblies for surface agitation, contributing to a more effective and reliable hazardous waste management solution.

This years' work demonstrated the viability of using remotely operated robotic systems for complex environmental management tasks, contributing to the broader mission of the U.S. Department of Energy's environmental remediation efforts. With continued development, the VCS has the capability to become a valuable tool in supporting the maintenance of nuclear storage facilities.

Subtask 18.6: References

[1] RPP-PLAN-43988 Rev.08A, "Technology and Innovation Roadmap, Rev. 8a," Washington River Protection Solutions, LLC, Richland, Washington, 2023.

[2] Department of Energy. Accessed on August 20, 2024. Site: https://www.energy.gov/

Subtask 18.7: Development of an In-Tank Sonar System for DST Applications

Subtask 18.7: Introduction

The U.S. Department of Energy's Office of River Protection (DOE-ORP) manages 177 underground storage tanks at the Hanford Site, containing 56 million gallons of hazardous waste in both liquid and solid forms, requiring accurate measurement for effective waste management and retrieval. Washington River Protection Solutions (WRPS) oversees the safe maintenance of these tanks, with accurate solids level measurements being essential for single-shell tank (SST) waste retrieval, double-shell tank (DST) operations, and waste feed delivery to the Waste Treatment Plant (WTP). The thickness and bottom profile of the floating sludge layer in the Hanford tanks is of interest to the site engineers to help with the emptying and the ultimate decommissioning of the tanks. Traditional methods using conductivity probes and tape measures to detect solid-liquid interfaces, however, are limited to point measurements directly below the riser, making them less efficient for broader waste management needs. A more efficient method is thus needed. FIU is therefore working with Hanford Site personnel to develop a sonar system that will be capable of mapping the bottom of the floating sludge layer. This information will help site engineers develop a plan of action for emptying the tanks.

Subtask 18.7: Objectives

The objective of this proposed research is to modify an off-the-shelf 3D profiling sonar system to image the profile of the bottom of the sludge layer in Hanford tanks, ensuring that the altered design and functional requirements of the system are in accordance with the WRPS document RPP-RPT-61163.

Subtask 18.7: Methodology

This subtask involves collaborating with Hanford Site personnel to design a sonar system capable of mapping the bottom of the floating sludge layer in the Hanford tanks. Figure 76 presents the sonar system conceptual design.

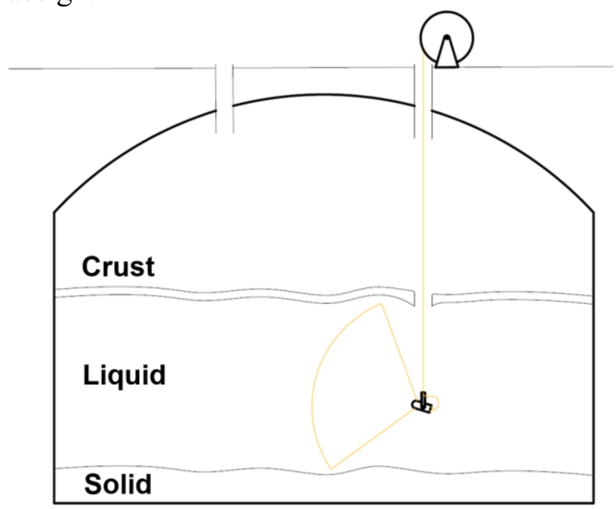

Figure 76. Sonar System for Hanford Tank Farms.

The system project encompasses the following three main phases:

- **Design of Deployment System:** The system will include a deployment frame comprising structural components and actuators designed to withstand the highly caustic tank waste and anticipated high temperatures. The frame will be deployable through a 4-inch riser and feature a mechanism that articulates the sonar into a position with a clear view of the sludge layer's bottom. Signal and power cables will be routed within the frame members wherever possible to minimize exposure to the tank environment. Additionally, the deployment reel will house the sonar signal/power cable in a flexible armored conduit, protecting it from the tank environment and damage during deployment or retrieval. The reel will also ensure precise control of the sonar's depth.
- **System Fabrication:** Once the system design is finalized, fabrication will begin, including the acquisition of components and any necessary modifications to ensure integration into the main system. The system will then be assembled and prepared for testing.
- **System In-house Testing:** After fabrication, the sonar system will undergo testing using a tank and riser mockup to evaluate its functionality. A draft report of the results will then be shared with WRPS.

Subtask 18.7: Results and Discussion

Illustrated in Figure 77, the Sonar's deployment system was designed to address the challenges posed by the Hanford Site and WRPS requirements. The frame was constructed out of aluminum, which is corrosion resistant, and machined in-house using a CNC machine. The actuator is an air cylinder this way it does not introduce any electronics inside the tank and brings the necessary strength to make the mechanism move. The mechanism was designed to actuate an air cylinder that is connected to a chain that moves to sprockets and in turn rotate the arm where the sonar is attached. The sonar is attached to the arm by two plates with spacers in between that allows space for the sonar cable.

Figure 77. FIU's In-Tank Sonar System Prototype.

The fabrication of the arm and holding plates for both the sonar and counterweight were made in-house with aluminum stock purchased by FIU, however, the connector between the chain and actuator was done in steel. CNC machines, illustrated in Figure 78, were used to cut the stock into the desired geometries and a milling machine was used for finishing operations, all done in FIU's manufacturing lab. Other components such as the chain, sprockets, and counterweight were purchased as finished products from outside vendors. The counterweight is a copper block chosen for its high density. shows images from the fabrication.

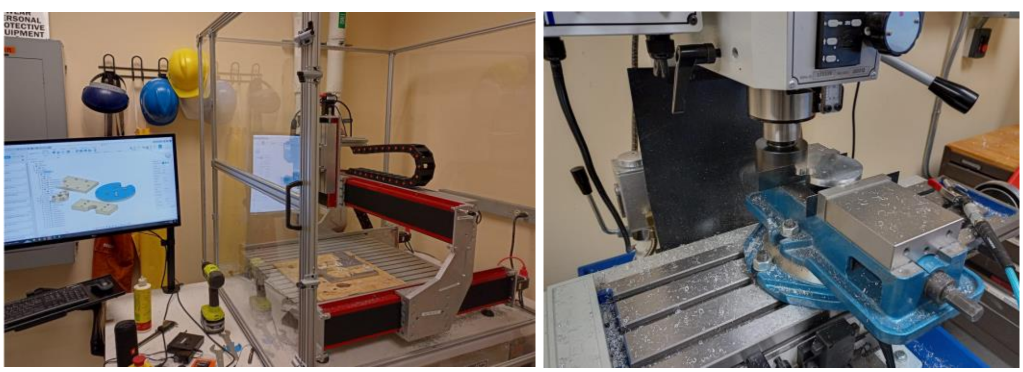

Figure 78. CNC used in fabrication of Sonar Mechanism.

The sonar gimble's control box, shown in Figure 79, are comprised of three solenoid valves one of them is a three-position valve and the other two are two position solenoid valves. There is also an air filter that guarantees no particles go into the piston from the airline the control box is connected. The logic is handled by a microcontroller and a relay module which are activated using mechanical switches. There are also to manual valves placed on the two two-position solenoid valves to restrict air flow allowing to adjust how strong the mechanism will move once activated.

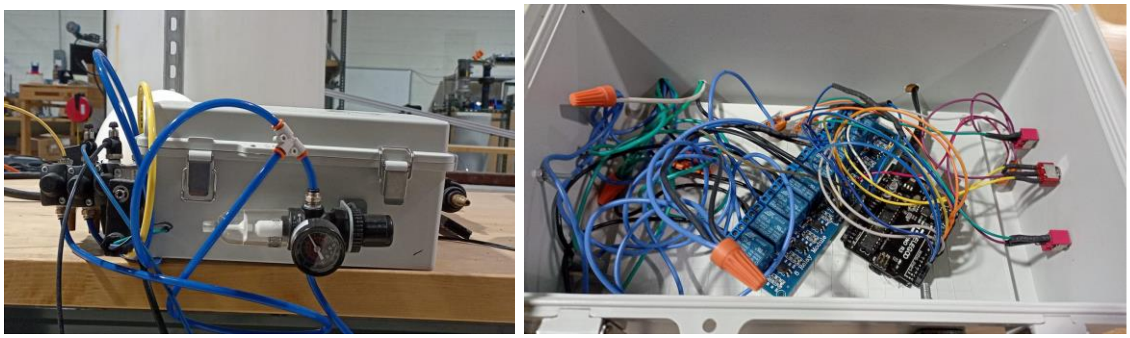

Figure 79. Sonar gimble's control box.

A series of comprehensive in-house tests, illustrated in Figure 80, were conducted to evaluate the gimbal control system and verify that the counterweight effectively assisted the system's movement. The tests also confirmed proper actuation of the cylinder by the control box. During testing, we identified a critical challenge: the system developed significant momentum during downward movement, making it difficult to achieve precise stops using only the control box. To address this issue, we implemented a mechanical stop solution. The stop component was fabricated using 3D printing technology and securely mounted to the counterweight's top mounting plate. Additionally, we integrated a smaller auxiliary piston into the frame, designed to engage with the 3D-printed stop component, providing reliable motion limitation.

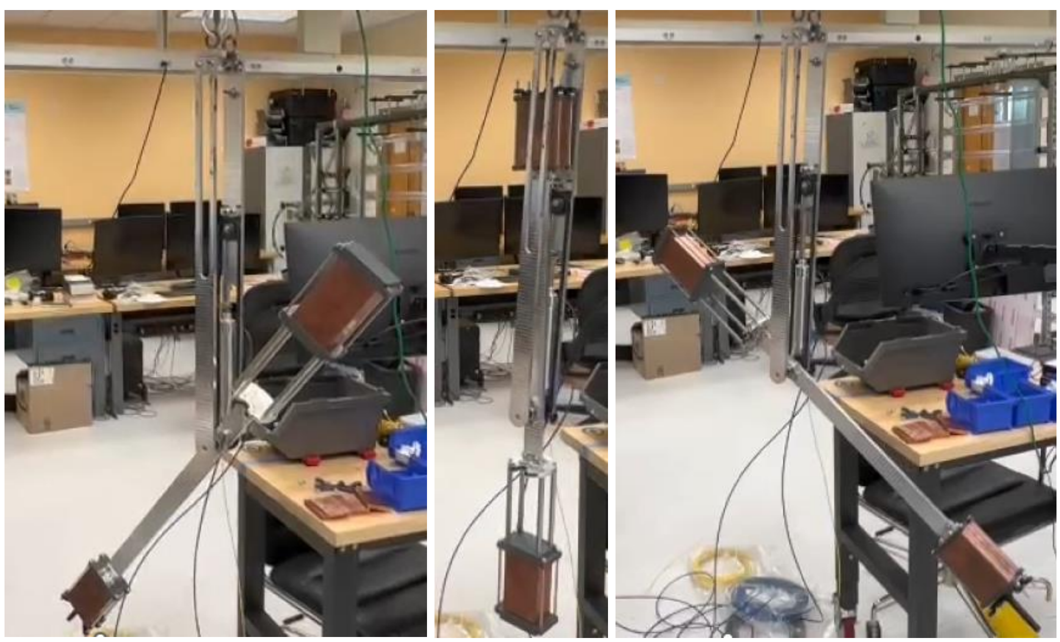

Figure 80. Gimble control tests.

Illustrated by Figure 81, further testing was performed at the Hanford site during the summer of 2024. Preliminary imaging tests with a 50-gallon tank containing objects like rocks and bricks evaluated the sonar's ability to detect and distinguish submerged features. The sonar was suspended and lowered using a hoist, and its settings, such as range, depth, and pulse duration, were adjusted to optimize data accuracy. The scans provided detailed imagery of the objects, laying the foundation for testing in larger environments.

Figure 81. 50-gallon tank imaging tests.

Subsequent tests transitioned to a medium-sized rectangular tank where the sonar was oriented at 90-degree angles to capture different perspectives. Illustrated in Scans highlighted objects such as bricks and a wooden plank, though limitations due to sound wave reflections in corners were observed.

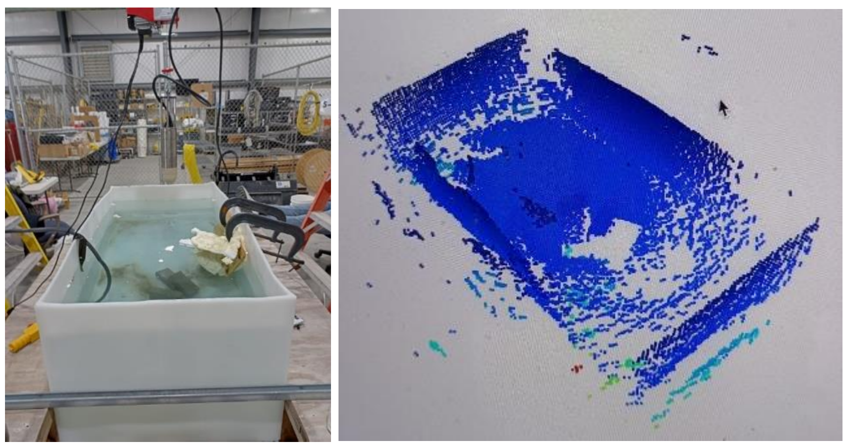

Figure 82. Rectangular tank imaging tests.

These initial test results provided critical insights that guided our system optimization for larger-scale deployments. The high-resolution scans revealed optimal sonar frequency ranges for different material densities, while the controlled depth variations established ideal scanning distances for maximum signal clarity. Based on these findings, we refined the pulse duration parameters to minimize signal interference and enhanced the filtering algorithms to better distinguish between closely positioned objects.

Cold Test Facility Demonstration

A significant achievement was reached during the system demonstrations at the Atkins Technology Center in Richland, where the sonar platform's imaging capabilities were presented to key stakeholders, field engineers and visitors. DOE Fellow David Rojas made substantial contributions during his 10-week internship with WRPS, focusing on optimizing the gimbal system's design and controls. Through extensive collaboration with WRPS stakeholders, Rojas create simulants with desired imaging features. The demonstration successfully validated the system's proof-of-concept, generating strong stakeholder support for continued development and future field deployment. Stakeholders particularly noted the system's potential for enhancing tank inspection capabilities and expressed interest in expanding its application scope in subsequent project phases.

Figure 83 shows the 30-foot mockup build by FIU Fellows in coordination with WRPS engineers at the Atkins Technology Center in Richland to demonstrate the sonar capabilities imaging Hanford's tanks.

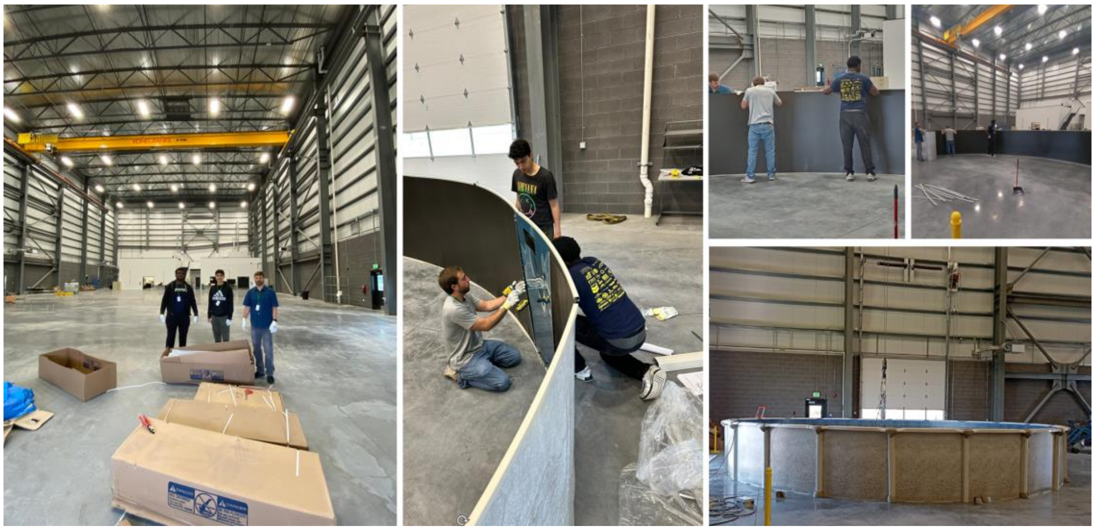

Figure 83. FIU's tank mockup at the Atkins Technology Center in Richland.

In the 30-foot-diameter pool, the sonar mapped submerged bricks, rods, and a foam crust simulant as illustrated in Figure 84. Mounted on a crane for maneuverability, the sonar conducted scans at various points. Parameters like transmit pulse and detection threshold were fine-tuned to enhance object detection and reduce noise. Initial scans revealed challenges, such as incomplete data and noise, but subsequent adjustments improved performance, producing more accurate representations of the pool's contents and structure.

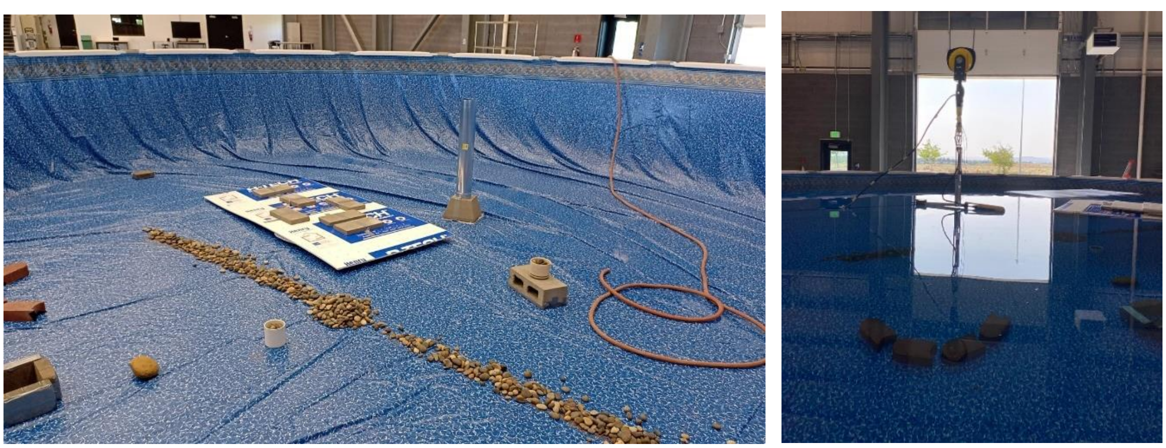

Figure 84. FIU's 30ft diameter pool with objects for sonar detection.

Figure 85 documents the DOE Fellows conducting cold test demonstrations at the Atkins facility. During these demonstrations, the Fellows systematically evaluated the sonar system's performance under controlled conditions, positioning the equipment over the test tank and adjusting operational parameters to optimize data collection. The testing phase was crucial for validating the system's capabilities and demonstrating its practical applications to WRPS stakeholders. The Fellows' hands-on involvement highlighted both the technical rigor of the testing process and the collaborative nature of the project between academic researchers and industry partners.

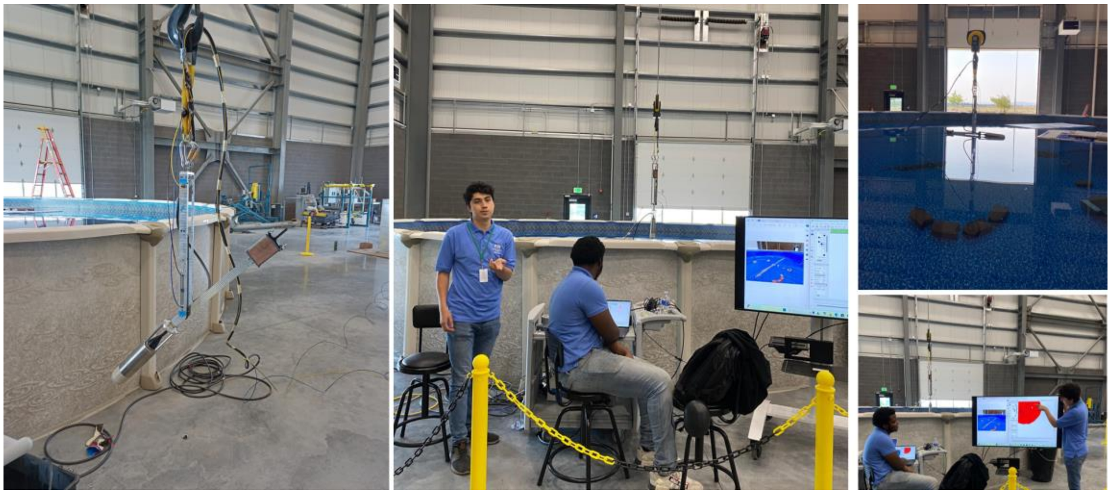

Figure 85. FIU's Fellows during cold test facility demonstrations.

The sonar system included various adjustable settings to optimize performance and data collection. The Maximum Range Slider limited the radial coverage of the sonar, with a maximum range of 10.0m and a restriction that it could not be set less than the Stop Depth. The Start Depth specified the depth below the transducer where sampling began, reducing multipath effects from proximity to the surface or nearby objects, and had a range of 0.2m to 5.0m. The Stop Depth, which worked alongside the Start Depth to minimize multipath, specified the depth beyond which data was not captured, with limits from 0.5m to 10.0m and a requirement to be at least 0.5m greater than the Start Depth without exceeding the Maximum Range.

Figure 86 shows sonar images captured during the demonstrations at Atkins facility. The Color Scale determined the number of meters represented by the range of the color palette and could be adjusted during scanning to modify height representation.

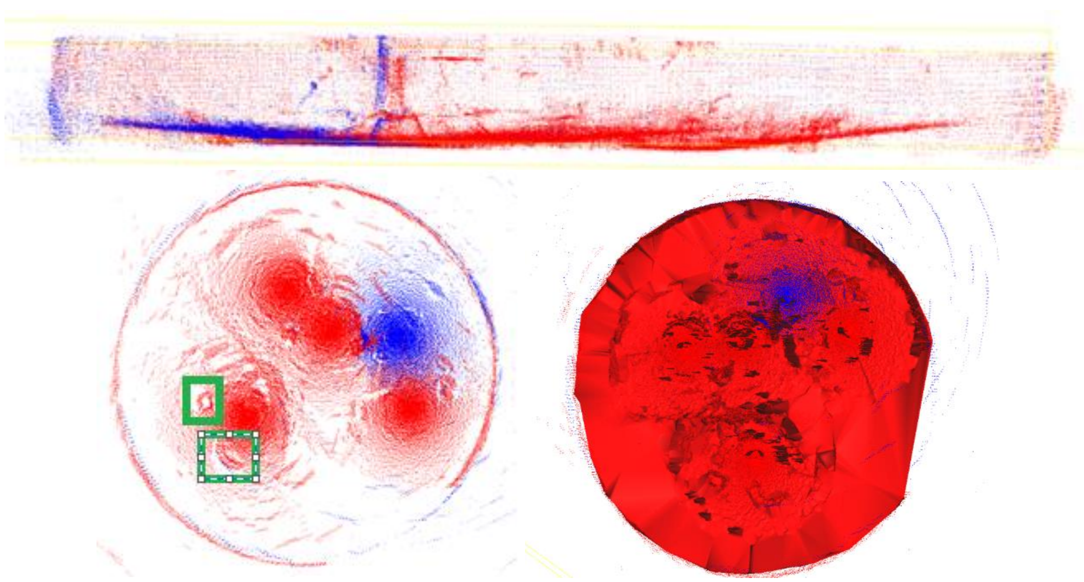

Figure 86. Sonar images captured during the demonstrations at the Atkins facility.

The Swath Arc defined the area for data capture by setting the arc swept by the sonar in 30-degree increments. The Velocity of Sound setting allowed compensation for sound speed in water to enhance accuracy, typically set at 1500 m/s but adjustable between 1400 and 1600 m/s. The Transmit Pulse controlled the duration of the acoustic transmit pulse, ranging from 10µsec to 250µsec, with shorter pulses providing higher resolution but lower gain. The Filter Window was used by the pulse echo detection routine to smooth data using a rolling average, adjustable from 1 to 20. Lastly, the Detection Threshold defined the signal level at which the sonar would begin detecting echoes, adjustable between 10% and 90%.

A map of the pool (the simulated tank) was reconstructed, displaying many features and highlighting the potential for mapping the topography of the tank. The ability to collect distance measurements from the point cloud also shows promise for developing methodologies to estimate the volume of settled waste at the bottom of the tank, as well as the crust layer. The furthest distance measured was the wall-to-wall span, which is the diameter of the pool, producing an error of only 1.3 percent.

Figure 87 shows video frames of the FIU's deployment efforts featured on WRPS social media.

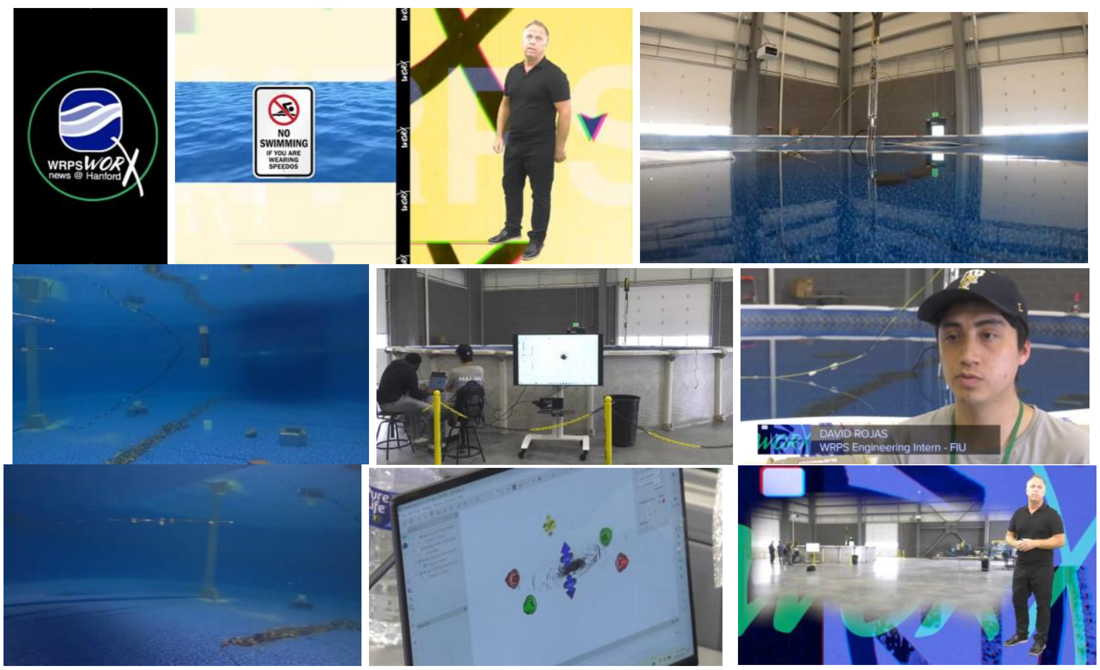

Figure 87. In-tank sonar demonstration video frames featured on Hanford social media.

The large demonstration testing validated the sonar's ability to map features across different scales, highlighting its potential for waste tank applications while identifying areas for further refinement.

Subtask 18.7: Conclusion

The work conducted demonstrates that, in concept, the use of a sonar probe to map the bottom of a tank waste topography is effective.

This research demonstrates that sonar technology can accurately map tank waste topography, offering a reliable method for measuring sludge levels and crust layers. The ability to generate 3D models presents opportunities for improving waste management processes at the Hanford site.

However, improvements in sonar hardware and software are necessary to enhance the system's performance and data accuracy.

Several lessons were learned during the project that can inform future improvements:

- The tank dimensions and design, particularly the ratio of tank width to height, play a crucial role in ensuring accurate measurements, with a 2:1 width-to-height ratio proving effective in our setup and recommended for future designs.
- The orientation of the sonar was found to significantly affect the accuracy of collected data, highlighting the need for precise control over the sonar's positioning to maintain consistency.
- The current mechanism for positioning the sonar lacks refinement, adjusting difficult and time-consuming; improving this control system would enhance accuracy and efficiency.
- The software library used, Open3D, was found to be inadequate for effectively manipulating sonar data and meshing multiple point clouds; switching to the more robust Point Cloud Library (PCL) is planned to address these limitations.

Finally, the scanning strategy should be adjusted to include multiple scans from different sections of the tank rather than relying on a single location, as this approach would likely yield more comprehensive and accurate results.

Subtask 18.7: References

1. RPP-SPEC-31604 2024, Functional Requirements and Technical Design Criteria for the Solid Liquid Interface Monitoring System Rev 1, Washington River Protection Solution Richland WA.
2. RPP-PLAN-63206 2020, Sampling Technology Program Plan Rev 1, Washington River Protection Solution Richland WA.
3. RPP-PLAN-43988 2024, Technology and Innovation Road Map Rev 9, Washington River Protection Solution Richland WA
4. Marine Electronics Ltd., User Manual for the 3D Sand Ripple Profiling Remote Sonar, Issue 1.1, 15th March 2010. Marine Electronics Ltd., Vale, Channel Islands.

TASK 19: PIPELINE INTEGRITY AND ANALYSIS

Subtask 19.1: Pipeline Corrosion and Erosion Evaluation

Subtask 19.1: Introduction

The Hanford Site Tank Farm has implemented a Fitness-for-Service (FFS) program for the Waste Transfer System. The FFS program, based on API-579-1/ASME FFS-1, examines structural parameters of the waste transfer systems to develop erosion/corrosion rates for relevant system components. The FFS information is acquired from opportunistic evaluations of pipelines that have been removed from service. FIU-ARC engineers work closely with key Hanford high level waste (HLW) personnel and the contractor, Washington River Protection Solutions, LLC (WRPS), to support the FFS program, deliver solutions for sensor evaluations, conduct bench-scale testing followed by data acquisition and analysis for corrosion and erosion assessment. Previous efforts at Hanford included the installation of sensors on a number of the POR 104 components, to provide real-time pipe wall thickness measurements. Due to various limitations, alternative approaches for remote permanently mounted pipe wall ultrasonic thickness measurement systems are being investigated.

FIU's efforts to support this scope have included investigating key options available in the market for remote, permanently mounted ultrasonic transducer (UT) and other sensor systems for HLW pipe wall thickness measurements and wear. Specific applications include straight sections, elbows and other fittings used in jumper pits, evaporators, and valve boxes. FIU assessed the use of various ultrasonic systems that are either commercially available or used previously at Hanford and selected the most promising systems for further evaluation. Two sensor systems were down selected. The Permasense UT sensor system and the fiber optic sensors from Cleveland Electric Laboratories (CEL) were acquired, and initial bench-scale validation testing was conducted. Following the initial bench scale tests, engineering scale testing was implemented on an in-house designed and installed test loop. The design loop has been established using 2- and 3-inch diameter straight and bend pipe sections to mount the sensors. The loop was eroded using a sand-water slurry and the Permasense sensors and the CEL sensors were used for thickness measurements [1,2,3,4,5,6]. The Permasense sensors were also tested for their performance in extreme environmental conditions under high humidity and temperatures. Finally, the feasibility of conducting radiation testing on those sensors was considered and a test plan was developed for implementation. Permasense UT sensors were used for thickness detection while the CEL sensors were used for anomaly detection. In addition, SRNL mass loss coupon erosion systems were evaluated for erosion and corrosion detection in the pipe loop at FIU. These included the SRNL coupons with the Pencil UT sensor [4,5].

FIU has successfully completed the sand water erosion tests on both carbon and stainless-steel coupons. Currently, FIU is investigating the effect of glass frit particle erosion and caustic simulant corrosion on the SRNL coupons. A bench scale mockup has been constructed and initial caustic simulant testing has been conducted. The static coupon immersion tests are also being performed in parallel. Benefits of this research include providing validation for new methods and technologies that will assist engineers in understanding the fault potential of HLW nuclear waste transfer components due to corrosion and erosion. By providing insights into determining if and when lines need to be removed/replaced, the unneeded excavation of transfer lines can be avoided, saving valuable time and resources. Also, more detailed and accurate guidelines can be developed governing the life expectancy of the transfer system and its components. By being able to have accurate predictions of points of failure from erosion, and by being able to monitor an entire pipeline's status in real-time, resources can be targeted to tackle preventative measures instead of reactive.

Subtask 19.1: Objectives

The motivation for this subtask is to assist DOE, WRPS and SRNL in providing realistic estimates of the remaining useful life of the components, to incorporate those estimates into future design plans and to automate the erosion corrosion monitoring. This subtask includes the investigation of various sensor systems and fluid flow dynamics to detect thinning in pipes and tanks along with real-time evolution of the wear using SRNL's mass loss/erosion coupons. Hence, there are three objectives for this task for structural health monitoring using various types of sensors. Including:

- Evaluation of SRNL's carbon and stainless-steel coupons for erosion testing.
- Caustic simulant-induced corrosion evaluation on FIU's custom bench scale flow loop.
- Development of data analytics and fluid flow dynamics-based models for automated erosion and corrosion detection.

Subtask 19.1.1: Evaluation of SRNL Stainless Steel Coupons for Erosion Testing using DWPF Glass Frit

Subtask 19.1.1: Methodology

The purpose of this research was to test and demonstrate that the SRNL erosion and mass loss coupons could provide an in-situ method for collecting erosion and mass loss rates from a pipeline using the stainless steel and carbon steel coupons during operation. Previous work included initial testing with the first set of carbon steel coupons provided by SRNL to FIU [4]. The application of these coupons was experimentally tested in an engineering scale pipe loop by circulating sand-water slurries of varying densities and grit sizes. The intended advantage of the replaceable coupons is their ability to easily calculate mass loss/gain and to gain insights into qualitative data such as erosion patterns on the inside of the pipes.

The past year's work included the feasibility investigation and initial testing of DWPF glass frit as a material for accelerated erosion in the pipe sections using the SRNL mass loss coupons and the Permasense Sensors. The present work evaluates:

- The structural integrity of the pipeline (FIU's Engineering scale test loop)
- Thermal integrity of the pipe loop under erosion experiments
- Erosion with multiple particles – sand and DWPF glass frit combination
- SRNL coupon material for hardness

Subtask 19.1.1: Results and Discussion

For this year, the objective was to conduct data analysis of all the experimental data obtained over the last 3-4 years and predict the remaining useful life of the pipe system and coupon material, thus indicating the structural stability of the current engineering scale pipe system.

Under this subtask, efforts were focused on completion of a final paper titled "*Pipeline Integrity Assessment in High Level Waste Transfer Systems - Experimental and Computational Fluid Dynamics (CFD) based Approaches*", that has been submitted to the Waste Management Symposia 2024 (WM2024). Additionally, the data analysis of all the erosion and corrosion experimental data obtained from extensive testing on the engineering scale bench loop has been processed to assess the level of degradation after about 4 years, starting from 2020 to 2023.

SRNL coupon test data was obtained from three different types of erosion testing - a) sand and water mixture, b) glass and water mixtures, and c) sand-glass and water mixtures. The logged data was converted to spreadsheets to create a database. This database was used to further create data visualization in the form of graphs. Some of the results are shown in the figures below. It is evident from the figures below that the sand erosion resulted in a higher level of degradation when compared to the glass bead erosion. Also, the combination of sand, glass and water mixtures for testing resulted in slightly higher values of erosion in the SRNL coupons.

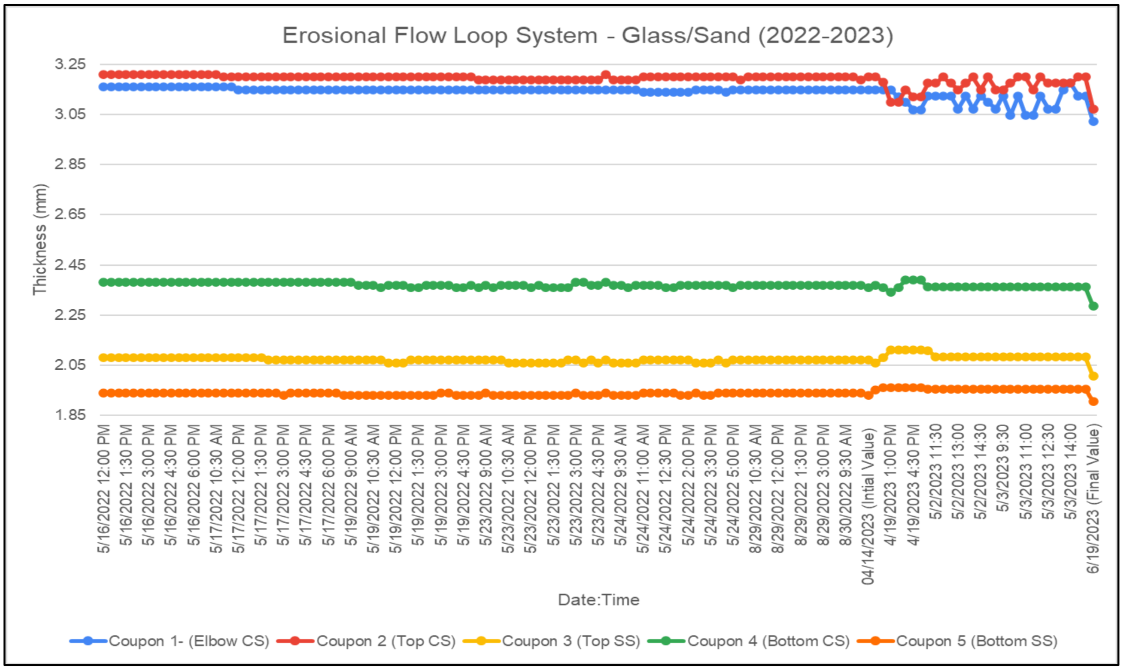

Figure 88. Erosion testing of SRNL coupons with glass simulants.

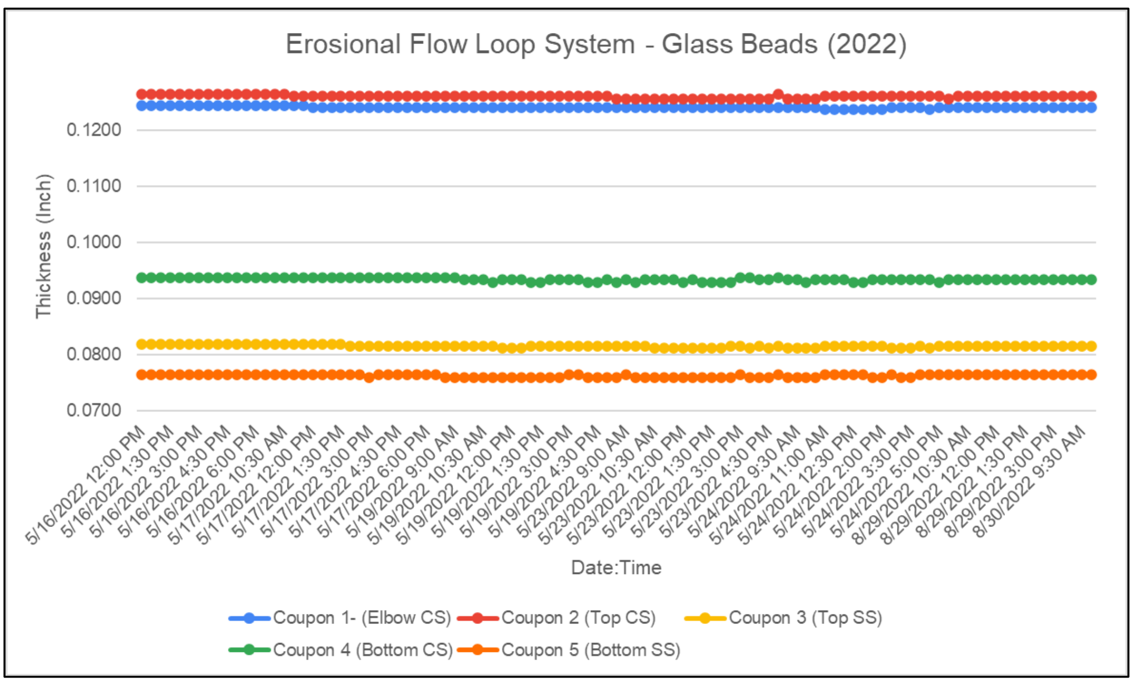

Figure 89. Erosion testing of SRNL coupons with sand simulants.

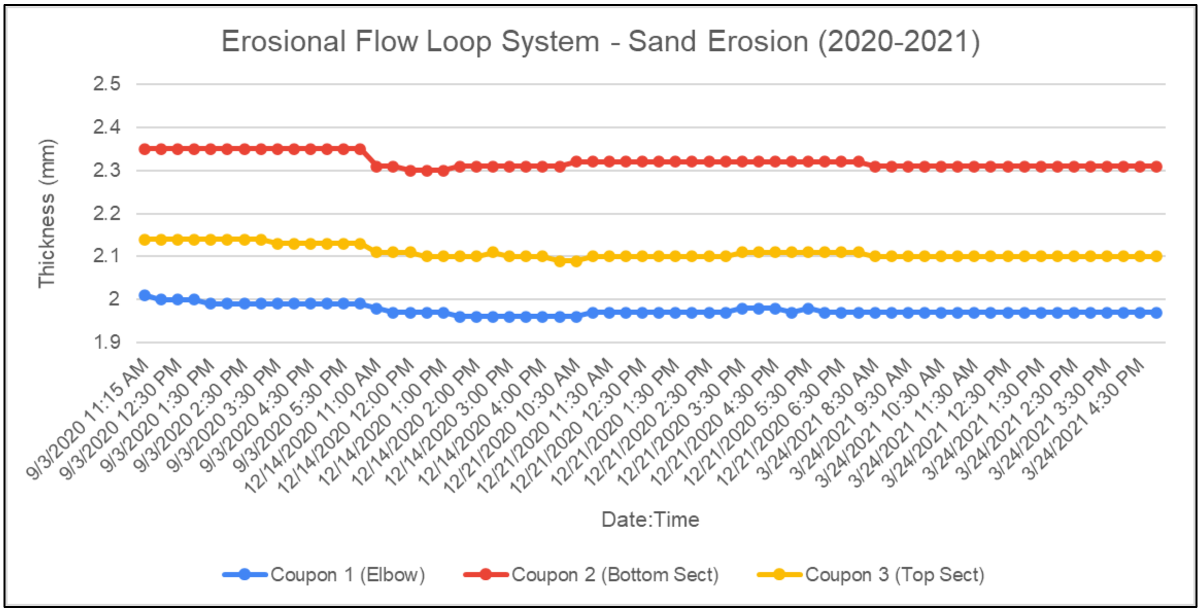

Figure 90. Erosion testing of SRNL coupons with sand simulants.

Also, with the pipe erosion data collected over several years, a database was created, and erosion data was analyzed for predictions. The results included sensor data from Permasense UT sensors, the pencil UT sensor for SRNL coupons and the traditional external UT sensor data. The database uses glass, sand, and water mixture test results from the engineering scale test loop. In addition, erosion image data is also collected and used for model development. Based on the data analysis, real-world turbulent erosion models were generated using COMSOL simulations depicting actual HLW pipeline conditions.

The FIU's Erosional Flow Loop System is an engineering scale flow loop that has been designed, built and tested for obtaining waste transfer pipe erosion data on the concept of particle erosion and fluid flow for several years. The information gathered from the system includes ultrasonic transducers and thermocouple data to determine the precise areal location of high erosional damage due to variations in particle sizes.

Table 3 introduces the libraries of data gathered over the years, all adequately organized and analyzed to obtain progressional information on the erosional effect. The information for abrasive sand precisely corresponds to the experimental values of the erosion rate for different sizes of sand from (2020 -2021). The same information for the Impact Glass beads is also obtained from the experimental values of only glass and water mixture flowing through the pipe system, only changing the size to observe the damage rate (2022). The information gathered corresponds to material loss among the internal pipeline walls and the mass loss coupon thickness measurement. The informational data has been modified to experiment with combining glass and sand particles within the water flow (2023). This enhances interaction and behavioral damage among the walls to understand the survival rates of different pipe components at such speed and pressure. The evaluation of the Permasense UT sensor has been safely recovered and analyzed to ensure proper analysis among the upper pipe components; this includes the 2-inch pipe section and the 3-inch pipe section. These sensors constantly monitor specific areas where we expect high erosional damage among the pipe system and provide the change of thickness and temperature at which the interaction occurs.

Table 3. Experimental Data Analysis Table with Erosion Results

Data Information	Date (Years)	Description
Erosion - Abrasive Sand	2020 -2021	Mass Loss Coupons Evaluation - Different Sand Sizes
Erosion - Glass Impact Bead	2022	Mass Loss Coupons Evaluation - Different Glass Sizes
Erosion - Glass Beads - Abrasive Sand	2023	Mass Loss Coupons Evaluation - Combination Effect of Glass & Sand
Permasense (UT) - 2 Inch (Straight Pipe)	2016-2018	Pipe Thickness Monitoring Evaluation - 2 Inch Straight Pipe
Permasense (UT) - 2 Inch (90 Elbow LR)	2016-2018	Pipe Thickness Monitoring Evaluation - 2 Inch 90 Elbow Long Radius
Permasense (UT) - 3 Inch (Straight Pipe)	2016-2018	Pipe Thickness Monitoring Evaluation - 3 Inch Straight Pipe
Permasense (UT) - 3 Inch (90 Elbow LR)	2016-2018	Pipe Thickness Monitoring Evaluation - 3 Inch 90 Elbow Long Radius

Table 4 and

Table 5 provide a visual representation of the new catalog of informational data we have corresponding to the Erosional Flow Loop System; the next step is analyzing the information and determining a pattern corresponding to the flow's physics.

Table 4. UT Measurements with Olympus Pencil Sensor for SRNL Coupons (sample database file)

Stainless Steel Coupons	Millimeter Measurement		
Time (AM/PM)	Coupon 1 (90-Degree Elbow) mm	Coupon 2 (Bottom Sect "3" inch) mm	Coupon 3 (Top Sect "3" inch) mm
9/3/2020 11:15 AM	2.01	2.35	2.14
9/3/2020 12:00 PM	2.00	2.35	2.14
9/3/2020 12:30 PM	2.00	2.35	2.14
9/3/2020 1:00 PM	2.00	2.35	2.14
9/3/2020 1:30 PM	1.99	2.35	2.14
9/3/2020 2:00 PM	1.99	2.35	2.14
9/3/2020 2:30 PM	1.99	2.35	2.14
9/3/2020 3:00 PM	1.99	2.35	2.14
9/3/2020 3:30 PM	1.99	2.35	2.13
9/3/2020 4:00 PM	1.99	2.35	2.13
9/3/2020 4:30 PM	1.99	2.35	2.13
9/3/2020 5:00 PM	1.99	2.35	2.13
9/3/2020 5:30 PM	1.99	2.35	2.13
9/3/2020 6:00 PM	1.99	2.35	2.13
Comment = Course Sand (3 Gallons) + Fine Sand (1 Gallon)			
12/14/2020 11:00 AM	1.98	2.31	2.11
12/14/2020 11:30 AM	1.97	2.31	2.11
12/14/2020 12:00 PM	1.97	2.3	2.11
12/14/2020 12:30 PM	1.97	2.3	2.1
12/14/2020 1:00 PM	1.97	2.3	2.1
12/14/2020 1:30 PM	1.96	2.31	2.1
12/14/2020 2:00 PM	1.96	2.31	2.1
12/14/2020 2:30 PM	1.96	2.31	2.11
12/14/2020 3:00 PM	1.96	2.31	2.1
12/14/2020 15:30	1.96	2.31	2.1
12/14/2020 4:00 PM	1.96	2.31	2.1
12/14/2020 4:30 PM	1.96	2.31	2.09
Comment = Fine Sand (11:30AM) 2gal + Sand Medium 20/30 (11:00AM) 2gal + Sand Coarse 6/20 (1:00PM) 2gal			
12/21/2020 10:30 AM	1.96	2.32	2.09
12/21/2020 11:00 AM	1.97	2.32	2.1
12/21/2020 11:30 AM	1.97	2.32	2.1

Graph HELP | Erosion - Sand (2020-2021) | Erosion - Glass Beads (2022) | Erosion - Glass+Sa

Table 5. Permasense UT Data Recording Database (sample) over the Years

3-Inch 90(deg) Elbow (Long Radius)				
Date:	Time:	UT Meas (mm):	UT Meas (In):	Temperature:
11/29/2016	11:52 AM	5.144	0.202519685	17.76
11/29/2016	1:37 PM	5.139	0.202322835	17.76
11/29/2016	1:42 PM	5.142	0.202440945	17.05
11/29/2016	1:46 PM	5.143	0.202480315	17.38
11/29/2016	1:51 PM	5.14	0.202362205	17.05
11/29/2016	5:56 PM	5.143	0.202480315	17.43
11/29/2016	11:58 PM	5.143	0.202480315	17
11/30/2016	6:01 AM	5.144	0.202519685	17.05
11/30/2016	12:06 PM	5.145	0.202559055	17.05
11/30/2016	6:08 PM	5.142	0.202440945	17.11
12/1/2016	12:11 AM	5.143	0.202480315	17.11
12/1/2016	6:14 AM	5.144	0.202519685	17.11
12/1/2016	12:16 PM	5.142	0.202440945	17.05
12/1/2016	6:20 PM	5.145	0.202559055	17.11
12/2/2016	12:23 AM	5.144	0.202519685	17.08
12/2/2016	6:26 AM	5.143	0.202480315	17.02
12/2/2016	12:30 PM	5.145	0.202559055	17.05
12/2/2016	6:32 PM	5.145	0.202559055	17.05
12/3/2016	12:35 AM	5.142	0.202440945	17.05

3-IN SP | 3-IN 90 | 2-IN SP | 2-IN 90

The Erosional Flow Loop System is equipped with advanced monitoring systems that benefit from experimental continuity within areas of high erosional movement. The figures presented below provide an overall assessment of the experimental data that has been collected over several years, initializing in 2016 and finalizing in 2023. These figures illustrate the gradual exchange between the pipeline walls and the flow interaction of simulants and water. By conceptualizing the erosional degradation of the specified area, a 90-degree elbow with a 2-inch-long radius allows for higher accuracy of predictability and comprehensibility of the standardized safety limit before total replacement. According to the ASME standard, a nominal 2-inch pipe section should have a standardized thickness of 0.154 inches. It is worth noting that this measurement may vary among different companies due to manufacturing differences. The 2-inch-long radius elbow from which the experimental data was derived is slightly above the standardized thickness, at 0.1709 inches within the acceptable range of the nominal 2-inch diameter. Observing the gradual differences of consistent pitting interaction from the simulants of glass impact beads and abrasive sand within the fluid flow provides an opportunity to comprehend the overall trend of erosional degradation within the infrastructural system. The 90-degree elbow initiated with 0.1709 inches and finalized with 0.1460 inches, providing informational data on the consistent trend of the system and its specific design.

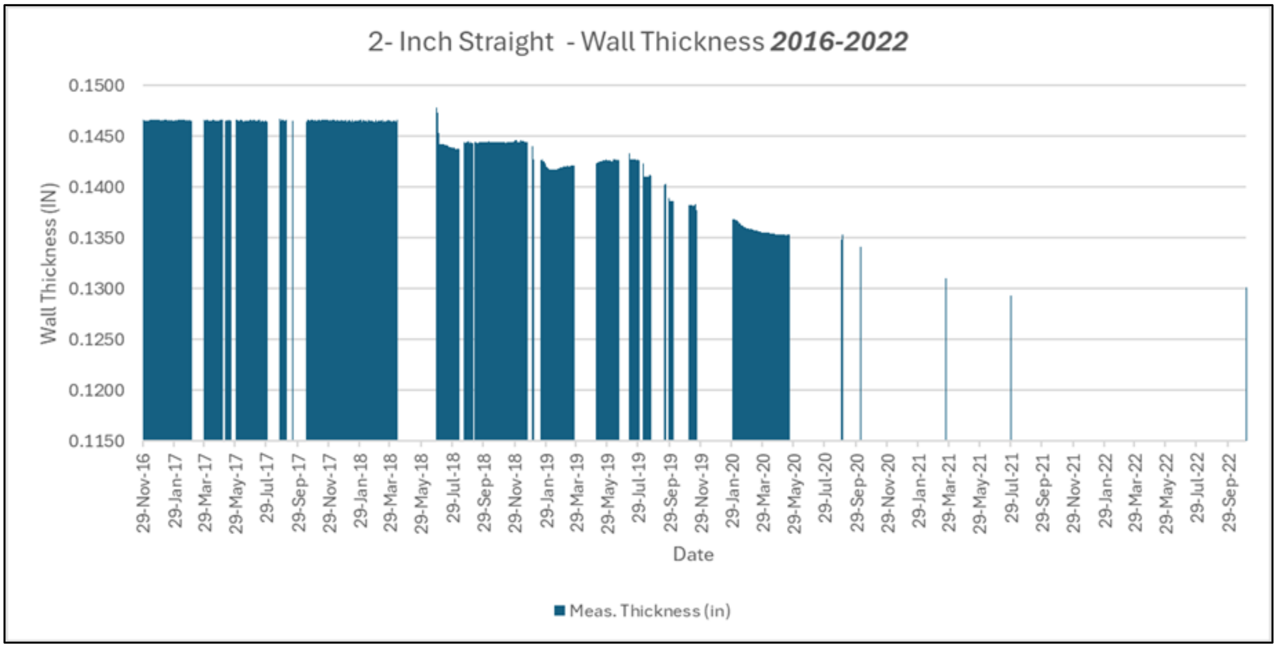

Figure 91. Pipe thickness changes at the 2-inch straight section of the loop as measured by the Permasense UT sensors.

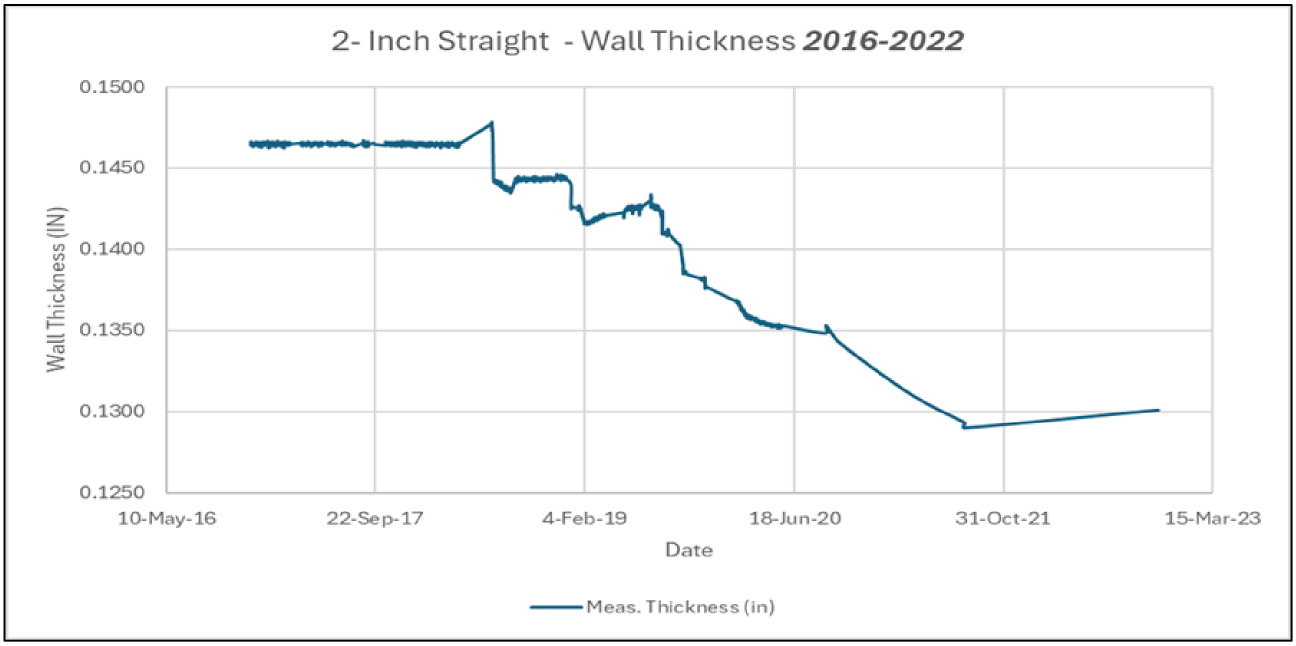

Figure 92. Comprehensive wall erosion in the 2-inch pipe section.

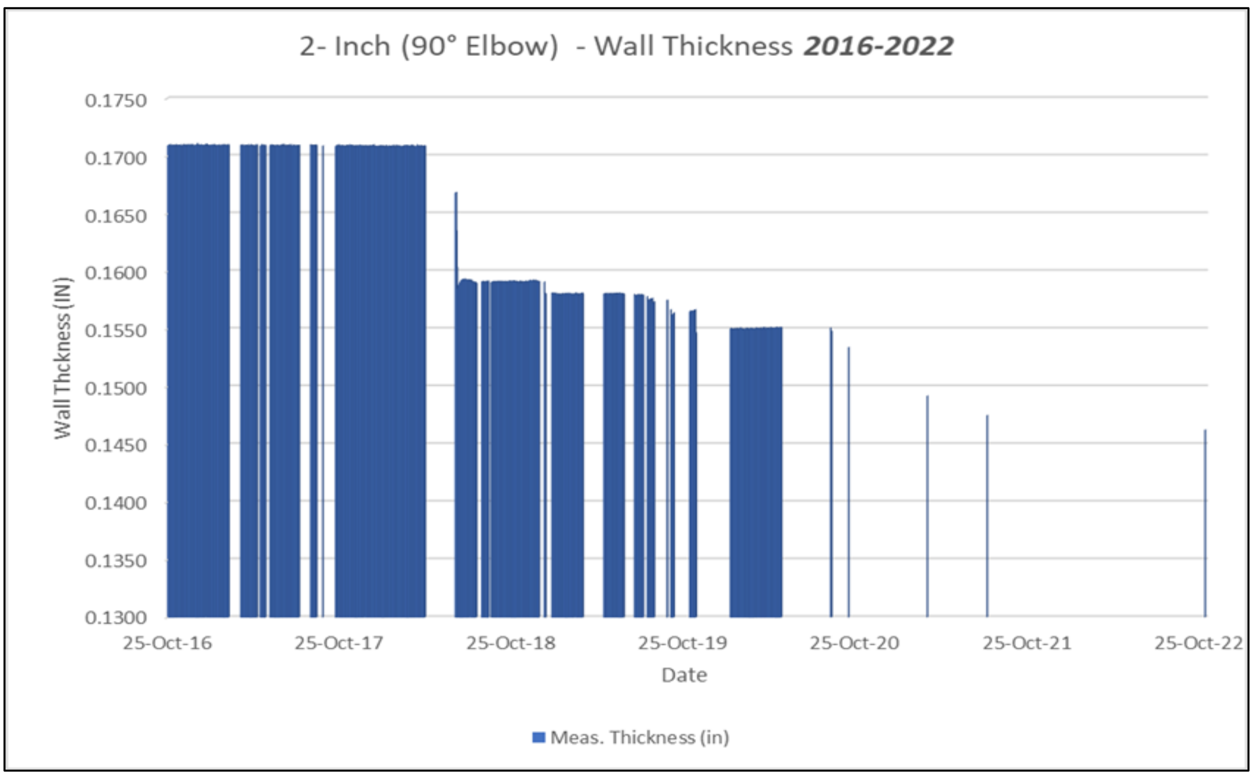

Figure 93. UT sensor readings for 2-inch elbow with test frequency.

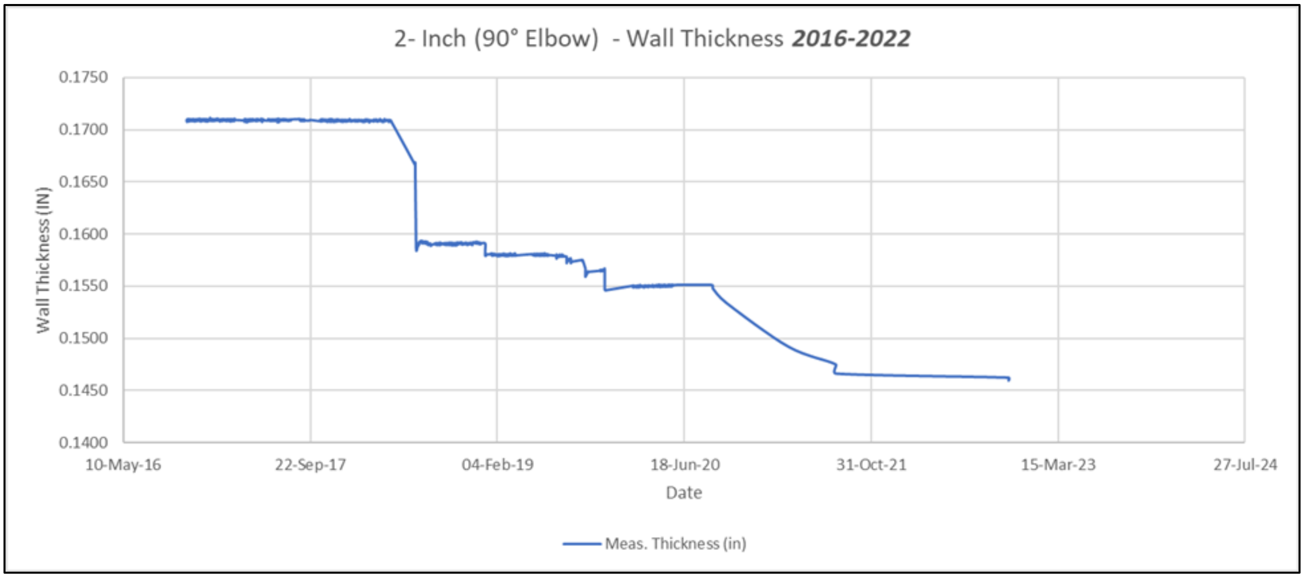

Figure 94. Erosion in 2-inch bend (elbow).

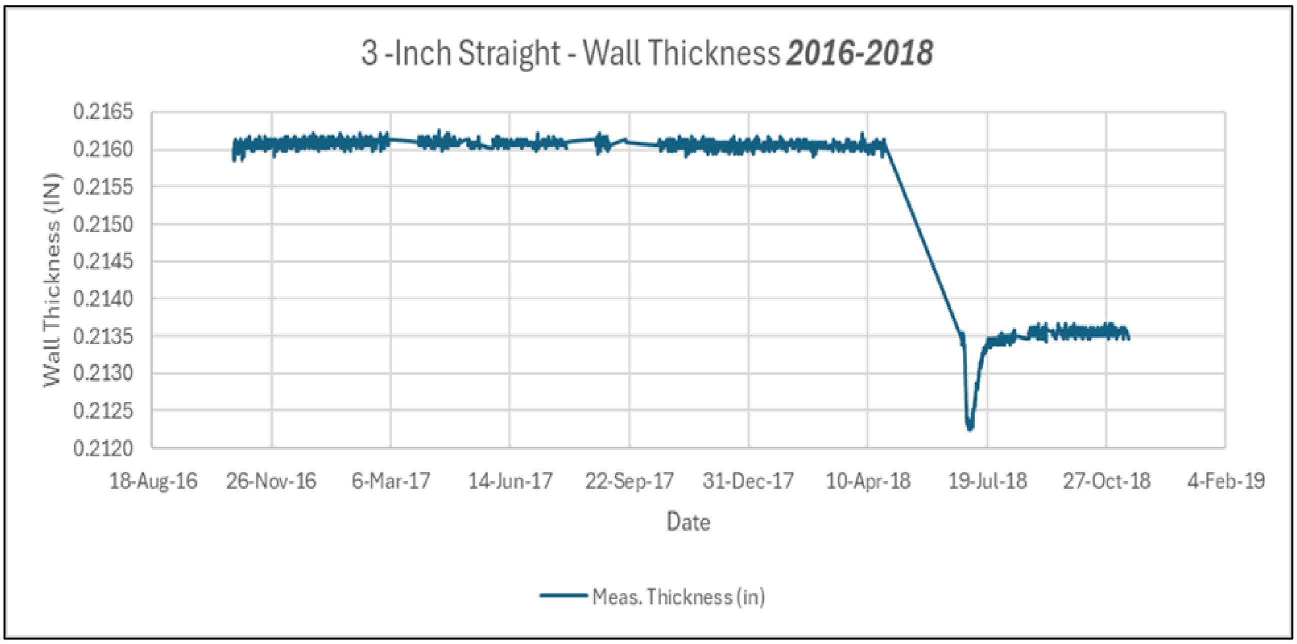

Figure 95. Comprehensive erosion in a 3-inch straight section of the pipe.

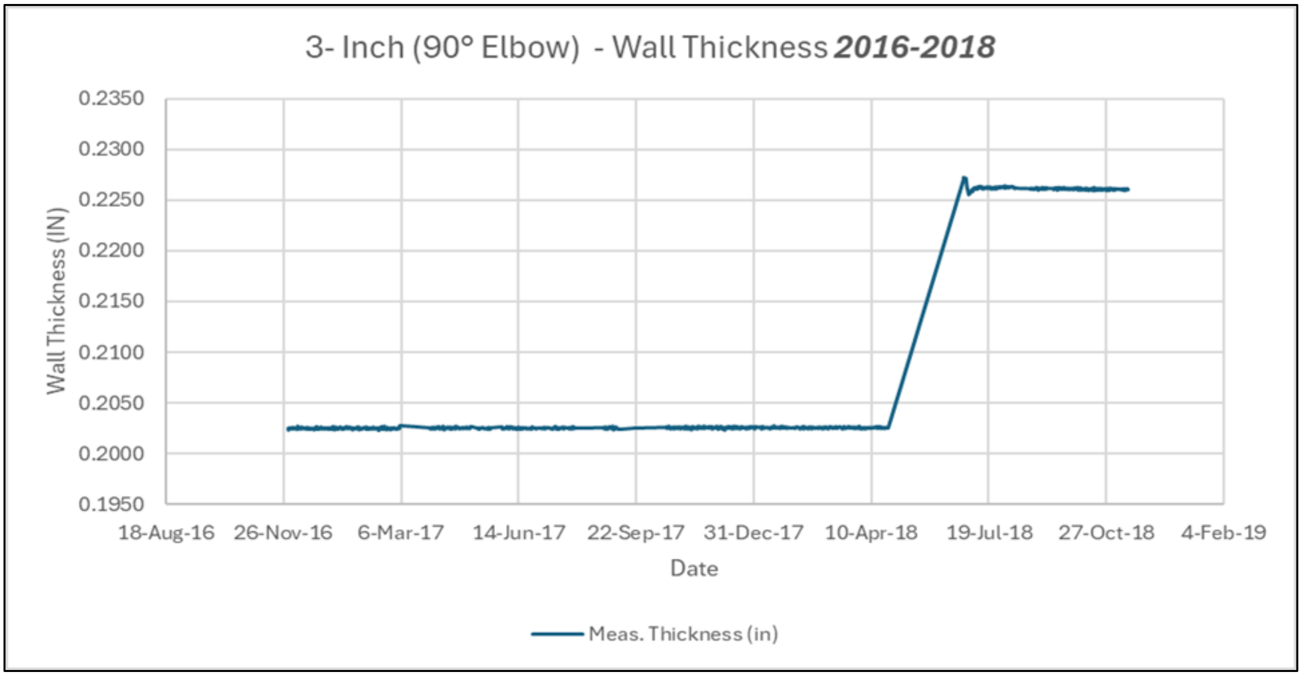

Figure 96. Erosion in a 3-inch elbow depicting sediment agglomeration at the bend.

The results have been analyzed to depict the erosion in pipes for both thickness changes and temperature changes. The analysis techniques include correlation, box plots, daily averages and trends, scatter plots with trend lines, and heatmaps. Some of the sample analysis results are shown in the figures presented next.

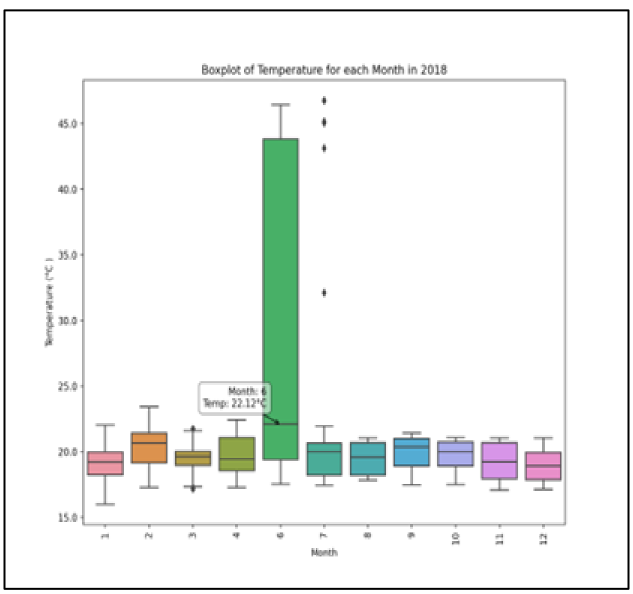

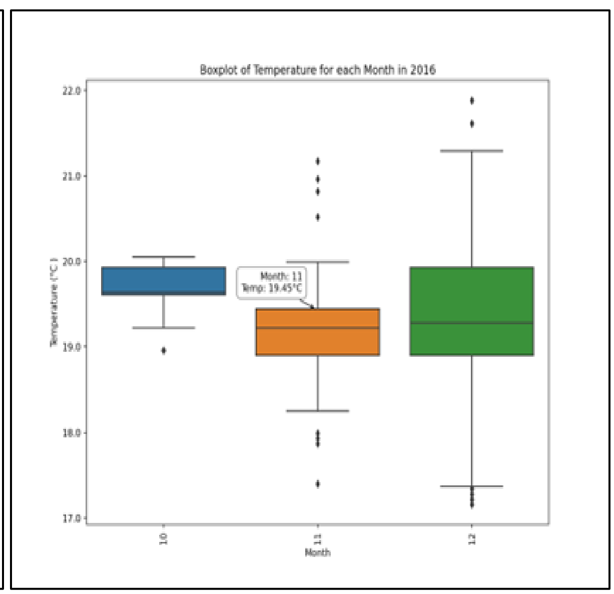

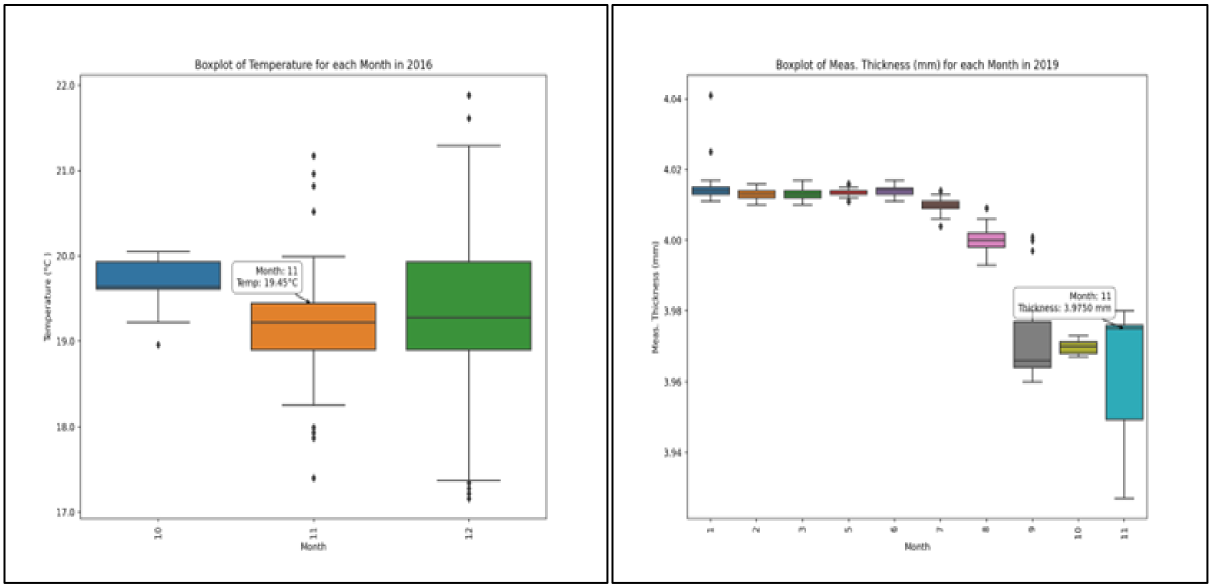

Figure 97. Box Plots for data analysis - temperature (top) and thickness (below).

As an example, the box plots for temperature are shown in the figures above, depicting temperature rise in June for the year 2018 while the monthly box plots depict a few outliers in each month. Similarly, for the measured thickness change (erosion) in pipes, the box plots show consistent thickness with minor outliers in November and December for the 2016 sample data set, while for the year 2019, they show consistent thickness from January to August, a significant drop in September, and increased variability in September and November.

Subtask 19.1.1: Conclusions

The real-time particle erosion effect on the SRNL coupons has been verified and validated on an engineering scale test bed using a combination of sand and glass replicating SRNL's DWPF glass frit. Experimental results showed much less change in erosion in stainless steel when compared to the carbon steel coupons. The integrity assessment of the pipe loop resulted in drastic changes in the carbon steel sections, particularly the elbow joints. The data for several years was integrated and analyzed using databases to provide useful conclusions.

Subtask 19.1.1: References

1. Aravelli A., McDaniel, D., Davila, C., "Real-time Erosion-Corrosion Detection in Waste Transfer Pipelines using Guided Wave Ultrasonic Sensors", Proceedings of the Waste Management Symposia 2018, Phoenix, AZ, March 18-22, 2018.
2. Aravelli, A., Thompson, M., McDaniel, D., Krutsch, M., McNeilly, M., Imrich K., Wiersma B., "Advanced Fiber Optic and Ultrasonic Sensor Systems for Structural Health Monitoring of Pipes in Nuclear Waste Sites", IMAPS 52nd International Symposium on Microelectronics (IMAPS), Boston, MA, Sep 30-Oct 3, IMAPS (2019).
3. https://srnl.doe.gov/tech_transfer/tech_briefs/SRNL_TechBriefs_UltrasonicThicknessMassLossMeasurement.pdf.

4. Aravelli, A., McDaniel, D., Thompson, M., Imrich, K., Wiersma, B., "Erosion-Corrosion Detection in Carbon Steel Pipe Loops using SRNLs Thickness and Mass Loss Measurement Coupons", Waste Management 2020 Conference, Phoenix, AZ, March 2020.
5. https://www.olympus-ims.com/en/shop/item/269-productId.570437480.html
6. Thompson, M., McDaniel, D., Wiersma, B., Aravelli, A. "Structural Health Monitoring Technologies for Wear and Anomaly Detection in Nuclear Waste Transfer Systems", Waste Management 2021 Conference, Phoenix, AZ, March 2021.

Subtask 19.1.2: Caustic Simulant Testing using the Bench Scale Flow Loop

Subtask 19.1.2: Methodology

The purpose of this subtask is to test and demonstrate that the SRNL coupons could provide static and dynamic methods for collecting corrosion rates from pipelines using stainless steel and carbon steel coupons. For this, a bench scale loop was custom designed and installed for testing replicate caustic simulants with various concentrations. The recipe for the salt solutions was prepared by SRNL scientists and transmitted to FIU for testing in the bench loop [1]. Static testing was conducted by immersing the coupons in bottles with 2, 4 and 6 Molar salt solutions, while the dynamic testing is conducted by placing the bench scale loop in a fume hood.

Past years' work included construction of the caustic bench loop and initial loop validation experiments using the 2M caustic solutions. This year's work includes:

- Evaluation of the coupons under 2, 4 and 6 Molar solutions – Experiments and data analysis.
- Bench loop troubleshooting and pump repair.
- Thermal effects on the pipe loop.

Subtask 19.1.2: Results and Discussion

FIU Year 4 Scope

In Year 4, the caustic simulant testing with new coupons obtained from SRNL will be conducted using both 2M and 6M concentrated salt solutions. Results obtained from the old coupons will be compared to those with new coupons for 2M salt solutions.

For the first quarter, testing with 6M salt solutions was initiated with the new coupons. As the experimental activity began, it was found that the loop was leaking, hence it was disassembled for troubleshooting. The pump sealant and rings had apparently failed and were therefore repaired. It was also observed that the pipe components were extensively corroded, and salt deposits were found at the bottom of the pipes. A cleaning schedule has therefore been arranged and rust removal solutions are being procured to clean the pipe loop prior to restarting the chemical testing. Some of the pictures from the loop repair and rust in the pipes (borescope images) of the dismantled loop are shown below. Upon repair and reassembly of the chemical loop, the 6M chemical testing will resume.

Figure 98. Borescope images of corroded internal structure of the pipe loop.

Figure 99. Disassembled loop for troubleshooting and cleaning.

This subtask mainly consisted of data collection and development of a database for both static and dynamic conditions for the chemical corrosion results. The lab work also included cleaning the chemical pipe loop for corrosion and reassembling the components and SRNL test coupons into the test section and beginning the 6M salt simulant testing. Additionally, efforts were put to initiate the writeup for a journal paper using the static coupon test data.

Informational data on the concept of chemical corrosion has been collected from both dynamic motions within a loop system and static submersion conditions. Varieties of structural formation of the materials, primarily carbon and stainless steel, were being used to manufacture the mass-loss coupon properties. Table 6 catalogs all current informational libraries of the data accumulated over recent years, focusing on the principles of statically submerged experiments, and organizing data based on years, visually representing the system's reaction to consistent contact with acidic salts (6M, 4M, or 2M). Experimental Weight Values provide the measurement and overall change of the weight of the coupons, either stainless or carbon steel, along with the rate at which the acidic salt reacts with the properties of the materials. Present data are being implemented into a new "Saturated and Dry" system providing consistent and factual weight measurement. Ultrasonic transducers have been recently implemented to accurately measure thickness at the coupons' tips due to their specific design. A new addition to the experimental values is the height measuring experiment, which verifies the thickness change of the tips and provides a standardized background to support the data information of the weight and thickness.

Table 6. Data Analysis Baseline Representing Collected Data Types

Data Information	Date (Years)	Description
Experimental Weight Values	2023-2024	Weight -Loss Experimental Values - (May 2023 to Current)
Averages of the Weight Values	2023-2024	Averaging the Weight-Loss Values - (May 2023 to Current)
Experimental Analysis Results	2021-2024	Gathering all the Weight Loss Values (2021 to Current)
Ultrasonic Sensor Data	2023-2024	Mass Loss Coupons - Ultrasonic Transducer Monitoring
Height Measurement	2024	Mass Loss Coupons - Height Loss Measurement

The dynamic motion of acidic salt is observed by utilizing the Chemical Corrosion Loop system, which furnishes valuable data for comprehending the flow dynamics and reactions within pipe walls. To enhance the system's performance, its design has undergone modifications and refurbishments, with a primary focus on restoring the inner surface to the optimal conditions. Employing meticulous procedures involving component immersion and static surface adhesion methods has effectively eradicated rust and salt deposits. Application of the biodegradable Evapo-Rust within statically submerged pipe components has been applied to clean them. In the image below, visual corrosion and debris of acidic salt are evident within the reducer/expander's threads and surface. Following 24 hours of submersion in the evapo-rust solution, the pipe components were gradually restored to their original metallic surface as evident in the right picture. These small-scale experiments on variations of carbon or stainless-steel formation have paved the way for the product's application within the inner surface of the pipe system without conflict.

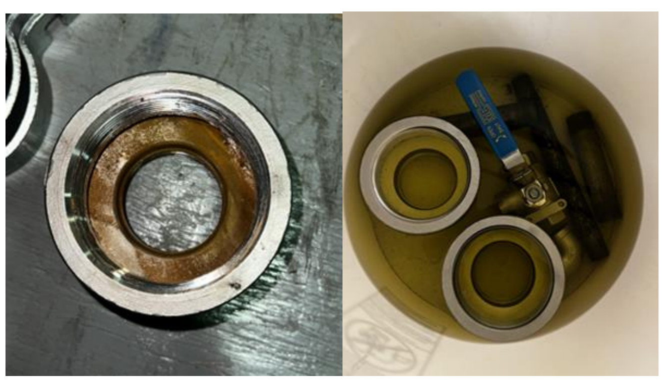

Figure 100. Pipe component cleaning between tests.

The following figures show the gradual change in the metal surface over time during the chemical simulant and the rust removal process to clean the pipe for the next iteration of testing. The figures illustrate the inner surface of the system after multiple cycles of 6 Molar solutions, the process and effectiveness of the rust remover on pipe component walls, and the severe maintenance required to restore the pipe system to optimal condition.

Figure 101. Chemical corrosion from Phase I testing (left and center) and clean pipe component (right).

As the conditions of the inner surface were met, the next step of the procedure was to modify the system's design to enhance the efficiency and comprehension of the corrosion damage of the fluid flow. Integrating an improved 3-inch pipe section sourced from SRNL marks a pivotal step toward improving the loop system's overall efficiency and reliability for the monitoring system. The figures below visually document the installation and final assembly of the newly integrated pipe section. The left figure illustrates the installation of the updated structure of carbon steel mass-loss coupons among the pipe sections. This revised component version includes three coupons on the upper surface, one at the bottom surface, and a new inclusion on the side surface, enabling a comprehensive assessment of corrosion damage as the flow expands and contracts within the component.

Figure 102. SRNL coupon assembly and loop testing.

Initial results of chemical corrosion with deposits on the SRNL mass loss coupons are presented in the figure below. It shows results of the five new mass-loss coupons after a singular experiment of continuous cycle motion of the acidic solution. These images will be the foundation for understanding corrosion development within the pipe system's walls.

Figure 103. Chemical corrosion on the SNRL coupons (posttest condition).

During this performance period, chemical simulant testing on the bench scale loop with 6M caustic solutions was completed. UT sensor data, temperature data, thickness changes, and visual borescope image data have been collected. The health of the pipe loop under caustic stressors is currently being evaluated. Results obtained are being drafted to submit the report deliverable. Images below show the caustic effect of the SRNL-developed 6M salt solution on the pipe's internal walls and the coupon surfaces.

Figure 104. Pipe wall damage near the expander (left) and wall damage and Coupon 1 hole (right).

Figure 105. Wall damage near Coupon 4 hole (left) and wall damage with chemical solution in pipes (right).

In the figures above, the wall damage is shown at various locations. These locations are near the reducer/expander and the SRNL coupon hole locations. It is evident that the wall damage due to caustic 6M solution is extensive on the carbon steel walls, while the stainless-steel reducer section is clean with almost no corrosion. Also, the section near Hole 1 shows a green surface which could be biological corrosion, compared to the black surface near Hole 4 (excessive chemical deposits on the carbon steel material). The last picture shows the borescope image with partially flooded pipes with 6M salt solution near the expander reducer section in the pipe loop.

Figure 106. 6M caustic test results for the SRNL coupons (Coupons 1 through 5 - left to right).

In addition to the borescope images in the pipe loop, the coupons removed from the loop were also checked for the surface damage due to caustic corrosion. The coupon images shown above indicate various levels of corrosion damage based on the location of the coupon in the loop. All coupons have shown greater area of corrosion (average surface area) except for Coupon 4 which was located very near to the reducer. It might be due to the dead region in the flow direction where there was almost no contact between the fluid and the coupon surface. Hence the results are in complete agreement with the physics of the loop and further validate the corrosion is caused due to the simulated chemical waste in the loop.

The research efforts conducted under this task with the 6-molar caustic solution were completed and the data derived is analyzed. Analyzing these values for wall-thickness degradation, thermal distribution, and localized Mass-Loss coupons will aid in determination of a realistic factor of corrosion deterioration within the pipeline systems. The Bench Scale Loop system currently holds a minimal supply of a 6-molar solution, which is statically maintained within the components to investigate the effects of the solution even if the system is nonoperational. Another situation that occasionally occurs is minor leakage, specifically in conjunction with the vertical straight section and the supply tank. This minor solution deteriorates the external surface of the vertical section resulting in salt crystallization, as shown in the figure below. The system still contains the caustic solution internally and salt deposits can also be found in certain regions. Maintaining both a visual inspection and ultrasonic reading where the salt is contained can help determine the rate and chemical reaction between the solution composition and the carbon steel characteristics.

Figure 107. External minor leakage salt formalization and rust deterioration.

Figure 108. Internal salt deposit within sectional regions.

Evaluating all the characteristics that comprehensively promote corrosion at an increased rate is undeniably valuable. The fundamental areas of corrosion offer quite a complicated and unpredictable pattern for the solution of the appropriate corrosion rate that inhabits the Bench Loop system. One of the significant factors that occasionally initiates accelerated rates of corrosion to degrade the surfaces can be through thermal influence. Noticeably, it is essential to recognize that the thermal capacity of such a minor-scale loop system will not exceed remarkable amounts of thermal distribution but can influence a chain of chemical reactions to occur, accelerating the rate of material deterioration as the 6-molar solution flows through the system. Figure 22 illustrates the interested localized regions that propose a thorough analysis of the overall thermal distribution.

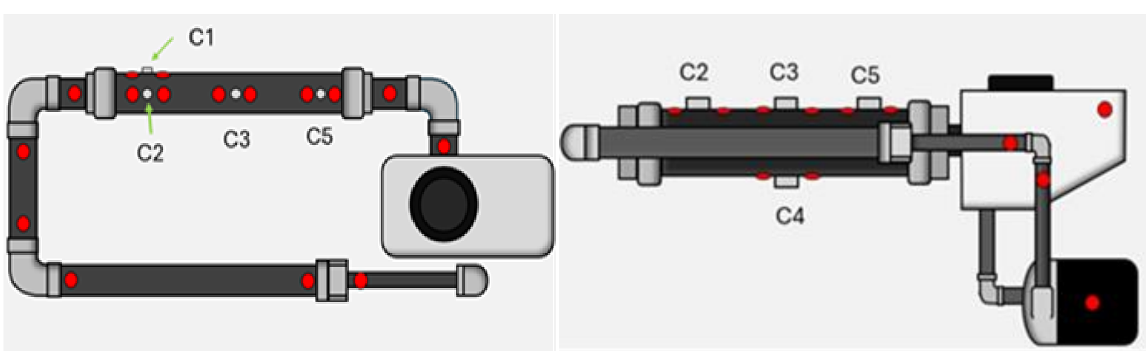

Figure 109. Localized regions of thermal analysis for the Bench Scale Loop System.

The selected regions were decided from a theoretical stance, proposing a "Before" and "After" thermal distribution between each component to convey a proper analysis of the loss of kinetic energy established by the escalated frictions of the solution flowing continuously. This continuous cycle can, in effect, influence the chemical response of the caustic solution and increase the corrosion effects on the surfaces, degrading the material at an accelerated rate and causing more unusual ruptures or leakage to occur. Table 7 demonstrates the differential temperature that the system embarks on and the impact that appears in the surrounding areas of the Mass-Loss coupons, providing guidance and solidification for the explanation of higher corrosion accumulation and material degradation of each localized coupon area.

Table 7. Thermal Gradient Analysis - Mass-Loss Coupons Region

	Avg of 10:00 AM - (°F)	Avg of 11:00 AM (°F)	Avg of 12:00 PM (°F)	Avg of 1:00 PM (°F)	Avg of 2:00 PM (°F)
(1) - ML Coupon Before	68.29	101.46	114.04	120.79	121.23
(1) - ML Coupon After	68.2	103.91	116.03	121.83	122.69
(2) - ML Coupon Before	68.4	103.7	114.88	121.5	123.48
(2) - ML Coupon After	68.27	104.2	115.65	121.72	123.25
(3) - ML Coupon Before	68.7	104.16	115.99	121.82	123.46
(3) - ML Coupon After	68.21	104.43	116.23	122.21	123.9
(4) - ML Coupon Before	68.28	106.21	117.84	123.46	125.32
(4) - ML Coupon After	68.28	106.03	117.79	123.14	124.92
(5) - ML Coupon Before	68.21	104.69	116.67	122.61	124.48
(5) - ML Coupon After	68.11	104.77	116.89	122.39	124.58

Although the thermal process was effectively portrayed by utilizing an Infrared Thermometer, it did impart complications when forming an appropriate reading, explicitly having the time to balance both wall thickness reading and thermal analysis while the system was operational. For this reason, advancing the monitoring process is a necessary obligation to effectively convey all the required thermal disruptions and increases that may occur. Utilizing a microcontroller will automate the process, maintaining a consistent thermal analysis of all sectional regions in the system, and applying a thermal K-type coupling will deliver a more accurate response to the heat transfer gathered from the external surface of the pipe components. These will be the following steps to both improve the accuracy of detailing the effects of corrosion behavior and the precise requirement for an overall system analysis.

Subtask 19.1.2: Conclusions

The effect of simulated caustic solutions replicating the chemical composition of HLW at Hanford and Savannah River sites is studied on waste transfer pipes. Two materials have been considered for corrosion due to the varying molar concentrations of the chemical simulants. Immersion experiments were conducted using SRNL's patented coupons. Visual inspection, weight change and thickness changes are quantified. Findings of the research summarize that carbon steel underwent high levels of caustic corrosion with 6M salt simulants over a period of 3 years. Results of static testing will be shared with SRNL for future material and design considerations. Based on the static test results, bench loop testing will be conducted with high concentrations of the chemical simulants and SRNL obtained new coupons.

Subtask 19.1.2: References

1. Wiersma, B. J., Peters, T. B., Poirier, M., "Simulant Recipes for Flow-loop Testing at Florida International University", SRNL-L3000-2020-00017, December 18, 2020.
2. https://www.olympus-ims.com/en/shop/item/269-productId.570437480.html\
3. Aravelli, A., McDaniel, D., Thompson, M., Imrich, K., Wiersma, B., "Erosion-Corrosion Detection in Carbon Steel Pipe Loops using SRNLs Thickness and Mass Loss Measurement Coupons", Waste Management 2020 Conference, Phoenix, AZ, March 2020.
4. Aravelli, A., Thompson, M., McDaniel, D., Krutsch, M., McNeilly, M., Imrich K., Wiersma B., "Advanced Fiber Optic and Ultrasonic Sensor Systems for Structural Health Monitoring of Pipes in Nuclear Waste Sites", IMAPS 52nd International Symposium on Microelectronics (IMAPS), Boston, MA, Sep 30-Oct 3, IMAPS (2019).
5. Thompson, M., McDaniel, D., Wiersma, B., Aravelli, A. "Structural Health Monitoring Technologies for Wear and Anomaly Detection in Nuclear Waste Transfer Systems", Waste Management 2021 Conference, Phoenix, AZ, March 2021.
6. A. Aravelli, D. Sinnott, R. Piloto, D. McDaniel, L. Lagos, B. Wiersma, "Simulant Based Particle Erosion and Chemical Corrosion in HLW Pipe Components", Waste Management 2023 Conference, Phoenix, AZ, March 2023.

Subtask 19.1.3: Automated Erosion and Corrosion Detection using fluid flow dynamics and advanced data analytics

Subtask 19.1.3: Introduction

Erosion and corrosion testing in the flow loop provides adequate data for developing automated erosion and corrosion detection process; and condition monitoring of the HLW pipe system components. This subtask investigates the use of experimental and flow simulation data to develop advanced algorithms for preventive and predictive maintenance of the tanks and transfer lines. This year's scope of work included:

- Computational Fluid Dynamics (CFD)-based flow model development in pipe components and loops using COMSOL and ANSYS.
- Machine learning model development for erosion corrosion detection in HLW transfer pipes.

Subtask 19.1.3: Methodology

This subtask involves CFD simulations for erosion corrosion detection and model development in data analytics. In the first quarter, fluid flow simulations using COMSOL software were conducted by developing corrosion models for particle flow in U-bends of the pipe sections. CFD models with turbulent flow conditions require high processing capacity of the system. Hence, a new Intel I7 processor was procured and integrated with the existing system to conduct high fidelity FEA simulations. Also, a new version of COMSOL (V6.2) was installed which significantly reduced the time for simulations. Using the new processor and the latest version of the software, flow simulations for water and sand particles were conducted for 1-inch diameter pipe bends (U-bends) with three methods of erosion. Details of the pipe section included:

- Nominal Diameter = 1 inch
- Outer Diameter = 1.315 inch
- Inlet Velocity = 16.5 m/s
- Mass Density of the Surface – 7,860 [kg/m^3] for the material (iron)
- Particle Density – 2,850 [kg/m^3] for the material density solid particles (silicon carbide).
- Particle Entrance Surface Diameter = 1 inch

Subtask 19.1.3: Results and Discussion

The pipe model, fluid flow in the pipe, and the particle flow simulation results are shown in the following figures.

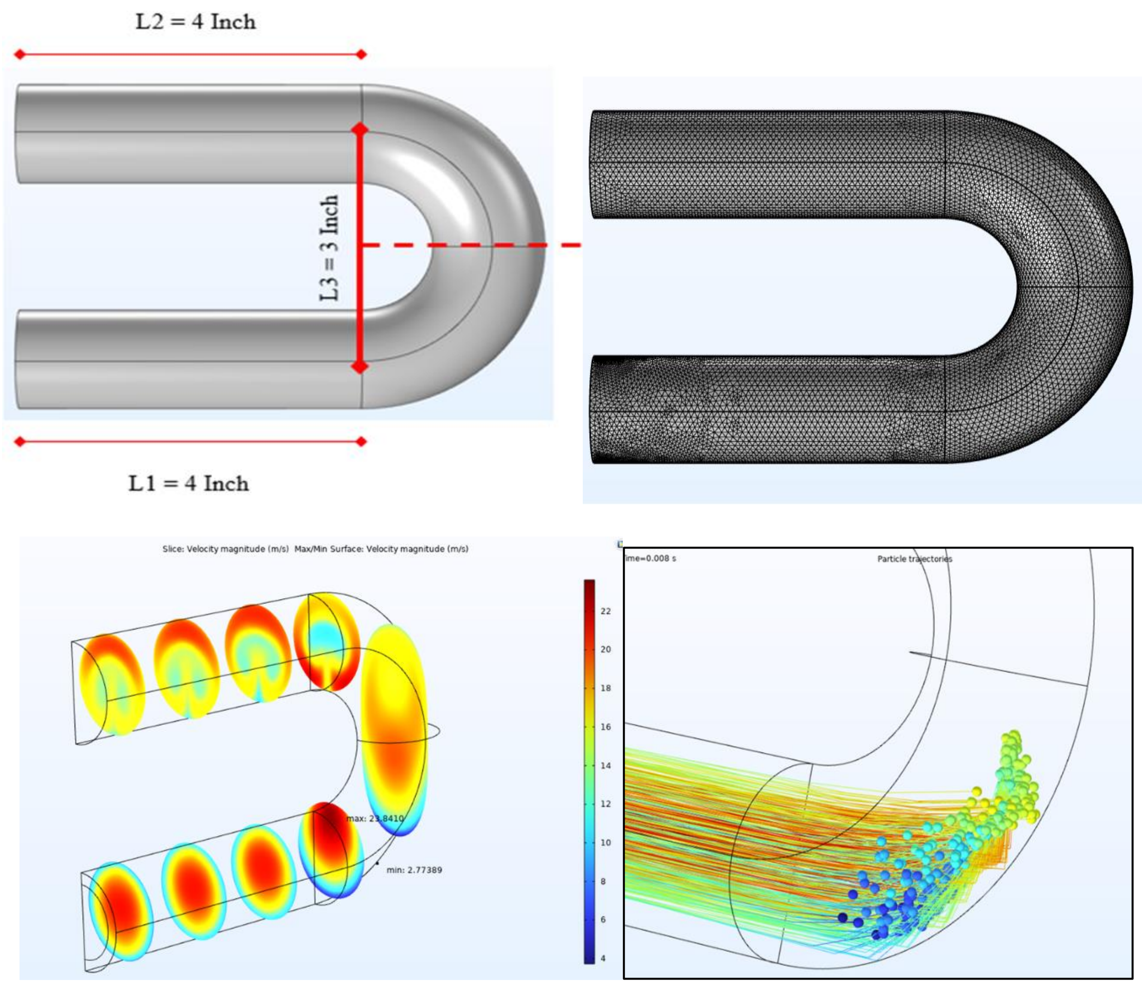

Figure 110. Pipe section (U-bend) simulation phases, including the CAD model, FE mesh, fluid flow and particle trajectories.

Understanding the dynamic motion of the fluid flow has given a more evident approach to estimating the areas of high pressure, high velocity, and the formation of dead zones. This approach of utilizing a simulation program allows for the manipulation of several geometries and the prediction of how the fluid flow would react in each case. Despite continuous improvements to optimize the accuracy and precision of these models, challenges persist, particularly in setting appropriate inlet velocity, managing pressure at the model's entrance, and precision with the mesh controls. Computational efficiency and mesh accuracy become increasingly crucial for precise flow predictions as we incorporate more informational data, such as velocity, pressure, and particle behavior. Figure 24 below depicts a carbon steel, schedule 40, with a 1-inch nominal diameter of a standard 180-degree bend elbow. While the specific geometry is not currently utilized within our system, its comprehendible usage is to attain the limitations and difficulties that the trajectories of the particles form with the change of design. The streamlined velocities provide an appropriate formation of the interaction of the fluid and boundary walls of the geometry. The turbulent flow model, specifically the k-w (spf) model, was chosen over the standard turbulent flow k-E (spf) model due to its more accurate mathematical calculations and consideration of wall interaction. The velocity inlet is maintained at 16.5 m/s for future comparison with other geometric models. Similarly, a static pressure of zero Pa is applied at the outlet for consistency in boundary conditions across simulations.

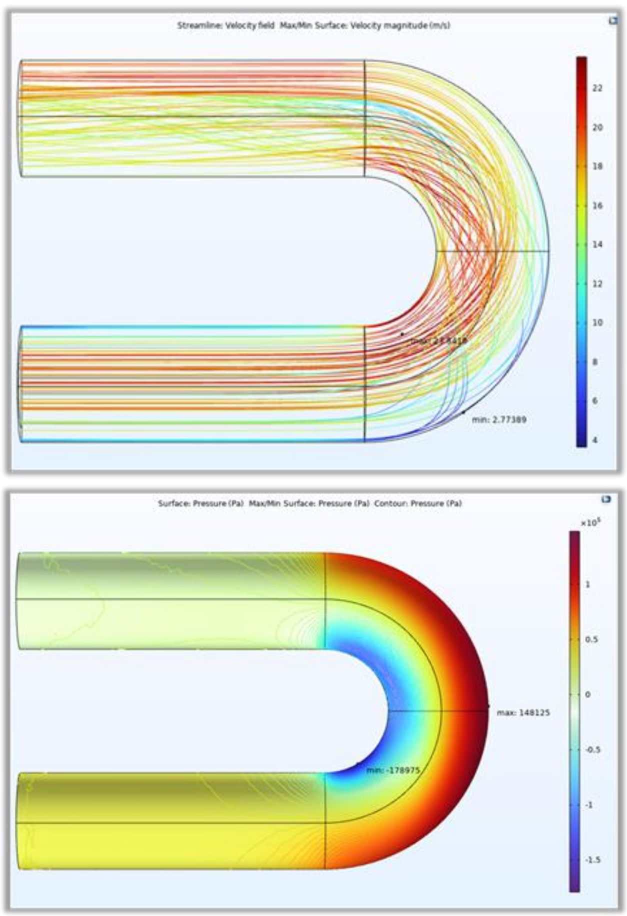

Figure 111. Pipe with U-bend - Flow velocity and surface pressure distribution.

After COMSOL simulates and mathematically approximates the geometry influencing the fluid flow, the next step is incorporating particle behavior within the turbulent flow. The inclusion of particles allows for approximating the areas that receive high erosional damage and estimating the erosional rates at which the walls become unsuitable for usage. The settings and formation of the particle are standard COMSOL particles, which is Silica Carbide with a density of 2800 kg/m^3 and diameter of 1.7*10^-4 m. These specific particles and size diameters are used to identify errors and compute a reasonable model for erosional damage. The figure below depicts the experimental values of the particle's trajectories and interaction with the boundary walls of the geometry. The three visual representations are of different erosional models that mathematically compute the erosional damage at varying rates. The left figure illustrates the Finnie Model, estimating the material removal rate from a surface due to particle impaction. The middle figure depicts the DNV Model, which considers the ratio of mass lost by the surface to the mass of incident particles, factoring in material properties and impact angle. The right figure showcases the E/CRC Model, which accounts for the ratio of mass lost from the surface to the mass of incident particles while also considering material hardness, particle shape, and impact angle.

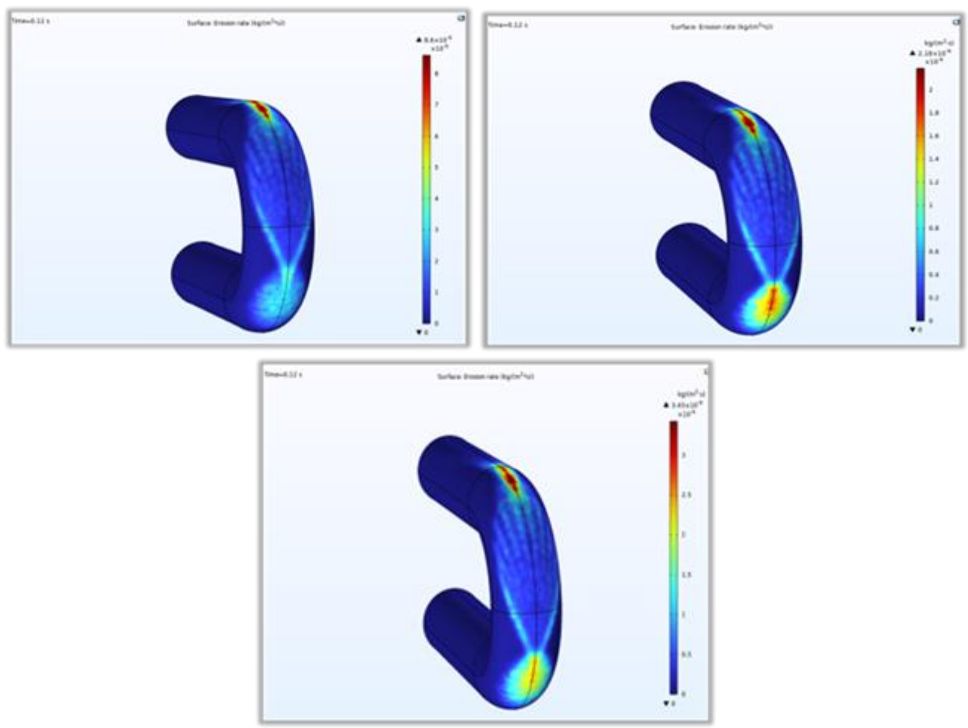

Figure 112. Erosion models depicting "hot spots" for erosion with particle impact at the bends with Finnie model (left), DNV model (middle) and E/CRC model (right).

The standard COMSOL particle settings are derived from practice examples involving a 90-degree Long Radius elbow, serving as an introductory framework for studying particle trajectories and understanding erosional rates. Its structural benefit is that it allows for a basis for the model and a standardized measurement of the erosional rate. The primary objective in simulating particles across variable pipe components is to accurately depict their response to realistic conditions, such as those encountered in the Erosional Flow Loop System and the Chemical Corrosion Loop. Currently, the particles under interest are those found in the Erosional Flow Loop System: The Abrasive Sand (20/30) and the Glass Impact Beads (size B). Realistically, the data for each particle reaction was recorded to provide a basis for the erosion rate each particle causes on the system's walls. The experimental values of the particles were recreated on the 90-degree Long Radius elbow to compare the difference of erosional damage due to density and size diameter. Figure 25 below (left) demonstrates the erosional damage caused by standard Silica Carbide particles (density: 2800 kg/m^3, size diameter: 1.7*10^-4 m), utilizing the Finnie model for mathematical computation. Figure 25 below (center) visually represents the Glass Impact Bead (size B), 2500 kg/m^3 density, 600 microns/0.0234-inch diameter, to determine the erosional damage that the density and size of the particles create on the same geometry and model of computation. Figure 25 below(right) depicts the erosional damages induced by Abrasive Sand (20/30), featuring a density of 1608.1 kg/m^3 and a diameter of 1270 microns (0.05 inches), providing insights into the effects of material and size variations of each particle.

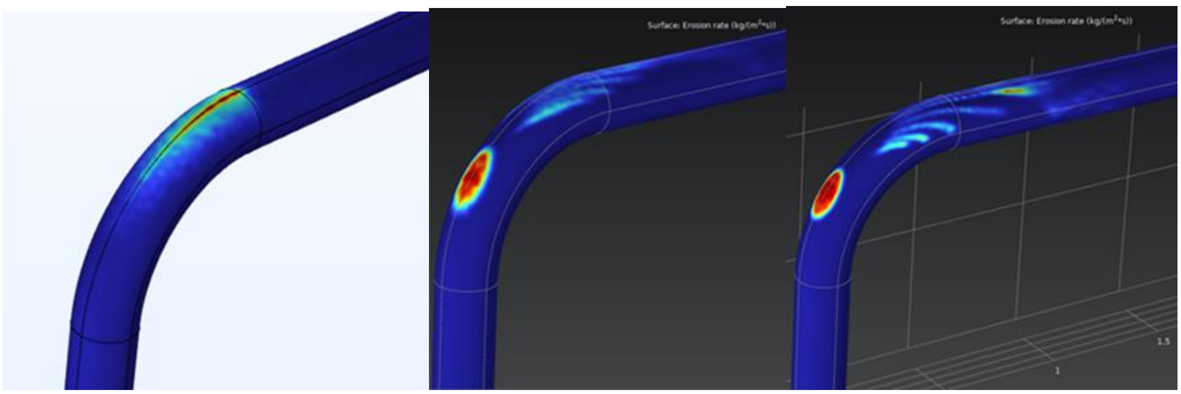

Figure 113. Erosion results with COMSOL models for the elbow (Finnie model (left), DNV model (center) and E/CRC model (right).

Finally, the research work done on this task resulted in an oral presentation by the task lead and a poster by the DOE Fellow at the 2024 Waste Management Symposia. The DOE Fellow supporting the task received an award for the Best Graduate Poster at the conference.

Under this subtask, the work continued to develop turbulent fluid flow models using FEA, considering cases such as U-bends and straight and elbow sections. The simulated CFD models were coupled with machine learning algorithms to predict erosion and corrosion-based pipe wear. COMSOL fluid flow models were developed for loop flow, and pipe erosion data generated with varying flow velocity (using simulations) was compared and verified with the experimental erosion data obtained from the testing in the lab. Erosion models were also developed using COMSOL. Some of the results are shown below, which depict special velocity distributions of flow in the pipe bend obtained using CFD. Intermediate velocities are predicted using the developed machine-learning models with interpolations. A comparative graph is also shown.

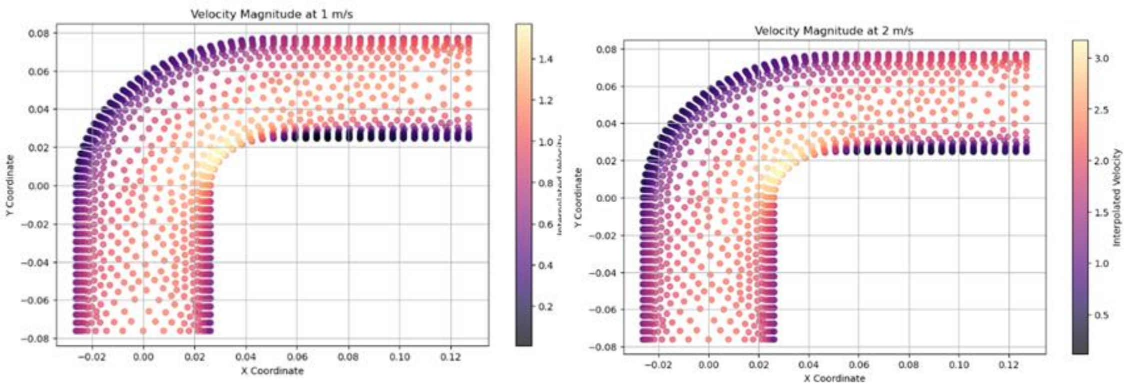

Figure 114. Spatial velocity distribution using CFD simulations (COMSOL).

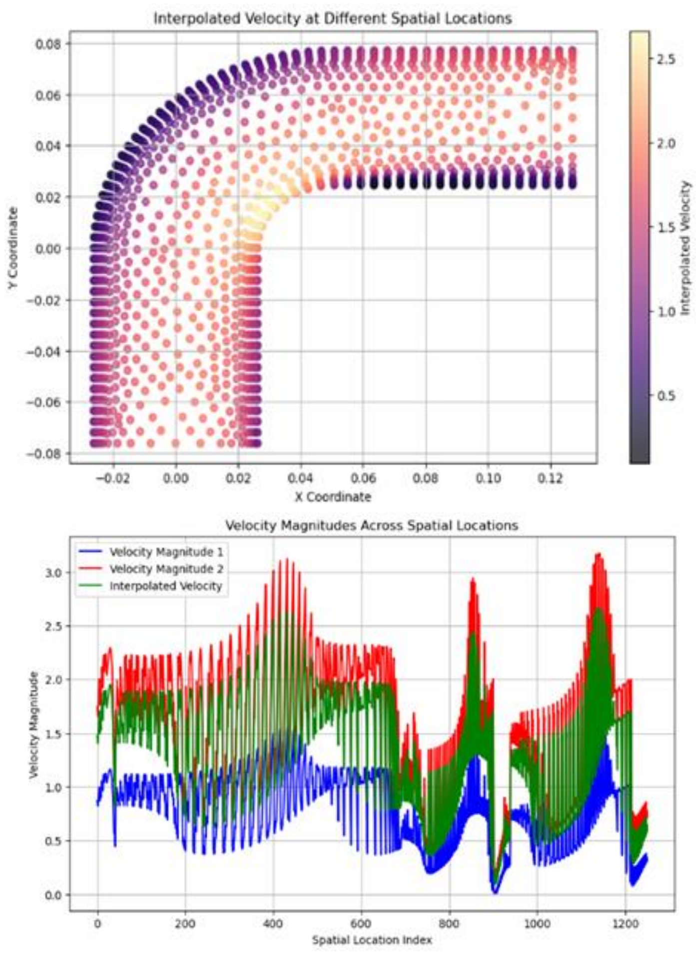

Figure 115. Interpolated velocities using machine learning models and comparison graphs.

One of the main objectives of an advanced computational fluid dynamic (CFD) analysis is to articulate the flow path of the fluid and comprehend the location that may have the highest rate of both erosion and corrosion impact. As previously mentioned, the locations of the thermal distribution are theoretically applied but do not emphasize the main areas where thermal heat is at its highest performance. To effectively portray the specific locations to set the sensor for the thermal distribution analysis, a scaled replica of certain sections of the loop system will be recreated to interpret both how the fluid interacts internally and the areas at which there is an immense temperate difference. Figure 28 illustrates the values and visual indication of thermal application using CFD simulation modeling.

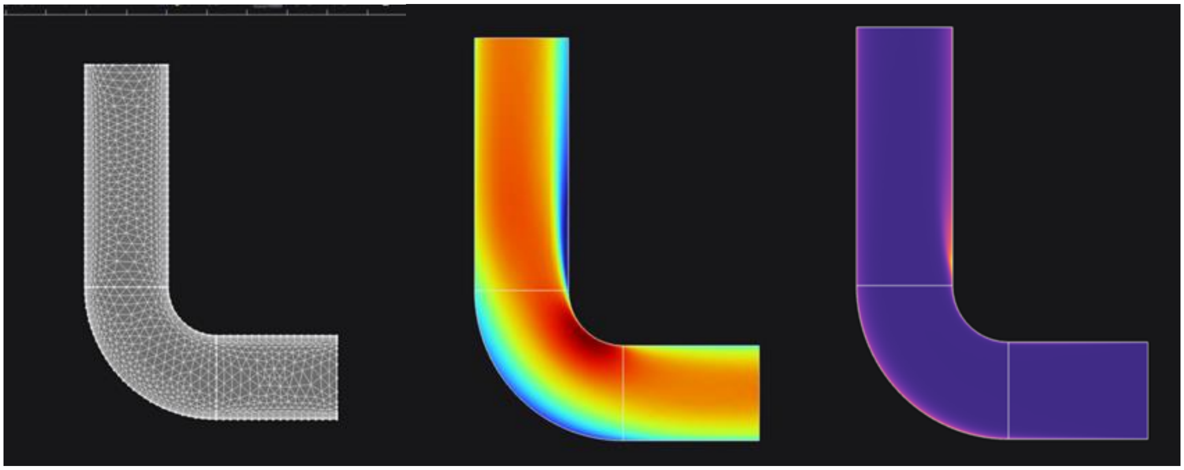

Figure 116. (a) Mesh Compilation, (b Velocity Fluid Flow, (c) Thermal Indication.

Subtask 19.1.3: Conclusions

Computational Fluid Dynamics (CFD) analysis was conducted to investigate the flow velocities and pressure changes in the pipe sections to identify hot spots (regions prone to high velocities/pressures). The research provides a basis to combine the CFD simulations with experimental results that can potentially be used to develop comprehensive realistic multi-physics-based models for flow in the HLW transfer process. The machine learning models developed using the particle erosion data can be used to predict erosion in pipes based on statistical methods. In the future, a comparative study of all simulant mixtures and their simultaneous effect can be investigated. This work can further be continued to examine the simultaneous effect of all simulants for more accurate erosion and corrosion prediction in the HLW transfer components, providing baseline data for infrastructure repairs and replacement as needed at several DOE sites.

Subtask 19.1.3: References

1. https://www.ansys.com/products/fluids/ansys-fluent
2. https://www.comsol.com/cfd-module
3. https://www.comsol.com/particle-tracing-module
4. Szegedy, C., Liu, W., Jia, Y., Sermanet, P., Reed, S., Anguelov, D., Erhan, D., Vanhoucke, V., & Rabinovich, A. (2014, September 17). Going deeper with convolutions. arXiv.org. https://arxiv.org/pdf/1409.4842.pdf
5. Tan, M., & Le, Q. V. (2020, September 11). EfficientNet: Rethinking model scaling for Convolutional Neural Networks. arXiv.org. https://arxiv.org/abs/1905.11946
6. Krizhevsky, A., Sutskever, I., & Hinton, G. E. (2012). ImageNet Classification with Deep Convolutional Neural Networks. NeurIPS Proceedings. https://proceedings.neurips.cc/paper_files/paper/2022/file/9f09f316a3eaf59d9ced5ffaefe97e0f-Paper-Conference.pdf

7. D. P. B. J. L. Kingma, "ADAM: A Method for Stochastic Optimization," in ICLR 2015, 2015
8. Y. An, X. Wang, R. Chu, B. Yue, L. Wu, J. Cui, and Z. Qu, “Event classification for natural gas pipeline safety monitoring based on long short-term memory network and Adam algorithm,” *Structural Health Monitoring*, vol. 19, no. 4, pp. 1151–1159, 2019.
9. K. Janocha and W. M. Czarnecki, “On Loss Functions for Deep Neural Networks in Classification,” *arXiv.org*, 18-Feb-2017. [Online]. Available: https://arxiv.org/abs/1702.05659. [Accessed: 09-Apr-2021].

TASK 20: CORROSION PROTECTION AND CHARACTERIZATION OF EM INFRASTRUCTURE

Subtask 20.1: Evaluation of Coatings for the H-Canyon Exhaust Tunnel

Subtask 20.1: Introduction

The H-Canyon is the only remaining chemical processing facility in America capable of reprocessing plutonium, highly enriched uranium, and other radioactive materials. The H-Canyon Exhaust (HCAEX) Tunnel used to contain and direct the exhaust air flow from the canyon chemical process areas to the sand filter system, where radioactive contamination is removed. After several structural integrity inspections of the HCAEX tunnel, mandated by mission requirements at the Savannah River Site, there is a great concern about the concrete structure degradation. Videos/pictures taken during inspections evidenced significant degradation of the interior concrete walls characterized by surface erosion exposing concrete coarse aggregates, rebars exposed in some tunnel sections and significant amount of concrete loss, all promoted by the aggressive environment inside the tunnel (primarily nitric acid vapors). The application of a protective coating on the degraded tunnel walls can mitigate and prevent further degradation, which constitutes the main goal of the investigation.

This is a multistage investigation including 1) the development and evaluation of aged concrete surfaces similar to the degraded HCAEX tunnel walls, 2) the identification and evaluation of potential coatings applied on the developed aged concrete surfaces, 3) the development and evaluation of a procedure and a robotic platform for the coating application and 4) the application (deployment) of the coating on the tunnel walls through the developed robotic platform.

Subtask 20.1: Objectives

The objective of this task is to investigate potential protective coatings that can be used to mitigate and prevent further degradation of the degraded concrete walls of the HCAEX tunnel. Concrete specimens with raw materials and mix design similar to the tunnel have been prepared and will be the substrate of the coatings. Potential coatings will be applied on aged and non-aged concrete surfaces similar to the tunnel degraded walls and further evaluated through accelerated aging tests at the laboratory. A comprehensive test plan for the evaluation of the coatings was prepared. After contacting several coating companies, FIU selected for the study various potential coatings including single and multiple layers with different compositions. Some of the potential coatings from different manufacturers, Carboline, Sherwin-Williams and Belzona, completed the evaluation. Also, another potential coating from Framatome company will begin the aging process and evaluation. A coating selection will be performed based on research findings. In line with the aforementioned objective, the following subtasks were executed to support the effort:

- Continue the evaluation of potential coatings through accelerated aging tests. The accelerated aging conditions will consider the worst-case scenario during the concrete aging experiments. Several variables of importance in the evaluation of the coating performance will be included in the study such as surface preparation, aging of the concrete surface and presence of rebar coating performance will be included in the study such as surface preparation, presence of rebar and others.

- Based on the preliminary results of the coating performance in aggressive environments, a ranking will be established. For this ranking, the results of various parameters under study will be considered such as visual inspection, failures degree, thickness, and others.

Subtask 20.1.1: Evaluation of Coatings through Accelerated Aging Tests

Subtask 20.1.1: Methodology

Based on lessons learned and results of the concrete aging process, the enhanced aging condition was selected for the accelerated aging of the coatings. The enhanced aging conditions consists of exposing the surface of the specimen to a 0.5M nitric acid solution. Once a week, the surface in contact with the acid solution is exposed to erosion by using a wire brush. This aging procedure combines the chemical and physical effect of the acid solution and the erosion, respectively. Concrete specimens, aged and non-aged and with and without embedded rebar will be used for the bench-scale testing. The abovementioned concrete specimens were the substrate for the evaluation of potential coatings.

Test plan

A factorial design of three variables at two levels was used leading to 8 different experiments. Table 8 below shows the test plan with the experiments for each coating. The single and synergistic effect of the variables were studied. The three variables under study are 1) surface preparation, 2) steel rebar presence and 3) aging of the substrate. Two levels of each variable were studied and represented in the table.

Four potential coatings, from different manufacturers Belzona, Carboline, Sherwin-Williams and Framatome were selected for the study. In previous reports, the results of the evaluation of Carboline, Sherwin-Williams and Belzona coatings were presented. In this report, the results of the evaluation of a polyurea coating system from Framatome company is presented.

Table 8. Test Plan for Accelerated Aging of Framatome Coating System

Test ID	F ID	**Aged/Non-aged surface**	**Surface Preparation (Yes/No)**	**Steel rebar (Yes/No)**
T1	FT1-1*	Aged	Yes	Yes
T2	FT2-1*	Aged	Yes	No
T3	FT3-1*	Aged	No	Yes
T4	FT4-1*	Aged	No	No
T5	FT5-1*	Non-aged	No	Yes
T6	FT6-1*	Non-aged	No	No
T7	FT7-1*	Non-aged	Yes	Yes
T8	FT8-1*	Non-aged	Yes	No

ID: identification, F: Framatome, *: there are three replicates for each test case and only “No 1” is represented in the table. For example, the replicates for Framatome’s T1 case would be FT1-1, FT1-2 and FT1-3.

Specimen preparation

Concrete samples of 4-inch diameter and 2-inch height were used as the substrate to evaluate potential coatings. The concrete samples were prepared in a previous stage of the investigation, using a mix design and raw materials similar to the tunnel. Some of the samples were aged through accelerated aging tests and others were not aged for comparative purposes. After the aging process, aged concrete surfaces with protruded coarse aggregates (uneven), exposed rebar (some cases) and chemical damage were obtained. The developed concrete specimens were used as the substrate of the coatings.

Framatome company received the concrete samples (aged and non-aged), already identified based on the test case (FT1 – FT8) and proceeded with the surface preparation and applying the coating. Only selected samples received surface preparation before the coating application (Table 8) including samples: FT1, FT2, FT7 and FT8 (Table 8). For each test case, three replicates were prepared. For example, for the T1 test case, the replicates identification are FT1-1, FT1-2, and FT1-3 (Table 8). The same identification process was done for the rest of the groups. Some of the samples have steel rebar, embedded or exposed, identified as FT1, FT3, FT5 and FT7 (Table 8).

To facilitate the aging process and evaluation, coated samples were grouped. Group 1 included FT1, FT2, FT3 and FT4 test cases, with two replicates each. Group 2 included FT5, FT6, FT7 and FT8 test cases, also with two replicates each.

Abrasive blasting with garnet media was the surface preparation method used on selected Framatome's samples, FT1, FT2, FT7 and FT8, before coating application. The rest of the samples, FT3, FT4, FT5 and FT6, did not receive surface preparation and served as a reference for comparative purposes. Once the applied coatings were cured, samples were sent to FIU laboratories for testing. Figure 117 shows the top view of the coated samples at the initial conditions (before aging started).

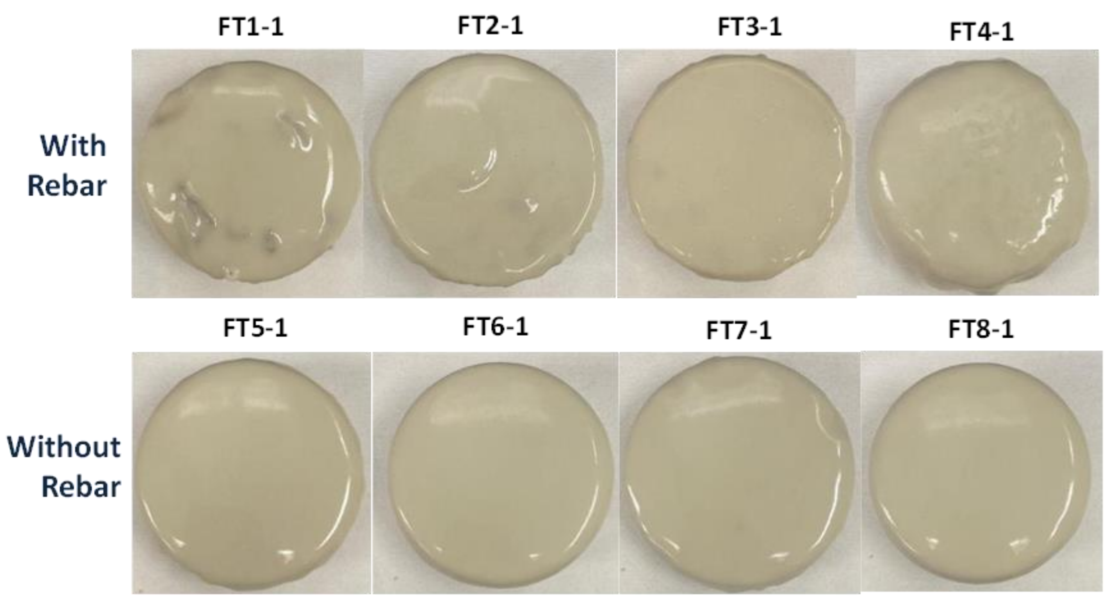

Figure 117. Top view of Framatome's coated samples, with (FT1, FT3, FT5 and FT7) and without (FT2, FT4, FT6 and FT8) surface preparation, at the initial conditions. Only replicate 1 is presented here, representative of all replicates.

Table 9 below shows the major characteristics of the Framatome polyurea coating system. The coating system proposed included a primer and a topcoat.

Table 9. Characteristics of the Framatome's Coating System

Coating	Characteristics
1. Prime coat. **Framatome-Nukote FP1 Fusion primer.** *Epoxy coating* 2. Finish coat. **Framatome-Nukote ST-M Polyurea.** *Polyurea coating*	- Coating system. Multiple coats. - Erosion and impact resistant coating (finish coat) - Environmentally friendly products - Fast curing

<u>Accelerated aging conditions</u>

The enhanced aging consists of exposing the samples (top coated surface) to a 0.5M nitric acid solution (pH = 0.3) and erosion for the time of the experiment. Once a week, samples were exposed to erosion using a wire brush. Figure 118 shows the schematic of the test setup developed for the exposure of the coated samples to the acid solution. A similar setup was used to age the concrete surfaces. The test setup was placed inside a fume hood to reduce the risk of operator exposure to nitric acid fumes.

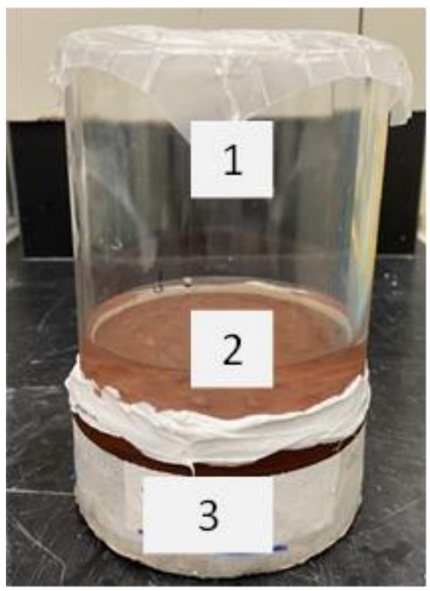

Figure 118. Test setup for coatings exposure to acid solutions. 1. acrylic tube with acid solution, 2. coating (brown color) covering the top surface of the sample, 3. concrete sample.

The procedure summarized below was followed for the evaluation of coated surfaces via the accelerated aging conditions.

I. *Initial data and visual inspection* - After labelling the samples, visual inspection and images of the coated surface are taken. This allows detection of possible failures on the coatings such as erosion, blistering, cracking, scaling and others. In addition, the initial thickness of the coating is measured. Images of the side and top views are taken.

II. *Measure impedance* - Impedance measurements are carried out with time at the open circuit potential (OCP) condition with 10 mV potential perturbation.

III. *Measure pH* - The acidic test solution in contact with the coated surface is collected for pH measurements. The pH values are recorded over time.

IV. *Measure coating thickness* - Ensure the sample is dry before making measurements. Place drops of water in selected locations. Record all 15 thickness measurements (3 measurements per location, 5 locations on sample) with the Positector 200 Thickness Gage and record the minimum, maximum and average of each sample.

V. *Visual Inspection* - Perform a visual inspection and document the exposed coated surface with photographs (side and top views) on a weekly basis. Inspect and record the presence of possible coating's failures.

VI. *Erosion of the coated surface* - The specimen is eroded with a small, circular wire brush in a circular motion across the samples' surface for approximately 1 minute.

VII. *Acid replacement* - Add 200 mL of the acid solution with adjusted pH or new in the corresponding acrylic container, exposing the coated concrete sample to the acidic environment.

VIII. Once a week, repeat steps II through VII for each sample.

Measurements

Several durability measurements such as visual inspection, pH changes of the acid solution, coating thickness, coating adhesion, failures identification/evaluation, impedance measurements, as well as surface characterization including x-ray diffraction (XRD), scanning electron microscopy with energy dispersive x-ray (SEM-EDS) and others will be performed for evaluating the potential coatings. Once a week the coating evaluation was conducted. Visual inspection and failure identification of the coated specimens was conducted before, during and after the aging tests. Possible failures that could be observed includes blistering, cracking, scaling and erosion. Images were also taken over time during the visual inspection to facilitate further inspection/evaluation of the failures observed. Other measurements included coating thickness and impedance. Because this is an ongoing investigation, surface characterization is not completed and will not be included in this summary document. Table 10 summarizes the measurements that will be used to evaluate the coating performance.

Table 10. Measurements to Evaluate Coating Behavior

Test	Age	Method
Visual inspection (failures)	Over time	ASTM D6577 [4]
Coating thickness	Over time	Coating Thickness Gauge
Water absorption	Over time	Electrochemical
Coating protective properties (impedance)	Over time	ASTM D6577 [4], Electrochemical
pH change (solution)	Over time	pH measures
Adhesion	before/after test	Pull-off test, ASTM D7234 [5], ASTM D4541[6]

Surface characterization (SEM-EDS, XRD, IR.)	before/after test	

Coating thickness measurements were conducted in 5 different locations of the coated surface of each sample, over time, using a Positector 200 Thickness Gage. For each location, at least three measurements were taken. Average values were calculated to get information of the coating's durability.

The evaluation of the failures (blistering, cracking, erosion, etc.) was performed by visual comparison between the samples studied (three replicates) and standard photographs specifically designed for each defect as well as the reference sample (not exposed), conforming to the ASTM D714 [7], ASTM D772[8], and ASTM D661 standards [9].

The pH of the acid solutions was measured with time to control and keep the concentration constant. By using the pH formula, the concentration of the acid solutions, 0.5M, was determined and compared with the original pH value (0.3). The deviation from the original value would indicate coating acid attack. The deviation calculated was used to determine the volume of concentrated acid to be added to keep the concentration of the solution constant.

Impedance measurements were also performed on the coated surfaces providing useful information about the coating durability. The impedance measurements were conducted over time using a PMC-1000 multichannel potentiostat, at the open circuit potential (OCP) condition with 10 mV potential perturbation. A three-electrode arrangement was used using a saturated calomel reference electrode as a reference electrode, a platinum mesh as the counter electrode, and the coated sample as the working electrode.

Subtask 20.1.1: Results and Discussion

This section was divided in the following subsections: 1) Visual inspection and failure analysis, 2) Coating thickness results, 3) Impedance results and 4) pH results. Because this is an ongoing experiment, only preliminary results are presented here.

Visual inspection and failure analysis

Figure 119 shows images of coated specimens before and during accelerated aging conditions. The samples presented here, with (FT1-1, FT7-1) and without (FT3-2, FT5-1) surface preparation, as well as aged (FT1-1, FT3-2) and non-aged (FT5-1, FT7-1) concrete substrates, before coating application, are representative of all test cases (FT1-FT8).

No blistering, cracking, or scaling failures were observed on the coated surfaces except erosion. A color change was also observed on the coated surfaces from day 15. The erosion of the surface promoted the detachment of some coating particles, which could impact the barrier properties of the coating.

The preparation of the substrate greatly determines the durability of the coating. In this study, selected samples received surface preparation (FT1-1, FT7-1) and for comparative purposes another group did not receive preparation (FT3-2, FT5-1). In general, no difference in the coating behavior among samples with and without surface preparation was observed, thus far.

The presence of exposed rebar before coating application, for example sample FT1-1, could eventually lead to coating failures. Peeling or detachment of the coating on top of the rebar was also not observed thus far. Once the steel rebar is oxidized, the corrosion products formed could lead to the coating failure.

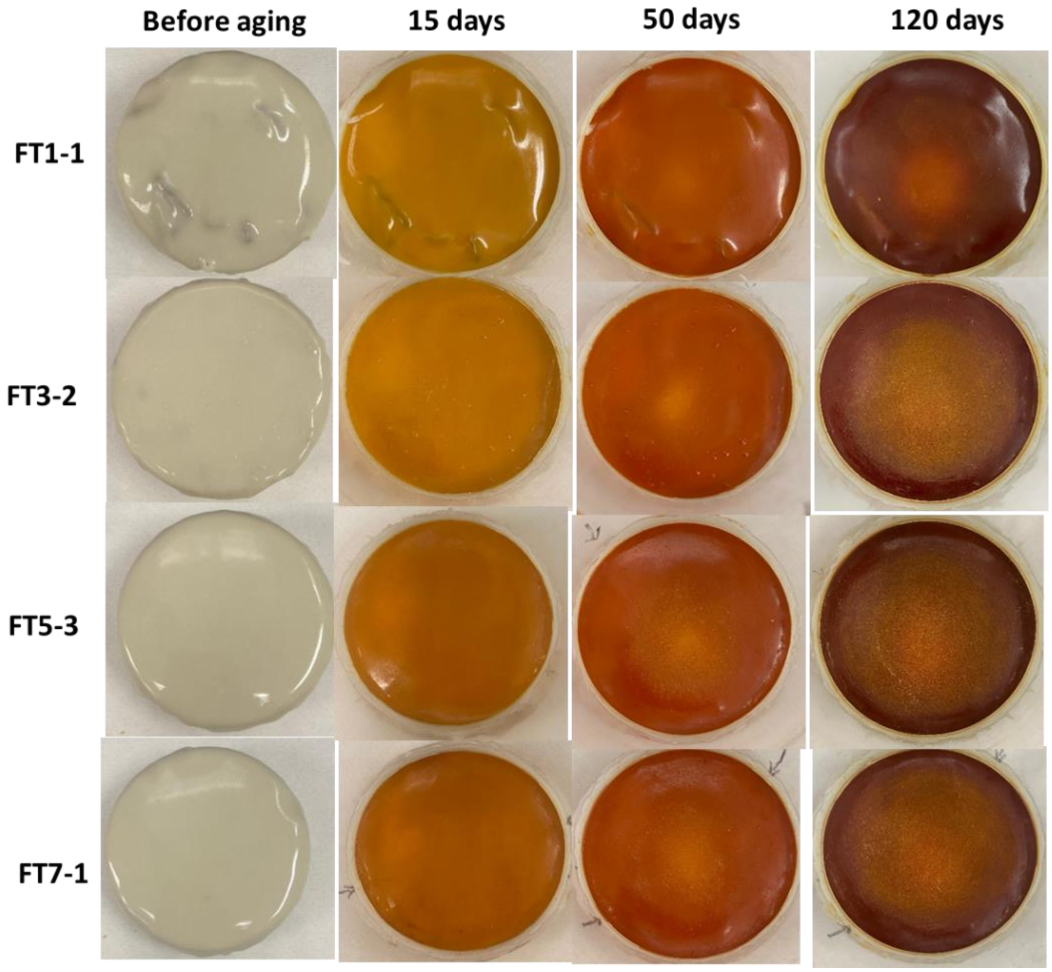

Figure 119. Images of top view of coated samples, with (FT1-1, FT7-1) and without (FT3-2, FT5-1) surface preparation, before and during accelerated aging.

Coating thickness

The thickness of the coatings gives quantitative information related to durability. Because the coatings are exposed to accelerated aging conditions, deterioration of their properties and possible decrease of the thickness is expected with the aging time. In addition, because a polyurea multilayer coating system, resistant to abrasion is being evaluated, a slower deterioration and consequently of the thickness is therefore expected.

Figure 120 shows the evolution of the coating thickness for selected samples of group 1 (FT1 and FT3) and group 2 (FT5 and FT7). All tested samples show a decrease in the thickness no matter the concrete surface conditions (aged and non-aged concrete, with and without surface preparation) before the coating's application. In addition, no major difference of the thickness was observed among the tested samples.

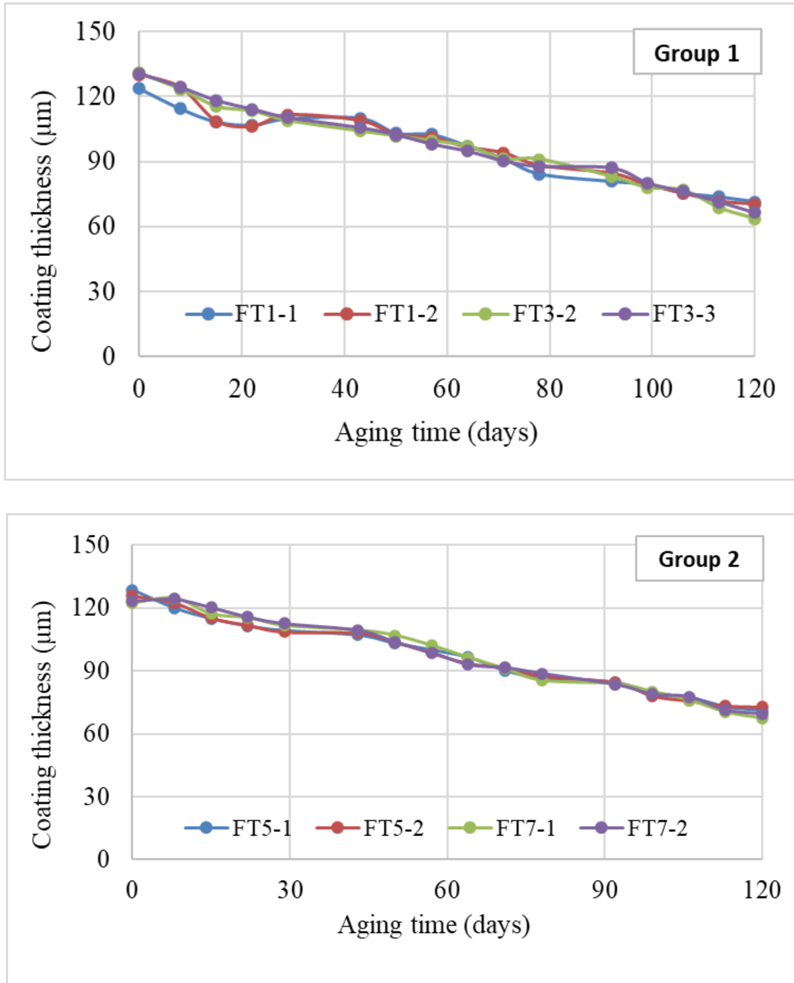

Figure 120. Thickness of selected coated samples, with (FT1, FT7) and without (FT3, FT5) surface preparation during accelerated aging. Group 1 (FT1 - FT4) and Group 2 (FT5 - FT8) .

The thickness loss of selected samples (FT1, FT3, FT5 and FT7) was calculated with the initial and final values. The calculated thickness loss ranged 40-47% of the initial value after 120 days of aging, no matter the surface condition of the samples, aged and non-aged concrete and with and without surface preparation.

Impedance results

Electrochemical impedance spectroscopy (EIS) is a very well-known technique for the study of coatings performance. It allows to measure the coatings resistance to the aggressive environment where it is exposed, that also relates with their barrier properties [10-12]. Baycon, one of the pioneers in coatings evaluation using electrochemical techniques, measured the resistance of three hundred different coating systems with their protectometer and related the values with performance in long-term corrosion tests. As a result, high and constant resistances were typical of good performance, > 10^8 –10^9 Ω.cm^2; rapid decreases to values below 10^6 Ω.cm^2 were typical of poor performance, and anything between these extremes was considered fair [10]. Mayne investigation agrees with previous findings and points that corrosion protective properties of organic coatings have an electrochemical character, as it can be explained by the coating resistance, hindering ions movement between cathodic and anodic areas [11].

Selected coated samples, with (FT2 and FT7) and without (FT3 and FT5) surface preparation and with (FT2 and FT3) and without (FT5, FT7) the aged concrete surface, were considered for this summary document. The selected samples are representatives of the eight test cases under study.

Figure 121 shows the evolution of the impedance modulus of coated samples with an aged concrete surface and with (FT2) and without (FT3) surface preparation at different aging times.

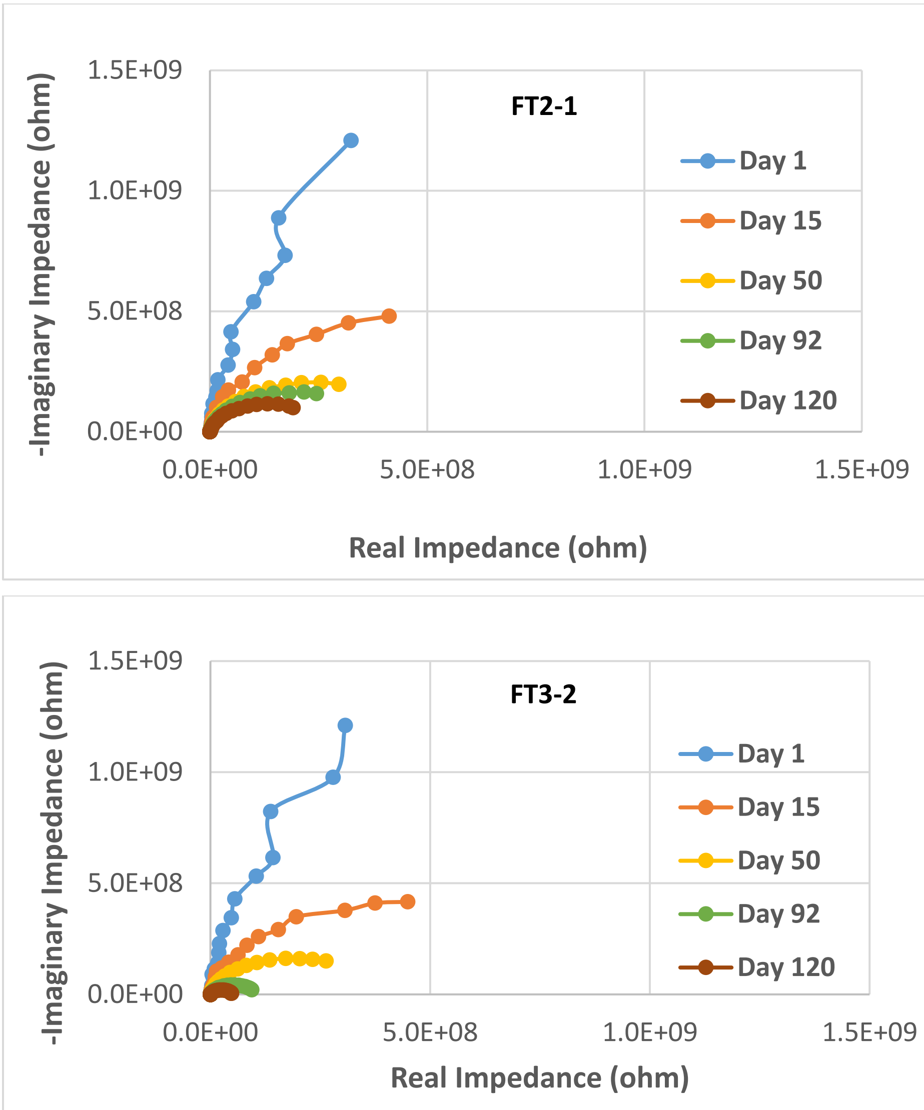

Figure 121. Nyquist plot comparison graph for selected coated samples with (FT2) and without (FT3) surface preparation of group 1.

The impedance decreases with the aging time up to values ranging 10^6-10^7 $\Omega.cm^2$ after 120 days of accelerated aging. Coated samples with surface preparation (FT2) showed greater impedance values (~10^7 at day 120) than samples without (FT3) surface preparation (~10^6 at day 120). This is indicative of greater resistance to the aging environment due to surface preparation. According to Baycon [10], impedance values between 10^6-10^7 are indicative of poor performance against the aging conditions.

Similar analysis was performed on selected coated samples (FT5 and FT7) of group 2 without the aged concrete surface. Figure 122 shows the impedance of coated samples with (FT7) and without (FT5) surface preparation at different aging times.

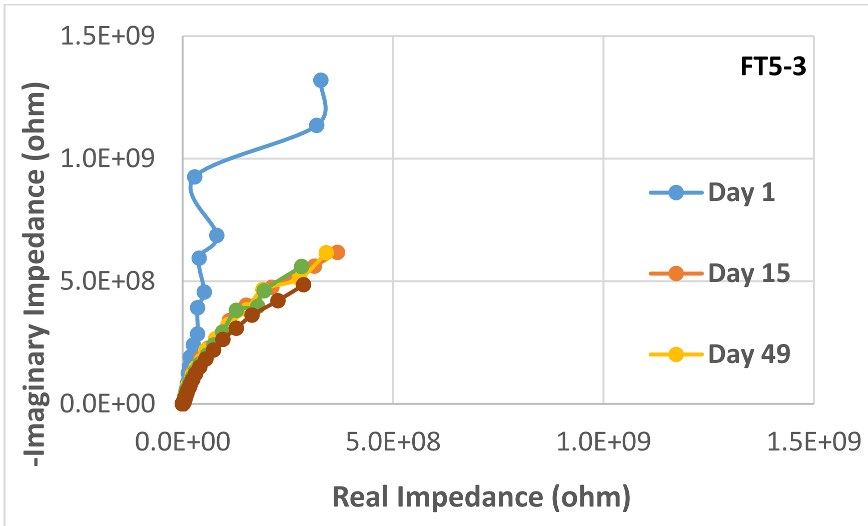

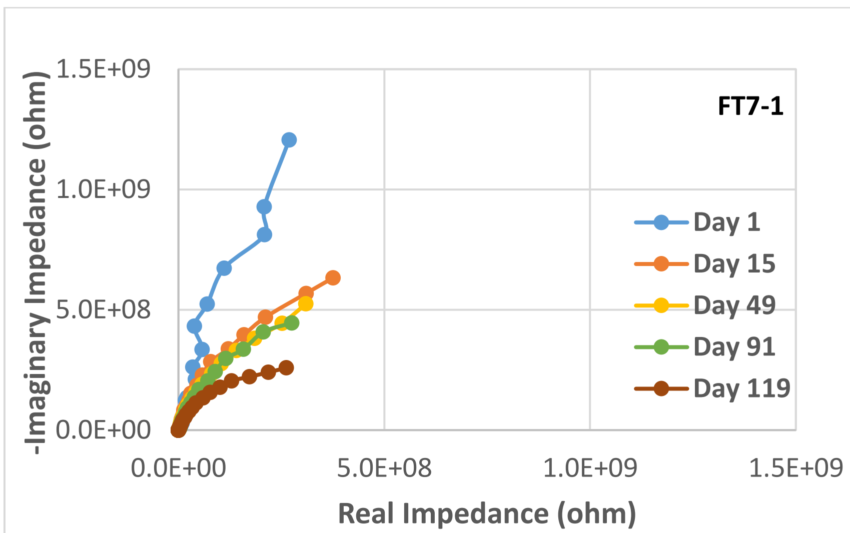

Figure 122. Nyquist plot comparison graph for selected coated samples with (FT7) and without (FT5) surface preparation of group 2.

For this group of samples without the aged concrete surface, the impedance also decreases with time for all the coated samples with and without surface preparation. However, after 120 days of aging, impedance values were above ~10^8 $\Omega.cm^2$ for both samples with and without surface preparation, indicating a good performance for all the test cases A major difference in the impedance was not observed between samples with and without surface preparation.

In summary, coated samples with the non-aged concrete surface (group 2) with and without surface preparation showed the best protective properties, with the highest impedance values. Coated samples with the aged concrete (group 1), has an uneven surface with protruded aggregates and exposed rebar (some cases) that is more prone to premature coating failure.

pH results

The pH of the nitric acid solution in contact with the coated samples was measured once a week. The idea is to keep constant the pH to 0.3 for the time of the experiment to have a solution with a concentration of 0.5 M.

The pH values of the acid solution of all the coated samples changed with the values between 0.12 and 0.40 during the accelerated aging. The changes in pH are indicative of interaction between the coating and the acid solution. Every week, if necessary, the pH value was adjusted to the desired value (0.3) by adding concentrated acid or diluting the solution. The concrete surface condition, aged and non-aged and with and without surface preparation, was not shown to influence the pH values.

Subtask 20.1.1: Conclusions

Visual inspection results showed no blistering, cracking, or scaling failures after 120 days of accelerated aging, except some erosion and a color change. The erosion of the surface increased with the aging time, leading to the detachment of some coating particles. The calculated thickness loss ranged 40-47% of the initial value after 120 days of aging, no matter the surface condition of the samples. Impedance results showed differences in the coating behavior depending on the concrete surface conditions, 1) aged and non-aged and 2) with and without surface preparation. Coated samples with the non-aged concrete surfaces depicted the highest impedance values ($>10^8$ $\Omega.cm^2$), indicative of a good performance after 120 days of accelerated aging. Surface preparation seemed to improve coatings resistance against the aging environment in coated samples with an aged concrete, with greater impedance values $\sim10^7$ $\Omega.cm^2$.

Subtask 20.1.1: References

1. Bob J. Gilliam et al. “Inspection and Assessment of the H-Canyon Ventilation System at the Savannah River Site”. Phoenix, Arizona. Waste Management Conference, 2015.
2. Staff Report, Defense nuclear facilities safety board. "H-Canyon exhaust tunnel fragility analysis input and assumptions". 2018.
3. Echeverria, M. et al. "Aging of concrete for the evaluation of repair materials to protect the HCAEX tunnel at Savannah River". Waste Management 2020 Conference, Phoenix, AZ, March 2020. (Best Poster of Track). Paper # 20301
4. ASTM D6577 “Standard Guide for Testing Industrial Protective Coatings”. 2019.
5. ASTM D7234-21 “Standard Test Method for Pull-Off Adhesion Strength of Coatings on Concrete Using Portable Pull-Off Adhesion Testers”. 2021.
6. ASTM D4541. “Standard Test Method for Pull-Off Strength of Coatings Using Portable Adhesion Testers”. 2017.
7. ASTM D714-02. “Standard Test Method for Evaluating Degree of Blistering of Paints”. 2017.
8. ASTM D772-18. “Standard Test Method for Evaluating Degree of Flaking (Scaling) of Exterior Paints”. 2018.

9. ASTM D661-19. “Standard Test Method for Evaluating Degree of Cracking of Exterior Paints”. 2019.
10. R.C. Bacon, J.J. Smith, F.M. Rugg, Electrolytic resistance in evaluating protective merit of coatings on metals, Ind. Eng. Chem. 40 (1) (1948) 161.
11. J.E.O. Mayne, Current views of how paint films prevent corrosion, J. Soc. 40 (1957) 183.
12. Echeverria M. et al. "Viability of Epoxy Siloxane Coatings for Preventing Steel Corrosion". Progress in Organic Coatings 92 (2016) 29-43.

Subtask 20.1.2: Establish a Ranking of Coating Candidates from Research Findings

Subtask 20.1.2: Methodology

In this investigation, four coating candidates, Carboline, Belzona, Sherwin-Williams and Framatome were selected for the accelerated aging and evaluation. The four coating candidates completed the aging and evaluation process.

The ranking was based on the coating's performance to the accelerated aging conditions, 0.5M nitric acid solution and erosion. Parameters considered for the ranking included the results on 1) visual inspection, 2) coating failures, 3) thickness loss and 4) impedance.

Subtask 20.1.2: Results and Discussion

Table 11 below summarizes the results of the evaluation of the four potential coatings after being exposed to 120 days of accelerated aging.

Table 11. Results of the Evaluation of the Potential Coatings after 120 days of Aging

Coating ID	Thickness loss range, (%)	Impedance (Ω), non-aged	Impedance (Ω), aged
Framatome (F)	40-47	$2.59.10^8$	$1.38.10^4$
Sherwin-Williams (S)	6-16	$1.16.10^9$	$1.15.10^4$
Carboline (C)	16-28	$3.00.10^3$	$<1.10^3$
Belzona (B)	13-33	$2.56.10^3$	$0.3.10^3$

Table 11 shows the results of thickness loss and impedance values of selected samples of the four potential coatings under study. Coating thickness decreased with the aging time for all tested coatings. The Framatome coating system showed the greatest thickness loss (40-47 %), followed by Belzona (13-33%), Carboline (16-28%) and Sherwin-Williams (6-16%) coatings after 120 days of aging. Also, Sherwin-Williams and Framatome coating systems offered excellent protective properties, with the highest impedance values, 10^8-10^9 Ω.cm^2, for the non-aged concrete samples, after 120 days of accelerated aging. The Carboline coating system and Belzona single coating showed impedance values, ranging 10^3-10^6 Ω.cm^2, indicative of bad-fair performance after 120 days of aging.

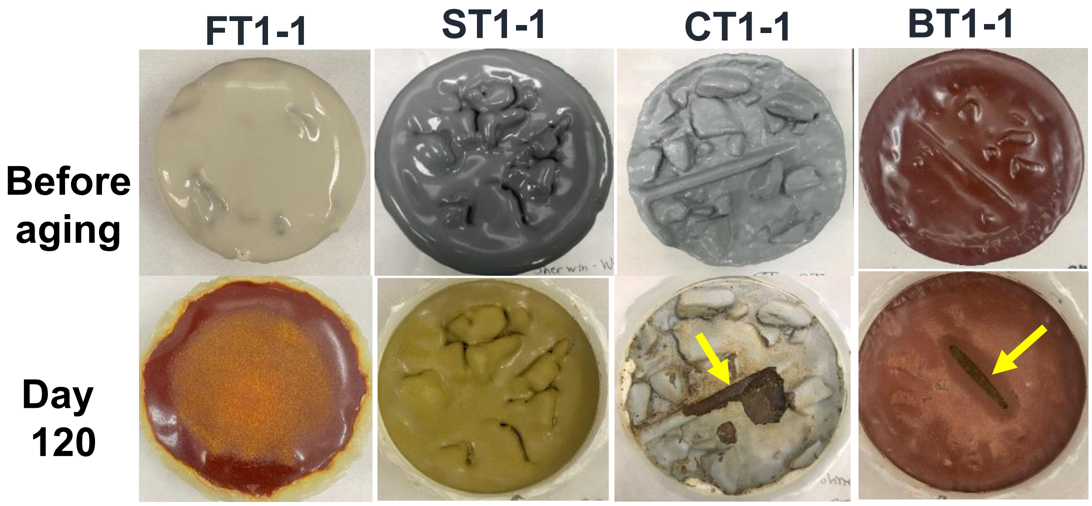

Figure 123. Top view of the potential coatings before and after 120 days of accelerated aging.

Figure 123 shows the images of the coated surfaces of the potential coatings. The top images show the condition of the coated surfaces before the aging started, with no degradation at this time. Only coated samples of group 1 (T1-1), with the aged concrete surface, steel rebar and surface preparation, are presented here, which are representative of this group. No major failures like blistering, cracking and scaling were observed on most of the samples, except erosion of the surface and some coating damage for Carboline and Belzona coatings. Color change was observed on some of the tested coatings, Framatome and Sherwin-Williams, related to coating degradation.

Subtask 20.1.2: Conclusions

Results suggest that Sherwin-Williams and Framatome coating system will offer greater protective properties than Carboline coating system and Belzona single coating in aggressive environments combining nitric acid attack and erosion. Sherwin-Williams coatings system showed the highest impedance values and less thickness loss over time.

Subtask 20.2: Corrosion Evaluation of Steel Containers for Hanford Integrated Disposal Facility

Subtask 20.2: Introduction

A current challenge for DOE and relevant DOE sites is to understand the durability of the steel containers that will contain low-activity waste (LAW) and secondary waste forms, encapsulated in glass and grout respectively, and that will be placed within the Integrated Disposal Facility (IDF) at Hanford. Currently, corrosion data of the steel containers at Hanford that is exposed to groundwater is limited. In addition, there is limited information on the corrosion behavior of container materials in groundwater that has also contacted grout waste forms following the initial container breach. It is of interest to study the corrosion of container materials when exposed to grout-contacted solutions to get information of the container-waste form (grout-waste form) interface.

Subtask 20.2: Objectives

The objective of this subtask is to evaluate material behavior of the containers in environments similar to IDF conditions and obtain site-specific corrosion data through electrochemical measurements. Various materials will be studied including 304 stainless steel (SS), 316 SS, carbon steel and others, and the effect of the ions concentration from the grout-waste forms on the corrosion behavior will be investigated. Obtaining such data can be used to predict the container's useful life. A new solution that simulates the IDF groundwater contacting the cement waste form inside the container will be used to study the container-waste form interface.

Subtask 20.2.1: Corrosion Behavior of Container Materials for the Steel Corrosion Study at Hanford - 304 Stainless Steel

Subtask 20.2.1: Methodology

In this section, information about the test plan, specimen preparation, test setup and electrochemical measurements is presented. Variables of interest in this study are the type of material and the effect of the grout-pore water solution concentration on the materials behavior to corrosion. Because this is a multiphase study, in this phase, corrosion data only for 304SS and 316SS container material in the solutions are obtained and presented.

Specimen preparation

The materials under study were 304 stainless steel (SS) and 316SS. Cold worked square bars, procured from McMaster, of 304SS and 316SS were cut to the dimensions of 0.75-inch height, 0.5-inch width and 0.5-inch thickness. The back of the sample was threaded, and a piece of 316 SS rod screwed to it to facilitate the electrical connection between the sample and the cables connected to the rod. Only the bottom squared section of the 304 SS and 316SS samples were under study, with an area of 1.61 cm2. The specimens were fixed in a cold resin allowing only one side of the square bar (bottom) to be in contact with the solution. The surface of the samples was cleaned with detergent to remove any grease, oil or dust from the surface. The surface was then grinded using a manual grinding machine and a series of grinding papers, 120, 300, 600, 800, 1000 and 1200. After grinding, the surface was polished with a cloth and a 1-micron diamond suspension to get a mirror finish of the surface. Finally, the surface was carefully washed with tap water and dried with compressed air, before storing in a desiccator until the beginning of the experiments.

Test setup and test solutions

A three-electrode arrangement was used to perform the electrochemical measurements including a reference electrode (saturated calomel-SCE), a working electrode (the sample, e.g., 304 SS or 316SS) and a counter electrode (a platinum mesh). Figure 124 shows the test setup inside a Faraday Cage which was used for the electrochemical measurements. The electrodes were in contact with the test solution and only the bottom surface of the sample (working electrode) was immersed in the solution during the experiment. A PMC-1000 potentiostat was used for the electrochemical measurements, connected to the computer through the VersaStudio software. A frequency response analyser FRA module, connected to the potentiostat, allowed the conduction of the impedance measurements. The ZSimpWinTM software was used for analyzing impedance data.

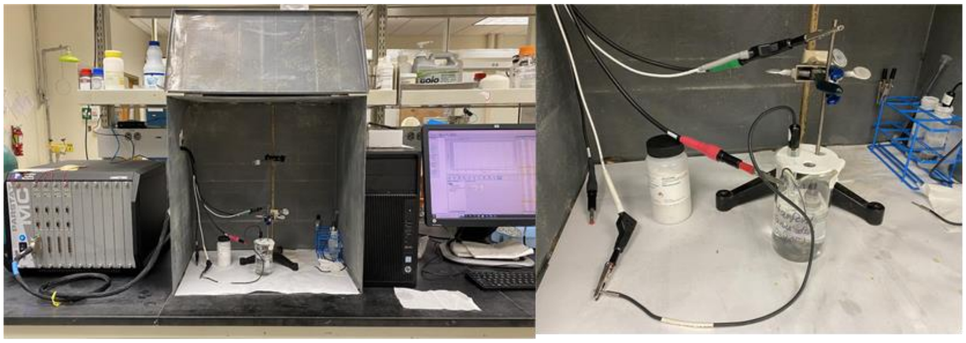

Figure 124. View of the potentiostat, the Faraday Cage and computer (left image) used for electrochemical measurements. Zoom of the experimental setup (right image).

The Hanford point of contact provided generic cast stone samples that would simulate the grout-waste forms in contact with the container material. In addition, the recipe to prepare a solution from the grout-waste forms, identified as grout-pore water (GPW) solution, was also provided. The GPW solution was used as the electrolyte for electrochemical testing. The GPW solution without dilution was considered as solution 1 and two other solutions, solution 2 and solution 3 were obtained from dilutions of solution 1.

Leach water from the grout-waste form were prepared as follows. First, the bulk grout-waste sample was crushed using a hammer. The powder obtained was then sieved to a particle size lower than 2 mm. DI water (1000.0 mL) then contacted 25 g of the powdered grout for 7 days on a mechanical shaker. The filtrate with pH 11.52 ± 0.08 obtained is the grout-pore water solution.

<u>Electrochemical measurements</u>

Electrochemical measurements included corrosion potential (Ecorr = OCP), electrochemical impedance spectroscopy (EIS), also known as impedance, and potentiodynamic polarization (PDP) or polarization.

The <u>impedance measurements</u> were conducted over time at the open circuit potential (OCP) condition with 10 mV potential perturbation and at a frequency range from 1MHz to 1 mHz. The impedance measurements were performed for a week, every 24 hours. The impedance measurements were conducted once the Ecorr was stabilized. For that reason, the Ecorr was measured for an hour or until the value was stable and then, the impedance measurement started. The experimental data was recorded and used to get various graphs such as the Nyquist and Bode plots.

The <u>PDP measurements</u> were conducted following the sequence below:

1. Measure corrosion potential (Ecorr) for 1 hour.
2. Run a PDP scan (single) with the parameters below:
    - Initial potential (V): -200 Vs OCP
    - Scan to 1V vs reference electrode or cut it off at 10 mA/cm^2
    - Scan rate (mV/s): 0.1667 mV/s

The PDP data was also used to get useful parameters such as the corrosion current (Icorr), the corrosion rate (R), the current density (icorr) and others, using the Tafel method. For this method, the material is polarized, typically on the order of ±10mV, relative to its Ecorr, the potential measured when no [net] current is flowing. As the potential of the material (working electrode) is changed, a current will be induced to flow between the working and counter electrodes, and the material's resistance to polarization (Rp) can be found by taking the slope of the potential versus current curve. This is known as a Tafel plot. The Icorr can be determined by the following equation [4].$Icorr = \frac{\beta_a \beta_c}{2.3\,(\beta_a+\beta_c)}(\frac{n}{I})^{-1} = KRp^{-1} = \frac{K}{Rp}$ (Equation 1)

Here, βa and βc are the anodic and cathodic Tafel slopes, respectively, in volts/decade, and n/I is the slope of the polarization curve around the Ecorr, corresponding to the polarization resistance. The term K is called the conversion factor or the Stern-Geary constant, assumed to be 26 mV for active steel and 50 mV for passive steel. When K is already known, the Icorr can be calculated based on the Rp obtained by the linear polarization. Then, if the surface area (anodic steel area), A, being polarized is accurately known, the current density (icorr) can be calculated by the following equation. [5].

$$i_{corr} = \frac{Icorr}{A} \quad \text{(Equation 2)}$$

The icorr can be also determined by cathodic Tafel extrapolation to corrosion potential. Here, icorr is in A/cm2, EW is the equivalent weight of steel (25.12 g/mol), ρ is the density of the steel (7.94 g/cm3) and F is the Faraday's constant.

Surface characterization

Surface characterizations techniques such as scanning electron microscopy and optical microscopy will be used to characterize the sample's surface and get information of the chemistry and morphology of the corrosion products that may form. For comparative purpose, same analysis will be conducted on non-tested samples and later compared with the results of tested samples. Because this is an ongoing investigation, at this time only images obtained using an optical microscope will be presented.

Subtask 20.2.1: Results and Discussion

Electrochemical test results for 304SS in GPW solutions

Impedance (EIS)

Figure 125 shows the impedance modulus versus frequency, for the 304 SS samples exposed to the grout-pore water (GPW) solutions 1, 2 and 3. The impedance modulus provides information about the corrosion performance or corrosion resistance of the material to the solution. For the GPW1, the impedance modulus is very similar on day 1 and on day 8 of the test, with a slightly increase at the end (lowest frequency), on day 8, from 1.15 E6 Ω to 4E7 Ω, respectively. This increment indicates good corrosion resistance of the 304SS in the GPW1 and possible formation and maintenance of the passive film.

For the GPW2 and GPW3 solutions, the impedance modulus follows a different trend on day 1 and on day 8, with greater impedance values on day 1 for most of the frequency range, from 1E6 to ~1 Hz, and very similar behavior and impedance values for both days, at the lower frequency range, 1E-1 to 1E-3 Hz. For the GPW2, it is also observed a slight increase of the impedance modulus value, at the lowest frequency, from day 1 to day 8, ~ 1E6 Ω to 1E7 Ω, which indicates good corrosion protection due to the passive film formation the material surface. For the GPW3, the impedance modulus at the lowest frequency for both days, overlaps, with values slightly lower, ~ 1E6 Ω, than GPW2 and GPW1. However, values are very similar and indicates good protection of the container material.

These results indicate that the concentration of the grout-pore water solution showed slight changes in the impedance modulus values, with greater values after days of immersion, day 8, having a beneficial effect on the corrosion protection. Also, the GPW1, showed higher impedance modulus than the GPW2 and GPW3, respectively.

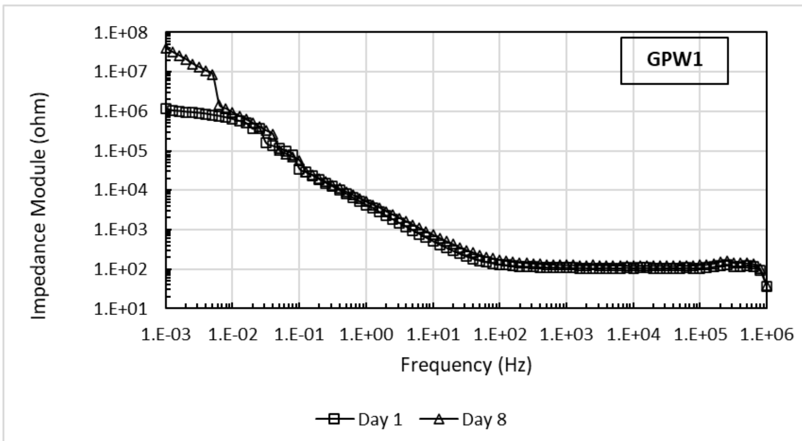

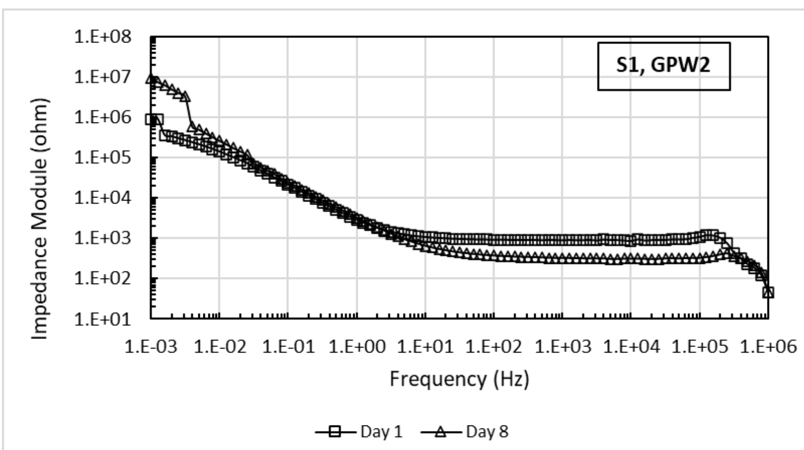

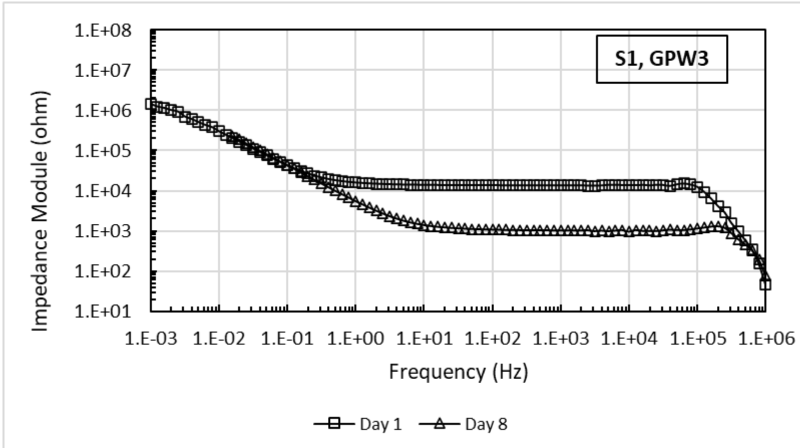

Figure 125. Bode plots for the 304 stainless steel container material exposed to grout-pore water solutions 1, 2 and 3 at different immersion times.

Potentiodynamic polarization (PDP)

Figure 126 shows the polarization curve of 304 SS specimen immersed in the grout-pore water solutions 1, 2 and 3. This graph offers insight into the electrochemical performance of the container material.

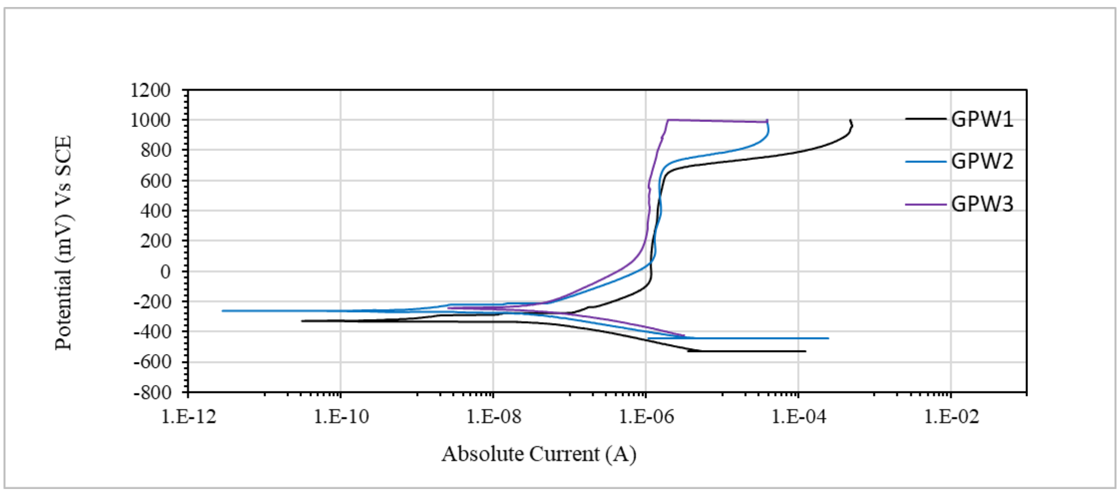

Figure 126. Potentiodynamic graphs for 304 stainless steel container material when immersed grout-pore water solutions 1, 2 and 3.

For the 304SS in grout-pore water solutions (GPW) 1, 2 and 3 (Figure 126), it is noticeable that the cathodic branches are controlled by electron transfer. For the 304SS in the GPW1, 2 and 3, solutions (Figure 126), the anodic branches are controlled by the diffusion, which is related to the passivity of the surface. For all the solutions, the anodic domain region shows three different parts. In the first part, the current increases, followed by a second part, a small quasi-passive region in which current is almost constant due to the formation of a passive film. This passive film breaks at certain critical potential, breakdown potential or Eb, ~ between 600 - 650 mV for the three solutions, at which current returns to increase quickly in the third part of the anodic domain region. This breakdown potential and rupture of the passive film was observed in the three solutions, almost same value for the GPW1 and GPW2 (~670 mV) and a little lower (~ 600) for the more diluted solution, GPW3.

Icorr and Ecorr were obtained from the Tafel method and icorr and R were calculated. Table 12 summarizes previous corrosion parameters for the 304SS when immersed in the three grout-pore solutions.

Table 12. Corrosion Parameters for 304SS in Grout-pore Water Solutions 1, 2 and 3

Test solution	Ecorr (mV vs SCE)	Icorr (A)	icorr (A/cm^2)	R (mm/y)
GPW1	-329.40	1.08E-06	6.70E-07	0.008
GPW2	-261.93	1.18E-06	7.32E-07	0.008
GPW3	-249.65	8.28E-07	5.13E-07	0.006

The Ecorr increases with the decrease in the solution concentration, from GPW1- GPW3. The higher currents were observed for the container material immersed in the solutions GPW1 and GPW2, with similar values ~ 1E-6 A. The sample exposed in the most diluted solution, GPW3, showed the lowest Icorr and higher Ecorr. The corrosion rate was also calculated, and the highest value is for the sample immersed in the GPW2, with the highest Icorr and icorr values.

The corrosion rates in mm/y were also calculated for the container material immersed in the three solutions. The corrosion rates of the material for the three solutions are very low, between 0.006-0.008 mm/y. Dominguez [5] created a scale of the corrosion resistance of the metallic materials with the corrosion rates in mm/year and their corresponding stability group. The R values for the three solutions indicates that the material is very stable. The lowest R values is for the material exposed to the GPW3 solution, the most diluted.

Electrochemical test results for 316SS in GPW solutions

Impedance (EIS)

Figure 127 shows the impedance modulus versus frequency, for the 316 SS samples exposed to the grout-pore water (GPW) solutions 1, 2 and 3. There is a marked difference in the impedance modulus trend between day 1 and day 8, when the sample is immersed in the most concentrated solution, GPW1. The impedance modulus for the GPW1, decreases from day 1 to day 8, from $1E^9$ Ω to ~ $1E^7$ Ω, however is a high impedance value indicating good corrosion protection. This is related to the formation of a passive layer on the surface.

For the GPW2, the impedance modulus follows a similar trend on day 1 and on day 8, with a slight increase on day 8, ~ $1E^7$, at the lowest frequency. For the GPW3, it was observed a similar behavior and values at the lowest frequency, however, at higher and intermediate frequencies ($1E^6$ – 1 Hz), impedance values for day 1 are higher than for day 8.

In general, the impedance modulus values observed, ~ $1E^7$ Ω, agree with good corrosion protection due to the passive film formation on the material surface. The highest impedance modulus is for the sample immersed in the GPW1 on day 1, ~ $1E^9$ Ω, compared to the two diluted solutions, GPW2 and GPW3, with values ~ $1E^7$ Ω.

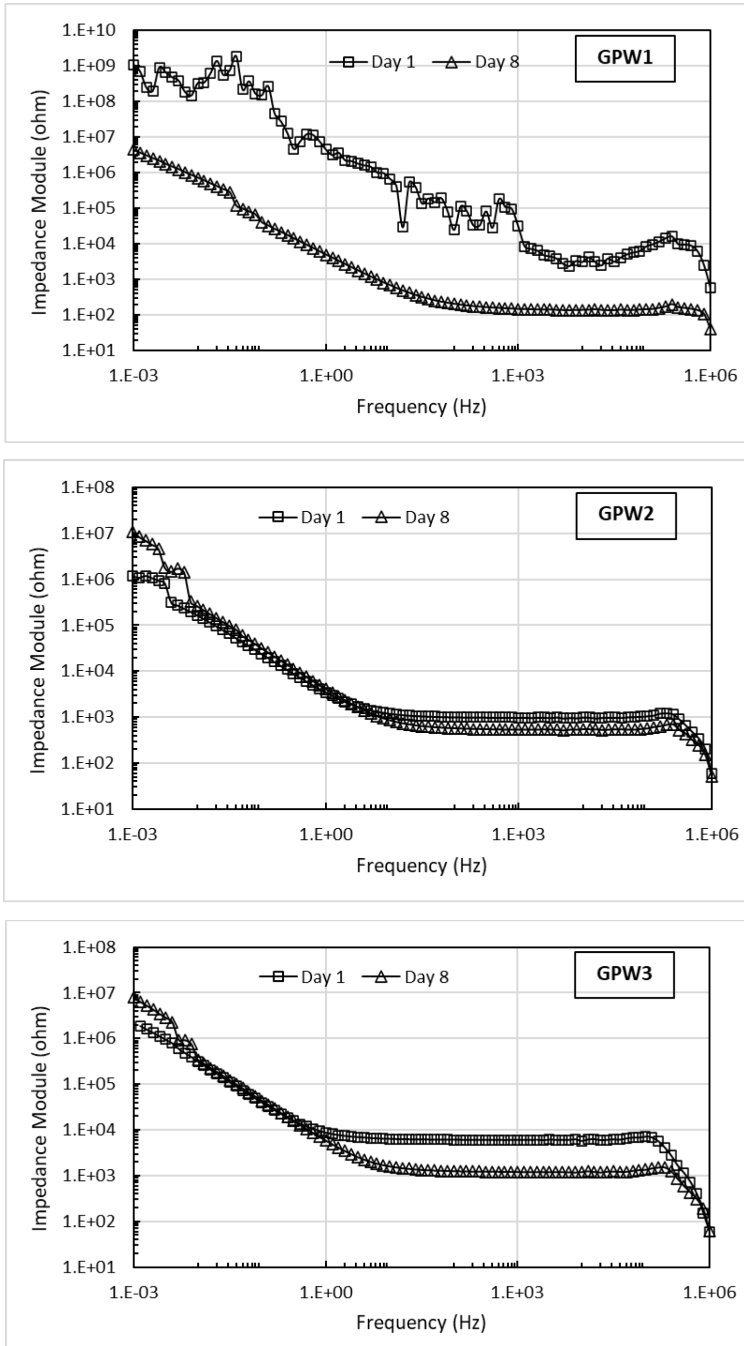

Figure 127. Bode plots for the 316 stainless steel container material exposed to grout-pore water solution 1, 2 and 3 at different immersion times.

Potentiodynamic polarization (PDP)

Figure 128 shows the polarization curve of 316 SS specimen immersed in the grout-pore water solutions 1, 2 and 3. It is observed how the cathodic branch, for the three solutions, are controlled by the electron transfer and the anodic by diffusion. Similar behavior was also observed for the 304SS container material.

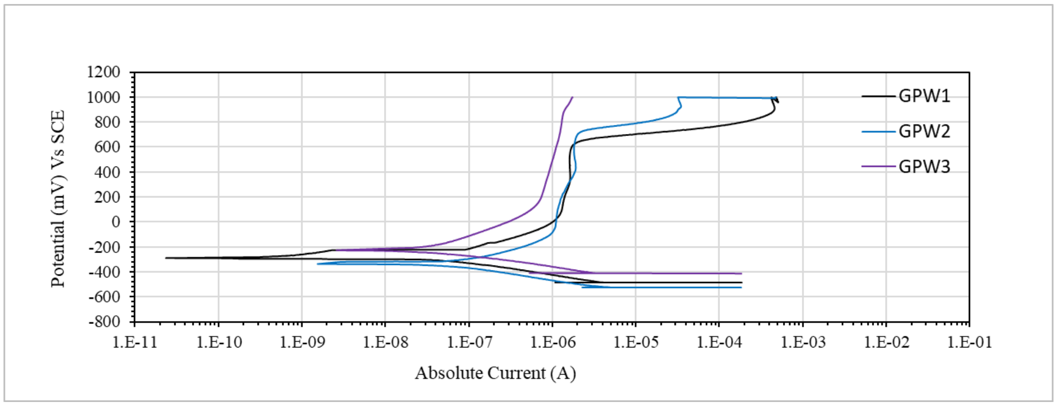

Figure 128. Potentiodynamic graphs for 316 stainless steel containers material when immersed in grout-pore water solutions 1, 2 and 3.

The anodic branch is characterized by three parts, first, a current increase is observed, follow by a slow increase of the current, related to the passive film formation, with small current fluctuations, more evident for the GPW1 and GPW2. The small current fluctuations could be related with the formation of some unstable pits that may not broke the passive film. This passive film breaks at certain critical potential, breakdown potential or Eb, ~ 585 mV, ~ 700 mV and ~850 mV for the GPW1, GPW2 and GPW3, respectively. Then, the current returns to increase quickly in the third part of the anodic domain region. This breakdown potential and rupture of the passive film was observed in the three solutions.

Table 13 summarizes important corrosion parameters for the 316SS when immersed in the three grout-pore solutions, including Icorr and Ecorr, obtained by the Tafel methods, as well as icorr and R that were calculated following specific equations.

Table 13. Corrosion Parameters for 316SS in Grout-pore Water Solutions 1, 2 and 3

Solution	Ecorr (mV vs SCE)	Icorr (A)	icorr (A/cm^2)	R (mm/y)
GPW1	-291.06	1.20E-06	7.44E-07	0.009
GPW2	-335.53	8.14E-07	5.05E-07	0.006
GPW3	-225.429	5.54E-07	3.43E-07	0.004

The highest corrosion current (Icorr) was observed for the container material immersed in the most concentrated solution, GPW1. The material exposed in the diluted solutions, GPW2 and GPW3, shows similar and lower Icorr values, ~ $1E^{-7}$ A. Current density (icorr) and corrosion rate (R) of the material were calculated following specific equations. Corrosion rates are very low, between 0.004 and 0.009 mm/y, for the three solutions, indicating very stable materials, based on Dominguez [5] stabilities group. This is in agreement with the protective passive film that should be formed on the surfaces. The lowest R values is for the material exposed to the GPW3 solution, the most diluted.

Surface characterization of the 304SS samples

Because this is an ongoing investigation, only the preliminary results of the characterization are presented here. It is expected to characterize the surface of the samples using various techniques including optical microscopy, scanning electron microscopy (SEM-EDS) and X-ray diffraction (XRD).

The surface of the 304SS samples were characterized using the optical microscopy technique. The intention was to identify the possible presence of pitting corrosion and study the morphology and dimensions of the pits. Images of the samples before and after the impedance measurements were taken at different magnifications.

Figure 129 shows images of the 304 SS before (reference sample) and after the impedance test, when exposed to grout-pore water solution 1 (GPW1). No pitting was observed on the images of the reference sample (top images). On the contrary, images of the sample after the test (bottom images) at 5X magnification show pittings formed on the tested surface. The same image was then 10X magnified (bottom, right image) and pittings were better visualized. The pitting lengths were measured and are between 14 and 38 μm.

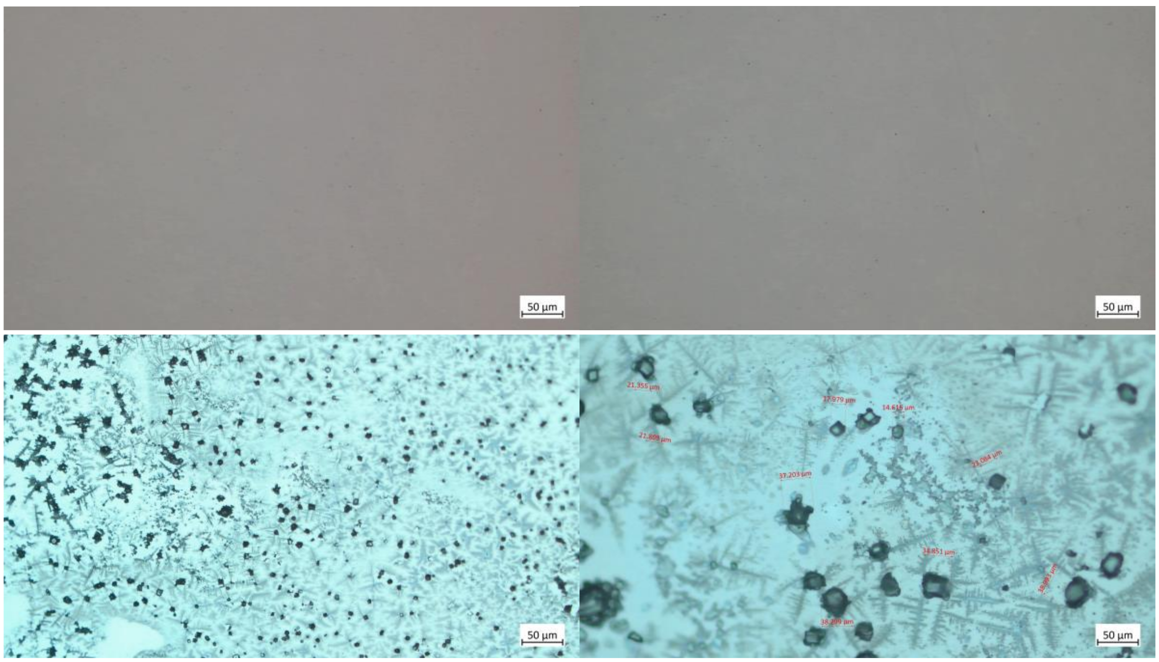

Figure 129. Images of the 304 stainless steel sample before (reference) and after the impedance test in grout-pore water solution 1 (GPW1) at different magnifications. Top images for the reference sample and bottom images for the sample after test.

Subtask 20.2.1: Conclusions

1. The impedance modulus values ~$1E^6$-$1E^7$ Ω for 304SS and 316SS agree with good corrosion protection due to the passive film formation on the material surface.
2. The highest impedance modulus is for the materials immersed in the most concentrated grout-pore water solution (GPW1) on day 1, ~ $1E^9$ Ω, compared to the two diluted solutions, GPW2 and GPW3, with values ~ $1E^7$ Ω.
3. Polarization graphs of 304SS and 316SS, in the three solutions, showed that the anodic branches were controlled by passive film formation followed by rupture of the film, due to pitting formation or some current instability.
4. The corrosion rates of 304SS and 316SS in the three solutions are very low, between 0.006-0.008 mm/y, indicating that the material is very stable.

Subtask 20.2.1: References

1. Marcus, F. and Mansfeld, F. “Analytical methods in corrosion science and engineering”. Taylor and Francis group. 2005.
2. Kruger, J. and Hardman, V. Kay. “Current understanding of pitting and crevice corrosion and its application to test methods for determining the susceptibility to such corrosion of nuclear waste metallic containers”. Center for Materials Science. Washington, D.C. 20234. 1982.
3. Hiromoto S. “Corrosion of metallic biomaterials” in Metals for Biomedical Devices, 2010, Book chapter.
4. R.A. Buchanan, E.E. Stansbury, in Handbook of Environmental degradation of materials, 2012.
5. J.A. Dominguez. “Introducción a la corrosion y protección de metales”. Ministerio de Educación Superior, La Habana, Cuba. 1987

CONFERENCE PARTICIPATION, PUBLICATIONS, AWARDS & ACADEMIC MILESTONES

Oral and Poster presentations (presenter is underlined)

M. Echeverria Boan, M., Baptiste (DOE Fellow), L. Lagos, and D. McDaniel, *“Electrochemical Performance of an Epoxy/Polyurea Coating System for the Protection of Degraded Concrete Infrastructures at DOE-EM Sites – 24503”*, Waste Management Symposia 2024, Phoenix, AZ, March 10-14, 2024 – Selected as “Best Poster” of Track 6 of Deactivation and Decommissioning. The manuscript achieved the rating of a “Superior” paper.

Bryant Pineda (DOE Fellow), *“Evaluating the Erosion and Corrosion Behavior in Nuclear Waste Transfer Systems - #24741”*, Waste Management Symposia 2024, Phoenix, AZ, March 10-14, 2024 – Selected as “Best Graduate Student Poster” in the student poster competition.

A. Aravelli, D. McDaniel, L. Lagos, B Pineda, B. Wiersma, *“Pipeline Integrity Assessment in High Level Waste Transfer Systems – Experimental and Computational Fluid Dynamics (CFD) Based Approaches”*, Proceedings of the Waste Management Symposia 2024, Phoenix, AZ, March 10 – 14, 2024.

B. Cintas, A. Abrahao, D. McDaniel, L. Lagos, D. Reid, K. Boomer, *“Development of Long-term Surveillance Unmanned Ground Vehicles for Nuclear Facilities Inspections”*, Proceedings of the Waste Management Symposia 2024, Phoenix, AZ, March 10 –14, 2024.

ACKNOWLEDGEMENTS

Funding for this research was provided by U.S. DOE Cooperative Agreement #DE-EM0005213. FIU’s Applied Research Center would like to acknowledge the commitment of DOE-EM to this Chemical Process Alternatives for Radioactive Waste project and to all the research being conducted as part of the Cooperative Agreement. The partnership between DOE EM and FIU has

resulted in the development and training of outstanding STEM students that will benefit this country as a whole.

APPENDIX

The following documents are available at the DOE Research website for the Cooperative Agreement between the U.S. Department of Energy Office of Environmental Management and the Applied Research Center at Florida International University: https://doeresearch.fiu.edu/SitePages/Welcome.aspx

FIU Year 4 Annual Research Review Presentations:

1. FIU Research Review - Project 1
2. FIU Research Review - Project 2
3. FIU Research Review - Project 3 - D&D IT ML
4. FIU Research Review - Project 4
5. FIU Research Review - Project 5
6. FIU Research Review - Project 4-5 – Carlos Rios
7. FIU Research Review - Project 4-5 – Fellow Aris
8. FIU Research Review - Project 4-5 – Fellow Aubrey
9. FIU Research Review - Project 4-5 – Fellow Melissa
10. FIU Research Review - Project 4-5 – Fellow Ocampo
11. FIU Research Review - Project 4-5 – Fellow Victor
12. FIU Research Review - Project 4-5 – Fellow Theophile
13. FIU Research Review - Wrap Up - Project 1
14. FIU Research Review - Wrap Up - Project 2
15. FIU Research Review - Wrap Up - Project 3 – D&D IT ML
16. FIU Research Review - Wrap Up - Project 4
17. FIU Research Review - Wrap Up - Project 5